MOLECULAR REGULATION OF LYSYL OXIDASE AND CONNEXIN 43 IN CARDIAC FIBROBLASTS: IMPLICATIONS FOR CARDIAC WALL STIFFENING AND CONDUCTION ABNORMALITIES

SRUTHI RADHAKRISHNAN

Ph.D. THESIS

2024

SREE CHITRA TIRUNAL INSTITUTE FOR MEDICAL SCIENCES AND TECHNOLOGY, TRIVANDRUM

An Institution of National Importance established by an Act of the Indian Parliament
(Act No.52 of 1980)
Dept. of Science and Technology, Govt. of India
www.sctimst.ac.in

MOLECULAR REGULATION OF LYSYL OXIDASE AND CONNEXIN 43 IN CARDIAC FIBROBLASTS: IMPLICATIONS FOR CARDIAC WALL STIFFENING AND CONDUCTION ABNORMALITIES

A THESIS SUBMITTED BY

SRUTHI RADHAKRISHNAN

TO

SREE CHITRA TIRUNAL INSTITUTE FOR MEDICAL SCIENCES AND TECHNOLOGY, TRIVANDRUM.

IN PARTIAL FULFILMENT OF THE REQUIREMENTS

FOR THE AWARD OF

DOCTOR OF PHILOSOPHY

2024

DECLARATION BY THE STUDENT

CERTIFICATE

I, **Sruthi Radhakrishnan**, hereby certify that I had personally carried out the work depicted in the thesis titled: **"Molecular Regulation of Lysyl oxidase and Connexin 43 in cardiac fibroblasts: Implications for cardiac wall stiffening and conduction abnormalities".** No part of the thesis has been submitted for the award of any other degree or diploma prior to this date.

Signature

Sruthi

*Radhakrishnan*Date

CERTIFICATE BY THE RESEARCH GUIDE

(*in institute letterhead)

Dr. Neethu Mohan

Division of Cellular and Molecular Cardiology

Department of Pathology

Sree Chitra Tirunal Institute for Medical Sciences and Technology

Trivandrum 695011, India.

This is to certify that **Sruthi Radhakrishnan**, Division of Cellular and Molecular Cardiology, Department of Pathology of this institute has fulfilled the requirements prescribed for the Ph.D. degree of the Sree Chitra Tirunal Institute for Medical Sciences and Technology, Trivandrum.

The thesis entitled, **"Molecular Regulation of Lysyl Oxidase and Connexin 43 in Cardiac Fibroblasts: Implications for cardiac wall stiffening and conduction abnormalities"** was carried out under my direct supervision. No part of the thesis was submitted for the award of any degree or diploma prior to this date. Clearance was obtained from the Institutional Animal Ethics Committee for carrying out the study.

Signature

Dr. Neethu Mohan

Date

CERTIFICATE BY THE RESEARCH CO-GUIDE
(*in institute letterhead)

Name of the Guide:

Division/Department:

This is to certify that (name of the student), department/division of …… of this institute has fulfilled the requirements prescribed for the Ph.D. degree of the Sree Chitra Tirunal Institute for Medical Sciences and Technology, Trivandrum.

The work under the thesis entitled,

……." was carried out under my direct supervision. No part of the thesis was submitted for the award of any degree or diploma prior to this date.

*Clearance was obtained from the Institutional Ethics Committee / Institutional Animal Ethics / Institutional Committee for Stem Cell Research / Other appropriate committees (if any, specify) for carrying out the study.

Signature

Name of the Co-guide

Date

The thesis entitled

MOLECULAR REGULATION OF LYSYL OXIDASE AND CONNEXIN 43 IN CARDIAC FIBROBLASTS: IMPLICATIONS FOR CARDIAC WALL STIFFENING AND CONDUCTION ABNORMALITIES

Submitted by

SRUTHI RADHAKRISHNAN

for the degree of

Doctor of Philosophy

of

SREE CHITRA TIRUNAL INSTITUTE FOR MEDICAL SCIENCES AND TECHNOLOGY, TRIVANDRUM

is evaluated and approved by

…… ……

(Name & Signature of the Guide) (Name & Signature of thesis examiner)

ACKNOWLEDGEMENTS

I am deeply grateful for the opportunity to pursue my doctoral studies in the Division of Cellular and Molecular Cardiology, Department of Pathology at Sree Chitra Tirunal Institute for Medical Sciences and Technology, Trivandrum, India.

It was a privilege to work under the leadership of two esteemed Directors, Dr. Asha Kishore and Dr. Sanjay Behari, whose support, along with the institute's excellent facilities, greatly enriched my research experience.

I sincerely acknowledge the Department of Science and Technology (WOS-A) and Indian Council of Medical Research, Government of India, for their financial support of this project and for providing the fellowship that made this work possible.

I express my profound gratitude to my esteemed guide, Dr. Neethu Mohan, for her unwavering support, insightful guidance, and invaluable encouragement throughout my doctoral journey. I deeply appreciate her consistent efforts to propose thoughtful improvements and her selfless commitment to mentoring. It has been a privilege and an honor to be her student.

I sincerely thank Dr. K. Shivakumar for his valuable guidance and encouragement. His extensive knowledge and critical thinking have been instrumental in ensuring the successful completion of my studies.

I extend my heartfelt gratitude to Dr. Anil Kumar P.R, Dr. Deepti A.N and Dr. Harikrishnan S, members of my Doctoral Advisory Committee, for their invaluable guidance, support and cooperation.

I extend my heartfelt gratitude to Dr. Sachin J. Shenoy, Division of In Vivo Models and Testing, for his expertise and dedication in performing rat surgeries and providing their care.

I sincerely thank Dr. Abhilash S.P, Department of Cardiology, for his guidance in interpreting ECG and ECHO data and Dr. Divya M.S for her guidance in histological analysis.

I extend my gratitude to the Deputy Registrar, Ms. Radha M and the Registrar, Dr. Santhosh Kumar B, for their invaluable support. I also take this opportunity to thank all the members of the Division of Academic Affairs, staffs of library, Computer division, DCE, Stores and purchase for their help.

I thank Dr. V. S. Harikrishnan, Mr. Manoj, Mr. Sunil, Mr. Biju and all members of Division of Laboratory Animal Science for their help during animal experiments. My sincere thanks to Dr. P. R. Umashankar, Ms. Jesna, Ms. Devika and all staff of the Division of In Vivo Models and Testing for assistance in animal surgery.

I warmly thank Dr. T. V. Anilkumar, Dr. Sabareeswaran A and all staff of the Division of Experimental Pathology for assistance in Nikon Microscope.

I also thank Dr. Lynda V. Thomas and all staff of Division of Tissue Engineering and Regeneration Technologies for assistance in Polarizer Microscope.

I am extremely thankful to the members of the Division of Cellular and Molecular Cardiology: Ms. Ramani, Ms. Hima, Ms. Sunitha, Mr. Sharon, Ms. Lathika, Ms. Sasikala, Mr. Najeeb for their help and support.

I am extremely thankful to Dr. Rajalakshmi P, Mr. James T, Ms. Resmi, Ms. Neena, Ms. Saritha, Ms. Sheeja and all other staff of the Department of Pathology for their assistance in tissue processing and sectioning.

I would like to express my heartfelt gratitude to my seniors, Dr. Harikrishnan V. and Dr. Allen Sam Titus for their guidance and training in molecular cardiology and my junior, Ms. Aswany for her support and friendship. I deeply appreciate the companionship and support extended by my colleague Ms. Indraja Devidasan. I cannot thank her enough for all of our scientific discussions and fostering a cheerful atmosphere in the laboratory.

I would like to acknowledge my parents, grandmother, sister, and in-laws in my personal and academic development. Their unwavering belief in me has been a constant source of motivation.

My thesis acknowledgement would be incomplete without mentioning my husband, Sooraj, who has been a source of support, inspiration and encouragement during all my Ph.D. struggles. A special mention to my son, Dhyan, who tells everyone that his mom is a "Scientist," upon which I must then add "not yet." I could not have made it this far without them.

Finally, I am indebted to Divine Power, who has been a guiding force in my life.

TABLE OF CONTENTS

LIST OF FIGURES

LIST OF TABLES

LIST OF ABBREVIATIONS

Ang II	Angiotensin II
ARBs	Angiotensin II receptor blockers
α-SMA	Alpha-Smooth Muscle Actin
AT1 receptor	Angiotensin II type 1 receptor
BSA	Bovine Serum Albumin
Cx43	Connexin 43
Cx40	Connexin 40
Cx45	Connexin 45
DDR2	Discoidin Domain Receptor 2
ECG	Electrocardiogram
ECM	Extracellular matrix
EMT	Epithelial-to-mesenchymal transformation
ERK1/2	Extracellular signal-regulated kinase 1/2
FSP-1	Fibroblast-Specific Protein 1
HRP	Horseradish Peroxidase
ID	Intercalated Disc
LOX	Lysyl Oxidase
MAPK	Mitogen-activated protein kinase
MI	Myocardial Infarction
MMPs	Matrix metalloproteinases
PDGFRα	Platelet-derived growth factor receptor α

POSTN	Periostin
RAAS	Renin Angiotensin Aldosterone System
SRF	Serum response factor
TGF-β	Transforming Growth Factor-β
VSMCs	Vascular Smooth Muscle Cells

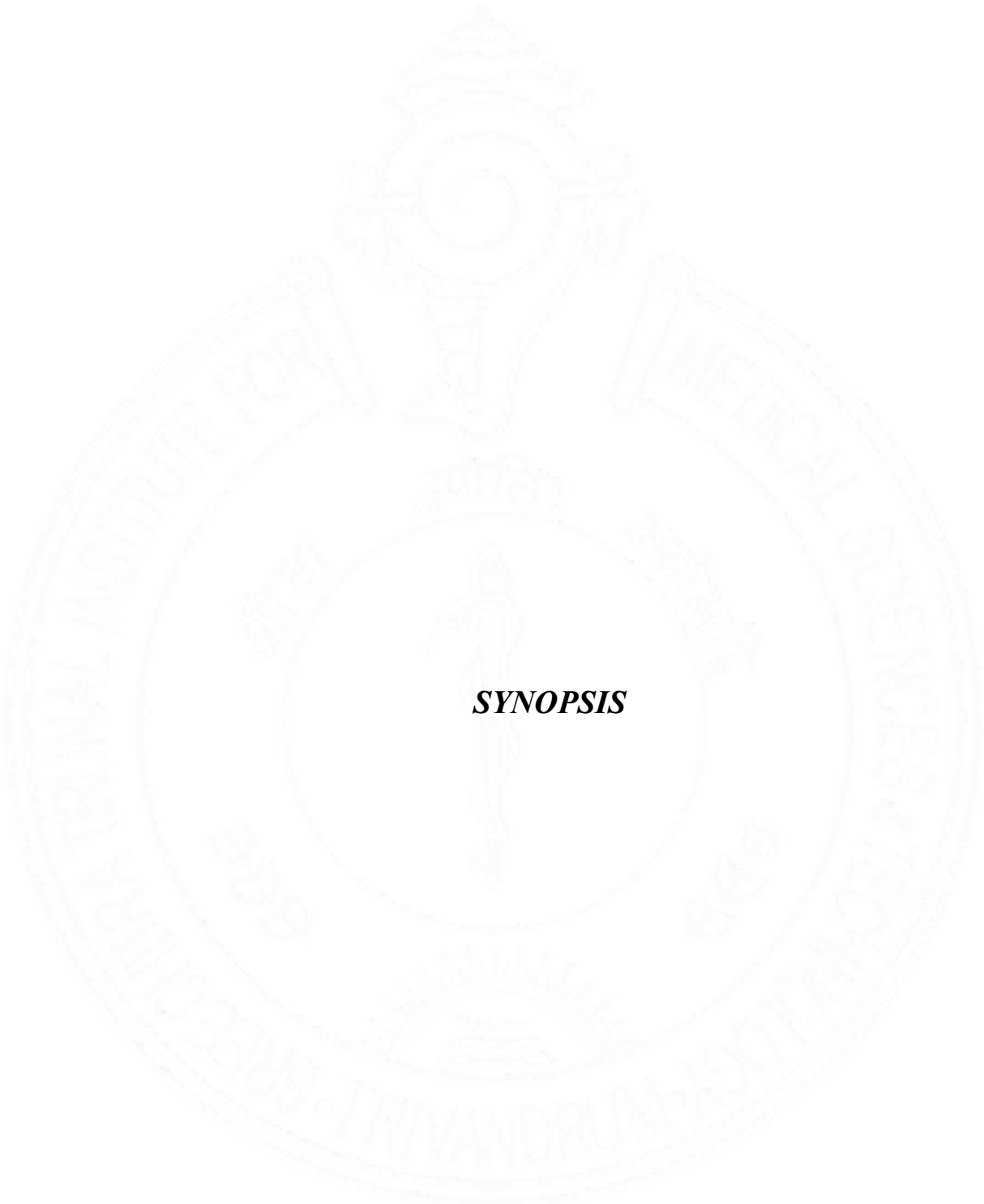

SYNOPSIS

Background: Cardiac fibroblasts derived from mesenchymal cells maintain the integrity of myocardial extracellular matrix. Following cardiac injury, quiescent cardiac fibroblasts transform into myofibroblasts, migrate to the site of injury, resist apoptosis, proliferate, synthesize collagen, and form a thick scar that protects the cardiac wall from rupture. However, excessive collagen deposition by the myofibroblasts results in maladaptive remodelling, manifesting in cardiac fibrosis. The two pathological consequences associated with cardiac fibrosis are a) cardiac wall stiffening that impacts the contractile properties of the heart, and b) conduction abnormalities impact the electrical properties of the heart. Profibrotic factors such as Angiotensin II (Ang II) and transforming growth factor-β1 (TGF-β1) are two major stimuli that regulate myofibroblast activity during cardiac repair. Cardiac wall stiffening is predominantly attributed to Lysyl oxidase (LOX), an enzyme that catalyzes collagen crosslinking. LOX has been implicated in various pathological conditions and contributes to increased left ventricular stiffness and dysfunction.

The conduction of electrical impulses in the ventricular region of the heart is propagated through gap junction proteins called Connexin 43 (Cx43) in electrically excitable cardiomyocytes. Cx43 is upregulated in cardiac fibroblasts post-myocardial injury and facilitates coordinated electrical activity between infarcted and healthy regions of the heart. However, as fibrosis progresses, prolonged coupling via Cx43 in cardiac fibroblast, and excessive collagen deposition together may induce abnormal spontaneous electrical activity, arrhythmias and conduction delay. Given the significance of collagen crosslinking and cardiac conduction in maintaining the

structural and functional integrity of the heart post-injury, exploring the molecular mechanisms that regulate these processes remains a subject of considerable scientific and clinical interest.

Extracellular matrix (ECM)-mediated changes have also been implicated in pathological remodelling of the heart. Periostin (POSTN), a matricellular protein with key roles in tissue remodelling, is upregulated following injury. Importantly, targeted ablation of POSTN-expressing fibroblasts has been shown to mitigate adverse cardiac remodelling. POSTN regulates various functions of activated myofibroblasts. However, whether POSTN regulates LOX and Cx43 expression in myofibroblasts remains unknown.

AIM: Against this backdrop, this study aimed to investigate the relationship between POSTN, LOX, and Cx43 and elucidate the molecular mechanisms by which POSTN regulates LOX and Cx43 expression.

The specific objectives are

1. To delineate the molecular basis of the regulation of LOX expression by Ang II and TGF-β1, focussing on the role of POSTN
2. To delineate the molecular basis of the regulation of Cx43 expression by TGF-β1, focussing on the role of POSTN
3. To correlate the levels of POSTN, LOX and Cx43 in a rat model of myocardial infarction

This thesis is divided into six chapters.

Chapter 1 provides an introduction to the research problem, offering a comprehensive overview on cardiac fibroblast and the function of the ECM. The chapter also briefly

discusses pathological remodelling processes, particularly cardiac fibrosis, and explores the associated pathological consequences, such as stiffening of the cardiac wall and conduction abnormalities. Furthermore, the chapter examines the importance of collagen crosslinking and the role of LOX in this process. The significance of gap junction proteins, with an emphasis on Cx43, has also been addressed. Additionally, the role of POSTN in cardiac fibrosis has been previously reported. Based on this research gap, a research hypothesis was formulated, and the objectives of the study were defined.

Chapter 2 presents a comprehensive review of existing literature related to the identified research problem. It offers an in-depth analysis of previous studies on cardiac fibrosis, highlighting key findings and gaps in the current understanding. This chapter systematically explores the various stages of cardiac fibrosis as well as the underlying molecular signalling pathways that contribute to its progression. Additionally, this section provides a detailed examination of myocardial infarction (MI) and its pathological consequences, outlining how MI serves as a critical factor in the development of cardiac fibrosis and its associated complications. Through this literature review, a contextual foundation was established, demonstrating the need for further investigation into the mechanisms and therapeutic targets relevant to cardiac fibrosis.

Chapter 3 comprises materials and methods used in this study. Cardiac fibroblasts were isolated from young adult male Sprague-Dawley rats using a standard protocol and characterized by immunofluorescence.

Objective 1: The regulatory relationship between POSTN and LOX in the presence of Ang II was established through the following experiments. The expression of POSTN and LOX was initially probed in Ang II-stimulated cardiac fibroblasts for different time points. Ang II-mediated POSTN and LOX expression was confirmed by silencing Angiotensin II receptor (AT1) activity. Further, by real-time PCR and western blotting, LOX mRNA expression, protein expression and activity were probed in POSTN-silenced Ang II-treated cells. The signalling pathway was elucidated by silencing POSTN and probing the activation of ERK1/2 and FAK. Downstream effectors were identified by silencing ERK1/2 and by silencing and inhibiting serum response factor (SRF) activity. Additionally, we also probed how Ang II mediates LOX expression via TGF-β1. To confirm this, expression of POSTN, ERK1/2, SRF and LOX were probed in TGF-β1-silenced cells. Appropriate controls were included in all experiments.

Objective 2: The regulatory relationship between POSTN and Cx43 in response to TGF-β1 was established through the following experiments. Initially, the expression of POSTN and Cx43 was probed in TGF-β1-stimulated cardiac fibroblasts. Further, expression of Cx43 was probed in POSTN-silenced TGF-β1-treated cells by western blot and immunostaining, and functional activity of Cx43 was determined by Lucifer yellow dye transfer assay. The signalling mechanism and downstream effectors in the regulation of Cx43 were elucidated by silencing POSTN, ERK1/2 and SRF.

Objective 3: In vitro results were correlated for the association of these proteins in an in vivo rat model of MI. MI was induced in adult male Wistar rats by ligating left anterior descending coronary artery. Rats subjected to surgical procedures but without

ligation were used as sham. Electrocardiogram (ECG) and echocardiography (ECHO) assessments were conducted to evaluate the cardiac performance and potential pathological remodelling. Histopathology, immunohistochemistry and western blot techniques were used to correlate the protein expression in the infarct zone of MI rats. The statistical significance of experimental results was analysed using a two-way analysis of variance (ANOVA) and Student's t-test. p-value of less than 0.05 was considered statistically significant for all comparisons.

Chapter 4 comprises the results. Cardiac fibroblasts were positive for DDR2, vimentin, and PDGFRα, and negative for endothelial marker von Willebrand factor. Ang II significantly upregulated the expression of both POSTN and LOX. POSTN silencing significantly reduced LOX activity and expression in Ang II-stimulated cardiac fibroblasts. siRNA-mediated silencing of POSTN decreased the Ang II-induced phosphorylation of ERK1/2 MAPK and upregulation of SRF. Moreover, the knockdown of ERK1/2 MAPK reduced Ang II-induced elevation of SRF and LOX expression. In addition, inhibition of SRF activity and SRF knockdown reduced LOX expression. The involvement of Ang II-dependent TGF-β1-mediated regulation of POSTN and LOX was investigated. TGF-β1 silencing in Ang II-stimulated cells abolished POSTN and LOX expression. Moreover, POSTN knockdown in TGF-β1-stimulated cells reduced LOX expression, activation of ERK, and upregulation of SRF. Together, these data suggest that POSTN has an obligate role in Ang II- and TGF-β1-stimulated LOX expression and is via ERK1/2 MAPK-dependent SRF pathway.

TGF-β1 upregulated POSTN and Cx43 expression. POSTN silencing significantly reduced Cx43 activity and expression in TGF-β1-stimulated cardiac fibroblasts.

Further, POSTN silencing decreased the TGF-β1-induced activation of ERK 1/2 MAPK. Moreover, the knockdown of ERK 1/2 MAPK significantly reduced TGF-β1-induced elevation of Cx43 expression. The TGF-β1-stimulated expression of LOX was attenuated on SRF silencing indicating that SRF mediates the transcriptional regulation of Cx43. Collectively, the findings establish that in response to TGF-β1 treatment, POSTN, ERK 1/2 and SRF act in concert to promote the transcriptional upregulation of Cx43.

Induction of MI in rats by coronary artery ligation was confirmed by blanching of the ventricular apex during surgery and variations in ECG such as bradycardia, atrial fibrillation, pathologic Q-wave and changes in echocardiographic recordings**.** ECG variations such as Qr pattern, and sinus tachycardia with ST elevation were observed at 1-week post-MI. Sinus rhythm with a Qr pattern and T-inversion at 4 weeks post-MI indicated pathological remodelling. ECHO recordings exhibited a reduction in wall movement and ejection fraction. Histology at 4 weeks showed LV wall thinning, myocyte damage and excessive collagen deposition. Immunohistochemistry and western blot analysis of the scar tissue showed that POSTN, αSMA, and LOX expression was upregulated within the collagen-rich scar tissue at the infarct zone. Total Cx43 expression in western blot and IHC was reduced within the collagen-rich scar tissue at the infarct zone. However, IHC data indicated that Cx43 staining was localized mainly to areas with high cardiac fibroblast density in the MI group.

Chapter 5 comprises the discussion on how the regulation of LOX and Cx43 by POSTN via activation of ERK1/2 MAPK and SRF in Ang II/ TGF-β1-stimulated

cardiac fibroblasts augment our understanding of the intricate mechanisms underlying collagen crosslinking and conduction abnormalities in the heart.

Chapter 6 comprises the summary and conclusion. The results demonstrated that POSTN plays a pivotal role in regulating LOX and Cx43 expression in Ang II- and TGF-β1-stimulated cardiac fibroblasts. Notably, the finding that POSTN, ERK 1/2 and SRF act in concert to promote the transcriptional upregulation of LOX and Cx43 which have manifestations in cardiac wall stiffening and conduction abnormalities respectively is both novel and significant. While POSTN-mediated regulation of Cx43 expression possibly represents a mechanism by which cardiac fibroblast may directly impact cardiac conduction, POSTN-mediated regulation of cardiac wall stiffening via LOX regulation possibly represents a mechanism by which cardiac fibroblast may indirectly impact cardiac conduction. Thus, it is tempting to postulate that POSTN may be a potential target for mitigating adverse structural and functional alterations in the heart post-MI.

CHAPTER 1

INTRODUCTION

Cardiovascular diseases represent a leading global health burden, with ischemic heart disease and myocardial fibrosis being the major contributors to end-stage heart failure. Despite advances in medicine, there remains a critical need for improved diagnostic tools and therapies for cardiac diseases, including cardiac fibrosis (Benjamin et al., 2019). Cardiac fibrosis is a hallmark of various cardiac pathologies, including myocardial infarction, hypertensive heart disease, diabetic hypertrophic cardiomyopathy, and idiopathic dilated cardiomyopathy, and it is a significant cause of morbidity and mortality. Following myocardial injury or infarction (MI), cardiomyocytes are lost due to ischemia, initiating a wound-healing response that involves the recruitment of inflammatory cells and the activation of tissue-resident cardiac fibroblasts. These fibroblasts play a critical role in remodelling the ECM, a process critical for maintaining cardiac structural integrity.

The ECM is a complex and mechanically stable scaffold composed of collagen, elastic fibers, fibronectin, laminins, proteoglycans, glycosaminoglycans, and glycoproteins. Its composition varies across tissues, but fibrillar collagen type I (85 %) and type III (11 %) predominate in the heart. These collagen fibers, which are regulated by cardiac fibroblasts, are essential for transmitting contractile forces and preserving the structural integrity of the heart (Frantz et al., 2010). The ECM undergoes degradation and resynthesis during myocardial injury to form a cardiac scar that protects the cardiac wall from rupture. This initial ECM deposition serves as a protective mechanism to stabilize injured tissue and maintain cardiac integrity. However, excessive ECM accumulation, particularly that of collagen type I, can become maladaptive and severely impair cardiac function.

Excessive collagen deposition and crosslinking significantly increase matrix stiffness. This stiffening hamper normal cardiac function by impairing the contractility and diastolic relaxation. Additionally, similar ECM remodelling is observed in interstitial fibrosis, which arises in response to pressure overload. In this context, sustained mechanical stress activates fibroblasts, driving excessive collagen synthesis and deposition. Increased stiffness and disorganized ECM remodelling also disrupt the electric coupling between cardiomyocytes, impairing efficient signal conduction. These combined effects exacerbate cardiac dysfunction, highlighting the need to better understand and target ECM remodelling pathways to mitigate fibrosis-related cardiac pathologies. (Travers et al., 2016).

Cardiac fibroblasts are key players in ECM synthesis, deposition, remodelling, and maturation, particularly in the response to structural and biochemical changes following cardiac injury. Upon injury, these cells undergo a phenotypic transition from a quiescent state to an activated myofibroblast phenotype characterized by enhanced proliferation, secretion, and ECM remodelling. This activation is driven by various stimuli, including cytokines, the renin-angiotensin system, growth factors, vasoactive peptides, and mechanosensitive signals, which engage specific receptors and activate downstream signalling pathways. Although significant progress has been made in understanding the mechanisms of fibroblast activation and collagen secretion, further research is needed to elucidate the processes of collagen crosslinking and increased stiffness of the cardiac wall.

Another major consequence of cardiac fibrosis is anisotropic conduction, inhomogeneity, and conduction delay, which can result in reentrant arrhythmias and

conduction blocks. Although fibroblasts were previously considered non-excitable and incapable of generating action potentials, recent studies have shown that they can electrically couple with each other and adjacent cardiomyocytes. In vitro studies have suggested that fibroblasts can propagate electrical signals over distances of up to 300 μm (Ongstad and Kohl, 2016). Emerging evidence indicates that fibroblast-myocyte coupling through gap junction proteins such as connexins and non-gap junction mechanisms can influence myocyte excitability. Such interactions within scar tissue may contribute to arrhythmogenesis (Wang et al., 2023). While connexins in cardiomyocytes have been extensively studied, their role in cardiac fibroblasts, particularly in the context of fibrosis, remains underexplored. Understanding the contribution of fibroblasts to normal and pathological cardiac function is critical for the development of therapeutic strategies for fibrotic heart disease.

Current treatments for cardiac fibrosis, including angiotensin-converting enzyme (ACE) inhibitors, AT1 receptor antagonists, β-blockers, and statins, primarily aim to mitigate excessive ECM deposition in the myocardium. ACE inhibitors and ARBs, such as lisinopril and losartan, have demonstrated benefits in reducing the collagen volume fraction, lowering type 1 pro-collagen levels, and improving left ventricular compliance, but only in patients with severe fibrosis. Eplerenone, which inhibits the aldosterone pathway, has shown significant antifibrotic potential, while sacubitril/valsartan, which combines ARB with neprilysin inhibition, effectively reduces fibrosis biomarkers. Tumor necrosis factor-α (TNF-α) plays a crucial role in promoting cardiac fibrosis; however, clinical trials using TNF-α antagonists, such as etanercept and infliximab, have failed to demonstrate improvements in mortality or

hospitalization rates and, in some cases, increased adverse outcomes. Colchicine, which is recognized for its anti-inflammatory effects, did not significantly reduce infarct size in clinical trials. Peroxisome proliferator-activated receptor-α (PPAR-α) agonists have been shown to reduce myocardial fibrosis and improve cardiac function in preclinical studies; however, excessive PPAR-α expression is associated with adverse cardiac effects, including lipotoxicity and hypertrophy. Similarly, while statins, particularly rosuvastatin, have shown antifibrotic and cardioprotective effects in experimental models, clinical trials have suggested conflicting results regarding their role in chronic heart failure. Although preclinical studies with anti-transforming growth factor-beta (TGF-β) or ALK5 antibodies have demonstrated reductions in fibrosis, these therapies are associated with adverse effects, including left ventricular dilation and increased mortality, highlighting the potential risks of targeting this pathway. Despite these advances, no current therapies have been conclusively shown to reverse fibrosis or improve clinical outcomes (Morfino et al., 2023). Hence, developing effective fibrosis-targeted therapies for myocardial diseases requires a comprehensive understanding of the molecular mechanisms that drive fibrotic remodelling.

Identification of the problem

A better understanding of the role of cardiac fibroblasts and the mechanisms underlying excessive crosslinking of the cardiac wall and abnormal cardiac conduction during fibrosis is essential for devising effective therapeutic strategies to control adverse cardiac fibrosis. Therefore, exploration of the molecular mechanisms involved in their regulation is of considerable scientific interest and clinical importance.

Research gaps

Excessive collagen crosslinking is a hallmark of cardiac fibrosis, contributing significantly to left ventricular (LV) stiffening and impaired diastolic function. This pathological process is largely mediated by Lysyl oxidase (LOX), a copper-dependent amine oxidase that plays a pivotal role in the post-translational modification of collagen. LOX catalyses the oxidative deamination of lysine and hydroxylysine residues in the telopeptide domains of collagen, generating reactive aldehyde groups. These aldehydes undergo spontaneous condensation reactions to form covalent crosslinks between adjacent collagen fibrils, thereby enhancing their tensile strength and resistance to enzymatic degradation (Smith-Mungo and Kagan, 1998). While crosslinking is crucial for maintaining the structural integrity of the extracellular matrix under normal physiological conditions, its dysregulation in pathological states leads to excessive matrix stiffening. In the context of cardiac fibrosis, elevated LOX activity has been implicated in the development of maladaptive myocardial remodelling, exacerbating LV stiffness, and diastolic dysfunction (López et al., 2010). Despite the critical role of LOX in collagen crosslinking, the molecular and cellular mechanisms underlying its regulation remain unexplored. Current evidence suggests that LOX expression and activity may be modulated by fibrogenic stimuli, such as angiotensin II and TGF-β1; however, the precise signalling pathways and transcriptional networks involved are not fully delineated (Laczko and Csiszar, 2020). This knowledge gap underscores the need for further investigation of the regulatory mechanisms of LOX, which could unveil novel therapeutic targets to mitigate

pathological matrix remodelling and improve cardiac outcomes in fibrotic heart disease.

Structural stiffening of the myocardium due to collagen accumulation has an impact on cardiac conduction. Emerging evidence suggests that excessive collagen deposition can lead to non-uniform conduction velocities and re-entrant circuits by creating electrical discontinuities and affecting gap junction functionality. Electrical coupling between ventricular cardiomyocytes and cardiac fibroblasts is mediated by the gap junction protein Connexin 43 (Cx43). Cx43-expressing fibroblasts were observed at 1 week post-MI, with their numbers progressively increasing up to four weeks following MI (Vasquez et al., 2010). Moreover, cardiac fibroblasts directly communicate with cardiomyocytes through Cx43 electrically linking infarcted and non-infarcted regions of the MI heart (Johnson and Camelliti, 2018). However, fibroblast coupling to cardiomyocytes in the long term induces abnormal spontaneous impulse formation (Yue et al., 2011). Despite extensive investigation of the role of Cx43 in cardiomyocytes, the regulatory mechanisms governing Cx43 expression in cardiac fibroblasts during pathological remodelling remain unexplored.

As a prominent member of the matricellular protein family, Periostin (POSTN) interacts with various extracellular components and cell-surface receptors during cardiac development and remodelling (Norris et al., 2009). It is usually present at negligible levels in the adult heart; however, it is highly expressed under pathological conditions and plays a significant role in ECM remodelling by promoting collagen fibrillogenesis (Conway and Molkentin, 2008). POSTN expression is upregulated in response to mechanical stress and pathological stimuli, such as angiotensin II and

TGF-β1, particularly in conditions such as myocardial infarction and cardiac fibrosis. As a secreted ECM protein that associates with areas of fibrosis, POSTN can directly interact with other ECM proteins, such as fibronectin, tenascin-C, collagen, and integrins. Targeted ablation of POSTN-expressing activated fibroblasts have shown to prevents adverse cardiac remodelling in mice (Kaur et al., 2016). However, the precise mechanisms through which POSTN influences collagen crosslinking and contributes to conduction abnormalities remain unclear. This gap underscores the need for further investigation to elucidate its role in collagen crosslinking and conduction abnormalities.

Broad objective

Angiotensin II (Ang II) and TGF-β1 are potent pro-fibrotic factor that has been implicated in the phenotypic transition of quiescent fibroblasts to active myofibroblasts. Moreover, Ang II and TGF-β1 are well known for their stimulatory effects on collagen expression in myofibroblasts (Campbell and Katwa, 1997; Petrov et al., 2002).

Against this background, the present study aimed to investigate the regulatory relationship between POSTN and LOX and its role in cardiac wall stiffening, as well as the interaction between POSTN and Cx43 and its implications for conduction abnormalities in cardiac fibroblasts stimulated with Ang II and TGF-β1.

Specific objectives

The following specific questions were addressed in this study.

1. To delineate the molecular basis of the regulation of LOX expression by Ang II and TGF-β1, focussing on the role of POSTN
2. To delineate the molecular basis of the regulation of Cx43 expression by Ang II and TGF-β1, focussing on the role of POSTN
3. To correlate the levels of POSTN, LOX and Cx43 in a rat model of myocardial infarction

CHAPTER 2

REVIEW OF LITERATURE

2.1 The Heart

The heart, a complex muscular pump, circulates blood through three divisions of the circulatory system: coronary (supplying the heart muscles), pulmonary (connecting the heart and lungs), and systemic (serving various body systems). It is composed of specialized cardiac muscles (myocardium) that maintain contractile rhythm for consistent pumping. The mammalian heart consists of four chambers, two upper atria, and two lower ventricles separated by the atrioventricular septum, along with valves and electrical nodes. Deoxygenated blood flows into the right atrium via the superior and inferior vena cava, and then moves through the tricuspid valve into the right ventricle, which pumps it to the lungs via the pulmonary arteries for oxygenation. Oxygenated blood returns via the pulmonary veins to the left atrium, passes through the mitral valve to the left ventricle, and is then pumped into the aorta for systemic distribution. Autorhythmicity of the heart is regulated by the sinoatrial (SA) node, the primary pacemaker located in the right atrium, and the atrioventricular (AV) node, which transmits excitation waves to Purkinje fibers along the interventricular septum and ventricular walls. A brief delay at the AV node ensures ventricular filling before contraction, and the cardiac cycle, comprising systole (contraction) and diastole (relaxation), produces a heartbeat. The coordinated contraction of the myocardium, along with ECM proteins, is vital for maintaining the rhythmic function of the heart.

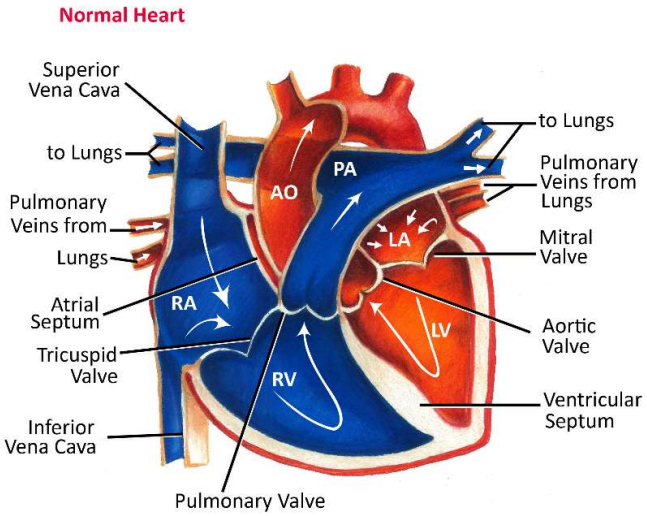

Fig 1: Structure of the heart

In adult mammalian hearts, cardiomyocytes constitute approximately 75% of the myocardial volume and are organized into laminar structures (Camelliti et al., 2005). These cardiomyocyte layers are embedded within an interstitial ECM network predominantly composed of fibrillar collagens. The cardiac ECM serves not only as a structural scaffold but also plays a critical role in the transmission of contractile force across the myocardium. Alongside type I collagen, the most abundant protein in the cardiac ECM, type III collagen, glycoproteins, glycosaminoglycans, and proteoglycans are also present (Silva et al., 2021). This matrix contains a reservoir of latent growth factors and proteases, which can be rapidly activated post-injury to initiate the repair processes. The interstitial ECM supports various cell types, integrating a complex cellular framework that includes myocytes, fibroblasts, endothelial cells, and immune cells, all contributing to the intricate architecture of the myocardium (Lother and Kohl, 2023).

2.2 Cardiac fibroblasts

Prior to the advent of sophisticated techniques, cardiac fibroblasts were largely disregarded in the context of cardiac development, function, and disease pathogenesis. As the primary producers of ECM, cardiac fibroblasts make up approximately 15–30% of the total cells in the heart and have been shown to play important roles in the development of the fetal heart and in maintaining homeostasis in the adult organ (Fernandes et al., 2023). Resident cardiac fibroblasts help preserve ECM integrity by regulating collagen turnover, a process involving continuous synthesis and degradation of ECM proteins (Frangogiannis, 2021). During cardiac development, fibroblasts influence cardiomyocyte proliferation through a fibronectin/β1–integrin-mediated pathway (Ieda et al., 2009). In young adult hearts, cardiac fibroblasts remain largely quiescent with minimal inflammatory or proliferative activity. Myocardial dysfunction was primarily attributed to the loss of cardiomyocytes following injury. However, recent advancements have unveiled the dynamic and multifaceted roles of cardiac fibroblasts in both healthy and diseased hearts. These studies have revealed that the impact of cardiac fibroblasts is highly context-dependent, ranging from beneficial under normal conditions to detrimental in disease states.

Physiological Settings: Under normal conditions, cardiac fibroblasts act as the "architects" of the myocardium. They orchestrate the production and maintenance of the ECM, the intricate scaffolding that provides structural support, and facilitates communication between cells. Fibroblasts also secrete growth factors and cytokines that regulate the function and survival of cardiomyocytes, thereby ensuring optimal

heart function. In addition, fibroblasts contribute to electrical conduction within the heart, ensuring a coordinated heartbeat (Souders et al., 2009).

Pathological Settings: Following cardiac injury, cardiac fibroblasts undergo phenotypic transformation. They are activated, proliferate rapidly, and transform into myofibroblasts. These myofibroblasts produce excessive amounts of ECM components, which leads to **cardiac fibrosis.** While initial fibrosis serves to create a scar and prevent rupture of the damaged heart wall, excessive fibrosis stiffens the myocardium, hindering the ability of cardiomyocytes to contract effectively. This ultimately contributes to heart failure (Frangogiannis, 2021).

2.2.1 Origin of cardiac fibroblasts

The concept of cardiac fibroblasts as a homogeneous cell population has been challenged by recent lineage-tracing studies, which have revealed them to be a complex and heterogeneous group with diverse developmental origins and phenotypic plasticity. During embryogenesis, fibroblasts primarily arise from the proepicardial organ via epithelial-to-mesenchymal transition (EMT), generating epicardial-derived cells (EPDCs) that invade atrial and ventricular tissues and differentiate into a fibroblast phenotype within the myocardium. Notably, mesangioblasts, bone marrow-derived multipotent progenitor cells, have also been implicated in the developmental origin of cardiac fibroblasts (Lajiness and Conway, 2014)

In healthy adult hearts, the fibroblast population is predominantly maintained by the proliferation of resident cardiac fibroblasts. However, following an injury, a dynamic recruitment process is initiated. While earlier studies proposed that cardiac fibroblasts

originate from heterogeneous pools of cells that require transdifferentiation to achieve a fibroblast phenotype, recent reports suggest that resident fibroblasts derived from the epicardium during embryonic development are the major source of disease-relevant activated fibroblasts or myofibroblasts in the adult heart. This is supported by the hypothesis that tissue-resident fibroblasts are geometrically interspersed between cardiomyocytes and possess the requisite molecular programming to facilitate a rapid response after injury (Tallquist and Molkentin, 2017). Similarly, research employing the endothelial/endocardial lineage-tracing mouse model Cdh5-Cre revealed that less than 1% of Cdh5-traced cells differentiate into POSTN-expressing cardiac fibroblasts following MI. Hematopoietic cells have also been implicated in the transdifferentiation into cardiac fibroblasts in response to ischemic injury. However, hematopoietic lineage-tracing studies have indicated that these cells make a minimal contribution to the cardiac fibroblast population. Notably, Tcf21 lineage-traced cardiac fibroblasts completely differentiated into POSTN-expressing myofibroblasts following injury (Fu et al., 2020).

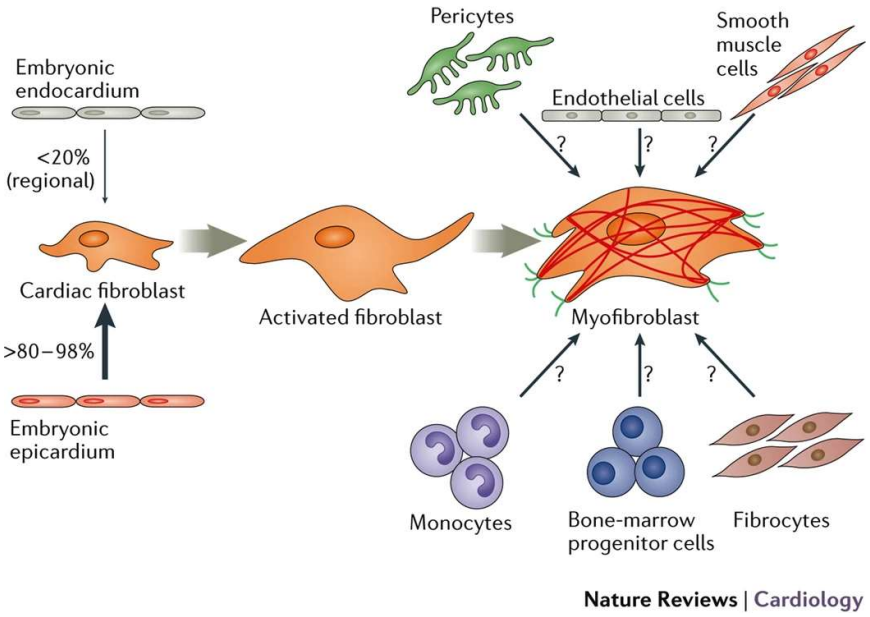

Fig 2: Origin of cardiac fibroblasts (Adapted from Tallquist and Molkentin, 2017)

2.2.2 Morphology and markers of cardiac fibroblasts

Fibroblasts are mesenchymal in origin. They are characterized by flat, spindle-shaped morphology and sheet-like extensions. They lack a defining basement membrane that distinguishes them from the other cell types. Activated fibroblasts demonstrate a prominent Golgi apparatus and an extensive rough endoplasmic reticulum, reflecting their increased biosynthetic activity. Identifying markers for the quiescent and active states of cardiac fibroblasts is of growing interest.

Discoidin Domain Receptor 2 (DDR2), a collagen-specific receptor tyrosine kinase, has emerged as a specific marker for cardiac fibroblasts owing to its robust expression and limited presence in other cell types (Souders et al., 2009). Platelet-derived growth factor receptor α (PDGFRα), a receptor tyrosine kinase, has emerged as a prominent

and specific fibroblast marker. Its precise expression pattern, coupled with its ability to bind platelet-derived growth factor B (PDGF-B), make it a valuable tool for fibroblast characterization and the study of fibroblast-mediated processes in disease contexts. Additionally, the utility of PDGFRα in inducible Cre-loxP systems has enhanced its application in genetic models, providing critical insights into fibroblast biology and pathophysiological mechanisms. (Fu et al., 2020). The transcription factor TCF-21 has been proven successful in elucidating the embryonic origin of resident cardiac fibroblasts from the epicardium (Doppler et al., 2017). These three markers, DDR2, PDGFRα, and TCF-21, collectively constitute the primary tools for identifying cardiac fibroblasts. Additionally, Vimentin and Fibroblast-Specific Protein 1 (FSP1) are widely used markers for cardiac fibroblast labelling, providing additional specificity for fibroblast identification. However, their broad expression limits their exclusivity. Vimentin, an intermediate filament protein, is abundant in fibroblasts but also expressed in endothelial cells. Similarly, FSP1, also known as S100 calcium-binding protein A4 (S100a4), has been extensively used as a fibroblast marker, although evidence suggests that it is commonly associated with immune cells (Moore-Morris et al., 2015).

Myofibroblasts, defined by prominent endoplasmic reticulum and contractile α-SMA filaments are activated cardiac fibroblasts that play a crucial role in scar tissue formation post myocardial injury (Rog-Zielinska et al., 2016). They are characterized by the expression of α-smooth muscle actin (α-SMA) and enhanced contractile activity. Although α-SMA expression is considered the gold standard for myofibroblast identification, Vascular Smooth Muscle Cells (VSMCs) also acquire a

myofibroblast-like phenotype with α-SMA expression and collagen production during injury (Rzucidlo et al., 2007). Hence, distinguishing these cells from vascular smooth muscle cells (VSMCs) poses a challenge.

Recent research suggests that POSTN acts as a specific myofibroblast marker. It is only expressed in adult tissues after injury. It is a secreted matricellular protein involved in the cellular adhesion and organization of collagen. Studies have shown that essentially all myofibroblasts in the injured heart, regardless of their prior lineage, express POSTN, making it a reliable marker for myofibroblast identification (Tallquist and Molkentin, 2017).

Interestingly, fibroblasts exhibit a dynamic expression profile and co-express markers typically associated with different cell types. Activated fibroblasts can upregulate transcription factors such as Wilms Tumor 1 (WT1), T-box 18 (TBX18), and TCF21, while subsets may express the myofibroblast marker α-smooth muscle actin (αSMA). Fibroblast Activation Protein is another marker that is associated with fibroblasts during fibrosis. Pathological activation also induces the expression of specific ECM proteins, such as ED-A fibronectin, which is pro-inflammatory and is associated with impaired cardiac function. The expression patterns of these markers vary depending on the disease model and fibroblast localization within the heart (Fu et al., 2020).

2.2.3 Cardiac Fibroblast Plasticity

Cardiac fibroblasts exhibit remarkable plasticity, transitioning into various cell states under pathological conditions. Myofibroblast differentiation from cardiac fibroblasts

has been extensively demonstrated through multiple lineage-tracing studies. While myofibroblasts were historically considered terminally differentiated and eliminated via apoptosis after infarct scar stabilization, recent lineage-tracing studies have revealed that Tcf21 lineage-traced fibroblasts persist beyond 8 weeks post-MI. These cells transition into matrifibrocytes, characterized by diminished αSMA expression and low levels of myocardial ECM proteins such as collagen I and III, while exhibiting high levels of cartilage ECM proteins, indicative of a partial transcriptomic switch toward a chondrocytic phenotype (Fu et al., 2018). Additionally, under certain conditions, such as injury-induced myocardial calcification, Col1a2 lineage-traced fibroblasts differentiate into osteoblast-like calcium-depositing cells via Runx2-dependent mechanisms (Pillai et al., 2017). Furthermore, Tcf21 lineage-traced fibroblasts have been shown to differentiate into adipocytes in response to a high-fat diet, a process typically suppressed by cardiomyocyte-secreted prokineticin-2 (Qureshi et al., 2017). Fibroblast transdifferentiation into endothelial cells has also been explored, with one study suggesting that ~35% of Col1a2 lineage-traced fibroblasts contribute to neovascularization post-MI by expressing endothelial markers, such as VECAD (Ubil et al., 2014). However, another group, using the same Col1a2-CreERT model and additional lineage-tracing systems, reported that neovascularization primarily results from the proliferation of pre-existing endothelial cells, and not fibroblast transdifferentiation (He et al., 2017). The discrepancies between these findings likely stem from the differences in the markers and antibodies used, underscoring the need for dual lineage-tracing systems to resolve these contradictions.

2.2.4 Factors and pathways that stimulate cardiac fibroblast activation

2.2.4.a Angiotensin II (Ang II)

Ang II is a key effector peptide of the renin–angiotensin–aldosterone system (RAAS) with critical roles in cardiac fibroblasts activation and cardiovascular pathophysiology. It exerts its biological effects primarily through the activation of angiotensin type 1 (AT1R) and type 2 (AT2R) receptors, with AT1R mediating most of its well-known prohypertensive and profibrotic actions. Ang II promotes vasoconstriction, sodium retention, and aldosterone secretion, thereby regulating blood pressure and fluid homeostasis. Additionally, it drives pathological remodelling in cardiovascular tissues by stimulating fibroblast proliferation, myofibroblast differentiation, and extracellular matrix deposition, thereby contributing to fibrosis.

2.2.4.a1 The renin–angiotensin–aldosterone pathway

The renin–angiotensin–aldosterone system is activated in remodelling hearts and plays a crucial role in myofibroblast activation. Stressed cardiomyocytes, immune cells, and fibroblasts produce renin and ACE, generating angiotensin II, which acts as a potent activator of cardiac fibroblasts through the AT1 receptor, thereby promoting fibroblast proliferation, migration, myofibroblast conversion, and ECM protein synthesis (Weber et al., 2013). In contrast, AT2 signalling inhibits these pro-fibrotic effects (Kurisu et al., 2003: 2). Angiotensin II stimulates fibrogenesis via PKC, ERK, and p38 MAPK

pathways, sometimes inducing TGF-β activation (Campbell and Katwa, 1997; Sano et al., 2001). Pro-inflammatory cytokines such as TNF-α enhance AT1 expression and increase fibroblast responsiveness to angiotensin II (Gurantz et al., 2005). Evidence indicates that aldosterone significantly contributes to fibroblast activation after myocardial injury by promoting fibroblast proliferation, migration, and matrix synthesis, partly through MAPK activation (Stockand and Meszaros, 2003). In addition to fibroblasts, aldosterone influences cardiomyocytes (Rickard et al., 2012), macrophages (Rickard et al., 2009), and lymphocytes (C Li et al., 2017), thereby initiating a fibrogenic program.

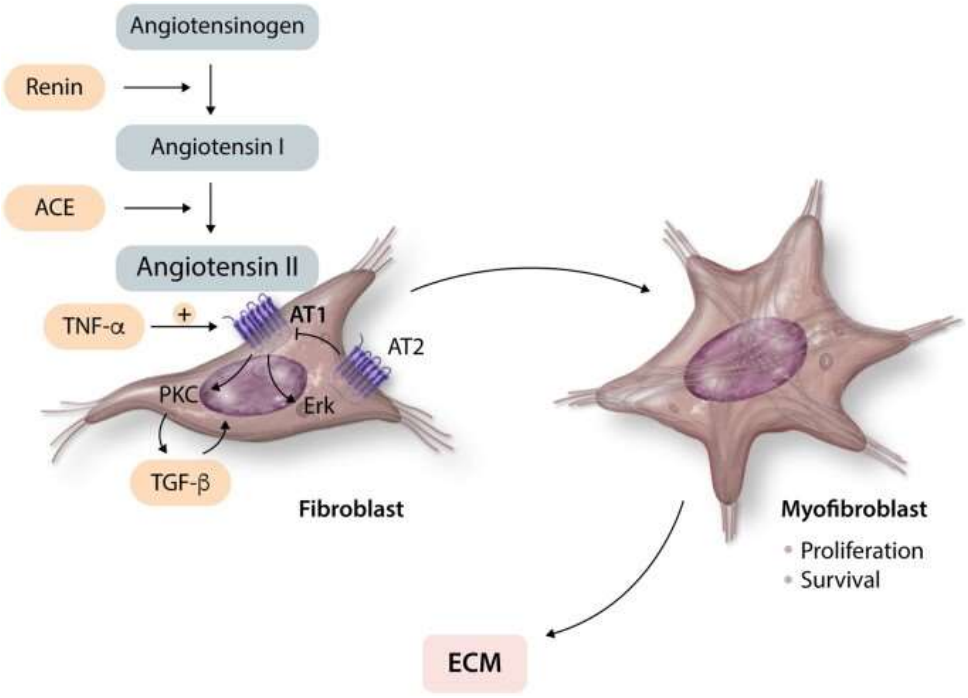

Fig 3: The renin–angiotensin–aldosterone pathway adapted from (Frangogiannis, 2021)

2.2.4.b TGF-β

TGF-β is a pleiotropic cytokine that plays a key role in the regulation of cellular processes, including proliferation, differentiation, apoptosis, and ECM remodelling. The TGF-β family consists of three isoforms in mammals, TGF-β1, TGF-β2, and TGF-β3, which exhibit both overlapping and distinct biological functions. TGF-β1 is the most widely studied isoform, and is critically involved in fibrosis, inflammation, and immune regulation. TGF-β2 plays essential roles in embryonic development, particularly in cardiovascular and skeletal formation, whereas TGF-β3 is implicated in palatal and lung development and may modulate TGF-β1 and TGF-β2 activities. All three isoforms are secreted in a latent form and require activation to bind to their serine/threonine kinase receptors comprising TGF-β receptor I (TβRI) and receptor II (TβRII). In the heart, TGF-β signalling is essential for myofibroblast activation and the production of ECM proteins, such as collagen and fibronectin, contributing to scar formation and tissue stiffening after myocardial injury. Dysregulation of TGF-β signalling has been implicated in pathological fibrosis, hypertrophy, and other cardiovascular diseases, making it a critical target for therapeutic intervention (Kubiczkova et al., 2012)

2.2.4.b1 TGF-β signalling pathway

The mammalian heart contains latent stores of TGF-β, which, upon injury, are rapidly activated to mediate the reparative response. This activation process involves

proteases, matricellular proteins, and integrins. TGF-β drives fibroblast activation, inducing myofibroblast conversion, ECM synthesis, and a matrix-preserving phenotype through increased integrin expression and protease inhibitor induction (Russo et al., 2019). TGF-β signalling begins with its binding to type II and type I receptors, and occurs via Smad-dependent and Smad-independent pathways. Binding to the ALK5 type I receptor activates Smad 3, promoting a matrix-preserving program that is critical for fibroblast activation post-injury (Bujak et al., 2007). Additionally, TGF-β activates Smad-independent pathways such as p38 MAPK, ERK, and TAK1, although the specific role of TGF-β in these signalling pathways has not been fully delineated (Molkentin et al., 2017; Wang et al., 2014).

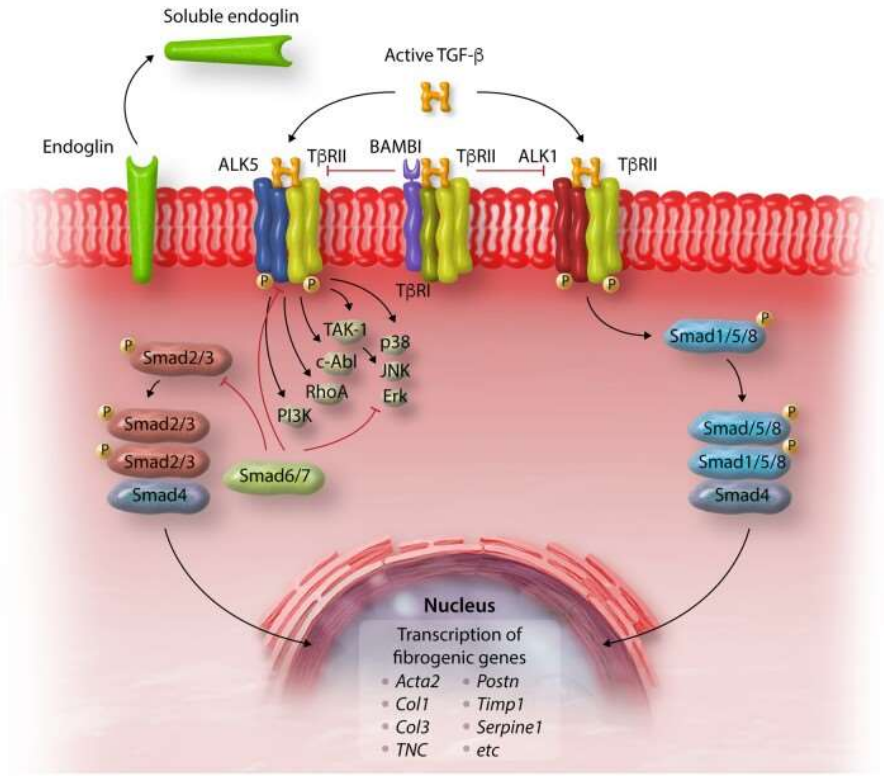

Fig 4: TGF-β signalling pathway adapted from (Frangogiannis, 2021)

2.2.4.c The β-adrenergic pathway

β-adrenergic (β-AR) stimulation activates fibroblasts and contributes to fibrotic cardiac remodeling with isoproterenol (Benjamin et al., 1989) and phenylephrine infusions (Farivar et al., 1995), as well as β2-AR overexpression (Nguyen et al., 2015), inducing significant myocardial fibrosis in vivo. This profibrotic effect may partly reflect fibroblast activation due to cardiomyocyte necrosis, immune cell activation, or fibrogenic mediator release. Direct β-AR stimulation in fibroblasts promotes proliferation via PI-3K (Colombo et al., 2001), p38 MAPK (Molkentin et al., 2017), and EGFR transactivation (Kim et al., 2002) pathways. The specific roles of β1- and β2-AR in fibrosis are not fully understood, although β-AR blockers have reduced fibrosis in some heart failure models, possibly by lowering blood pressure or cardiomyocyte death. Recent evidence suggests that β3-AR signalling in cardiomyocytes may have anti-fibrotic effects (Hermida et al., 2018).

2.2.4.d Mechanosensitive signalling pathways

Cardiac fibroblasts can also be activated by mechanical stress and sensing forces through mechanosensitive receptors, such as integrins, ion channels, G-protein coupled receptors, and growth factor receptors (Barnes et al., 2018). These receptors initiate downstream signalling cascades, including FAK, MAPK, RhoA/ROCK, and PI-3K, which promote matrix transcription and structural remodelling. Mechanosensitive activation likely evolved to safeguard the tissue integrity from mechanical stress. However, in the heart, prolonged mechanical tension can lead to persistent fibroblast activation, excessive collagen deposition, and maladaptive

myocardial remodelling. Additional mechanosensitive pathways, including the MRTF/SRF axis and YAP/TAZ system, detect cytoskeletal changes and regulate the transcription of fibrogenic genes, thus playing a crucial role in fibroblast activation across various cardiac pathologies.

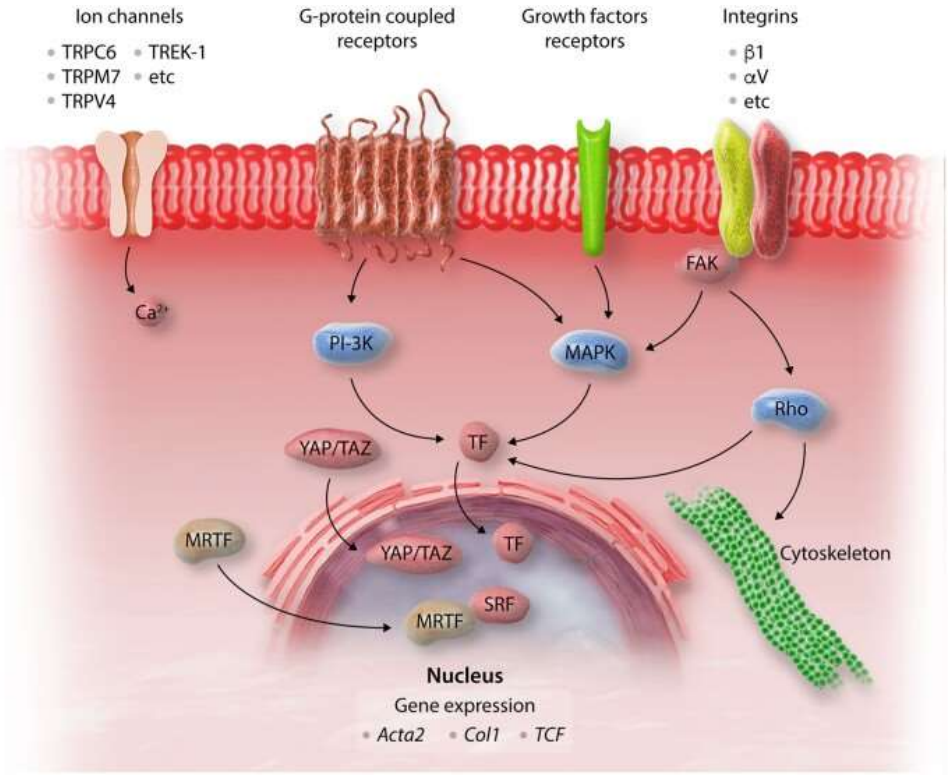

Fig 5: Mechanosensitive signalling pathway adapted from (Frangogiannis, 2021)

2.3 The cardiac ECM

Myocardial cells are embedded in an ECM composed of a network of structural proteins and macromolecules, with fibrillar collagen as the predominant component, representing approximately 85% of the collagen in non-human primates and rodents. Type III and V collagens comprise approximately 10-15% and 5% of the total

collagen, respectively, maintaining a balance within the healthy myocardium. However, in fibrotic tissue, collagen type I increases to nearly 90% of the total collagen content. Cardiac fibroblasts exclusively synthesize fibrillar collagens, ensuring collagen homeostasis through regulated synthesis and degradation (Weber, 1989). The myocardial ECM is organized into three interconnected layers, the epimysium, perimysium, and endomysium, which support cardiac structure and function. The endomysium envelops individual myocytes; the perimysium integrates groups of cardiomyocytes into muscle bundles; and the epimysium encases the entire cardiac tissue. This structured collagen framework transmits forces generated by myocytes to facilitate cardiac contraction and relaxation, while preventing myocyte displacement, maintaining ventricular geometry, and averting deformation and rupture.

Collagen fibers gain high tensile strength through LOX-mediated cross-linking, which prevents sarcomeres from overextending. Typically, collagen fibers resist physical disruption unless ventricular pressures surpass 100 mmHg, with infarcted ventricular rupture occurring at pressures above 600 mmHg. Collagen also forms intercellular connections that link the ECM to intracellular cytoskeletal proteins, enabling myocardial stretching to influence gene expression. In addition to fibrillar collagens, non-fibrillar collagens, such as types IV and VI, are found in the cardiomyocyte basement membrane. Collagen type IV interacts with laminin, perlecan, and entactin to create a sheet-like structure in the basement membrane, whereas collagen type VI connects type IV and type I collagens, anchoring the basal lamina to the interstitial matrix (Weber et al., 1989). Cellular fibronectin is another crucial ECM component that is involved in cardiac development and pathology. It contains binding sites for cell

receptors and pro-fibrotic factors, such as TGF-β, as well as growth factors, such as VEGF, BMP1, and FGF, thus acting as a key regulator of myocardial cell signalling. During wound healing and fibrosis, fibronectin undergoes alternative splicing of the ED-A variant, which promotes fibroblast activation (Valiente-Alandi et al., 2018).

Table 1. Components of the ECM in normal adult hearts

Categories	Components
Glycoproteins	
Collagens	
Fibrillar collagens	Collagen I, III, V
Nonfibrillar collagens	Collagen IV, VI
Matricellular proteins	Thrombospondins, SPARC, Tenascin, Osteopontin, POSTN, CCN
Others	Elastin, Fibronectin, Laminin, Fibrillin
Proteoglycans	
Cell surface proteoglycans	Syndecan, Glypican
ECM proteoglycans	Aggrecan, Perlecan, Nidogen
Small leucine rich proteoglycans	Biglycan, Decorin, Asporin, Fibromodulin, Podocan
Glycosaminoglycans	Hyaluronate, Chondrotin sulfate, Heparin sulfate, Dermatan sulfate
Proteases and inhibitors	MMPs, ADAMS, ADAMTS, TIMP

Table 1 is adapted from (Li et al., 2018)

2.4 The cardiac ECM post-MI

Following MI, cardiomyocytes undergo necrosis and are irreversibly lost because they lack the ability to regenerate, initiating a complex wound-healing process mediated by cardiac fibroblasts. Myocardial repair after infarction progresses through three overlapping phases: inflammation, proliferation, and maturation, each of which is characterized by dynamic molecular and cellular events. During the inflammatory phase, ischemia rapidly activates latent matrix metalloproteinases (MMPs), which are driven by reactive oxygen species (ROS) generated by necrotic cardiomyocytes, fibroblasts, endothelial cells, and infiltrating leukocytes. This activation degrades the ECM and generates matrikines, such as collagen-derived peptides, which stimulate immune cells and fibroblasts, while provisional ECM networks composed of fibrin and fibronectin facilitate leukocyte infiltration and modulate inflammatory signalling via integrin and Toll-like receptor (TLR4) pathways. During the proliferative phase, phagocytes clear ECM fragments, activate anti-inflammatory pathways, and promote deposition of a cell-derived matrix enriched with fibronectin, hyaluronan, and proteoglycans. This matrix supports fibroblast-to-myofibroblast transformation and angiogenesis, aided by matricellular proteins, such as thrombospondins, Osteopontin, SPARC, and POSTN, which localize and modulate growth factor signalling to regulate cellular plasticity and tissue repair. In the maturation phase, myofibroblasts deposit ECM proteins, including collagens I and III, fibronectin, and proteoglycans, with scar maturation marked by increased activity of cross-linking enzymes, such as LOX. This leads to the formation of a dense, cross-linked collagen scar that enhances tensile

strength but also increases passive stiffness, contributing to diastolic dysfunction in the remodelled myocardium (Frangogiannis, 2017).

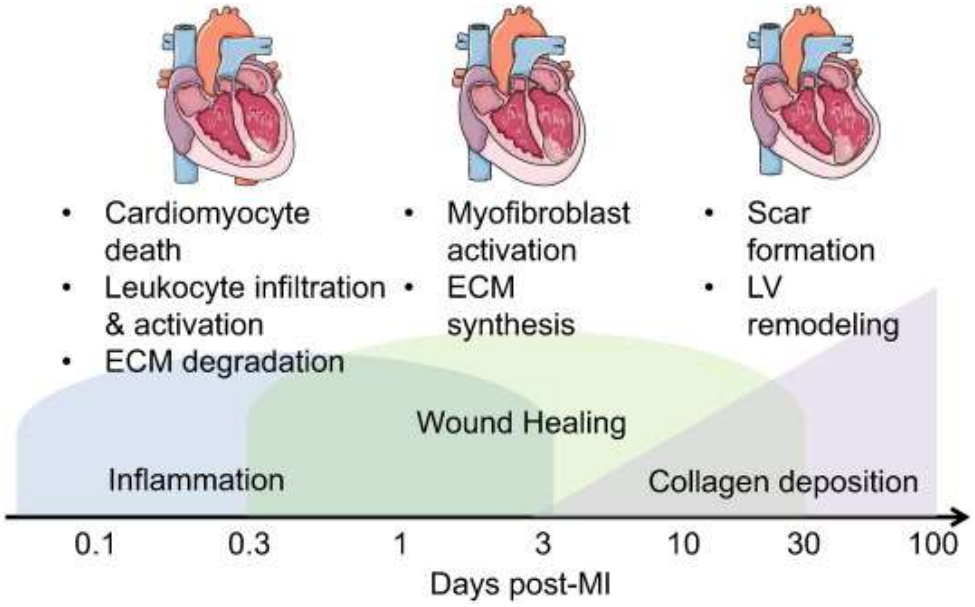

Fig 6: Cardiac ECM post-MI adapted from (Nielsen et al., 2019)

2.5 Cardiac fibrosis

Cardiac fibrosis refers to the excessive deposition of ECM proteins in the cardiac interstitium. This is accompanied by cardiac pathologies. Although cardiac fibrosis often correlates with adverse outcomes, it is not always the primary cause of dysfunction. The adult mammalian heart has limited regenerative capacity and generally heals by forming a scar. Thus, in many cases, cardiac fibrosis is a reparative process in which ECM deposition replaces dead cardiomyocytes to form a collagen-based scar (Frangogiannis, 2019). Although non-contractile, the scar is essential for maintaining structural integrity and preventing mechanical complications such as

cardiac rupture. In other cardiac conditions, fibrosis mainly affects the interstitium and arises gradually, without substantial cardiomyocyte loss. For example, systemic hypertension leads to progressive interstitial and perivascular ECM deposition, which stiffens the myocardium and impairs diastolic function. Aging, obesity, and diabetes also contribute to myocardial interstitial fibrosis, reduce ventricular compliance, and potentially play a role in heart failure with preserved ejection fraction (HFpEF) (Frangogiannis, 2021). Therefore, cardiac fibrosis is not a singular condition amenable to uniform treatment; it is a pathological response that may be either adaptive or maladaptive depending on the underlying pathophysiological context.

Fibrosis has a multifaceted detrimental effect on the myocardium.

- Myocyte atrophy: Excessive collagen deposition results in encapsulation of myocytes in collagen tendrils leading to reduced workload contributing to heart failure progression (Cowling et al., 2019)
- Increased tissue stiffness: The deposition of stiff, cross-linked collagen type I by myofibroblasts hinders diastolic function (González et al., 2019).
- Disrupted electrical conduction: Collagen disrupts connexin-mediated cell-cell communication, promoting arrhythmias (Rodríguez-Sinovas et al., 2021)

2.6 Cardiac wall stiffening

ECM remodelling and excessive collagen crosslinking following cardiac injury play a crucial role in the development of cardiac fibrosis. In cardiac fibrosis, the stiffness of

the fibrotic myocardium is almost 2-10 times stiffer than that of normal healthy myocardium (~8–10 kPa) (Wang et al., 2019). This condition is pathologically characterized by enhanced collagen type I deposition and an altered ratio of collagen type I to type III. The collagen type I/III ratio varies depending on the underlying etiology of fibrosis (Hinderer and Schenke-Layland, 2019). For example, MI models demonstrate a pronounced increase in type I collagen relative to type III collagen. Given that type I collagen fibers are stiffer than type III collagen fibers, their increased deposition results in greater tissue rigidity. As the concentration of rigid, cross-linked type I collagen fibers increases, the passive tissue stiffness correspondingly increases (López et al., 2012). This hardened tissue further perpetuates fibrosis by activating mechanosensitive pathways and releasing latent TGF-β, a key profibrotic factor (Zhu et al., 2022). Cardiac wall stiffening is predominantly attributed to LOX, an enzyme essential for collagen crosslinking that catalyses the accumulation of excessively crosslinked collagen.

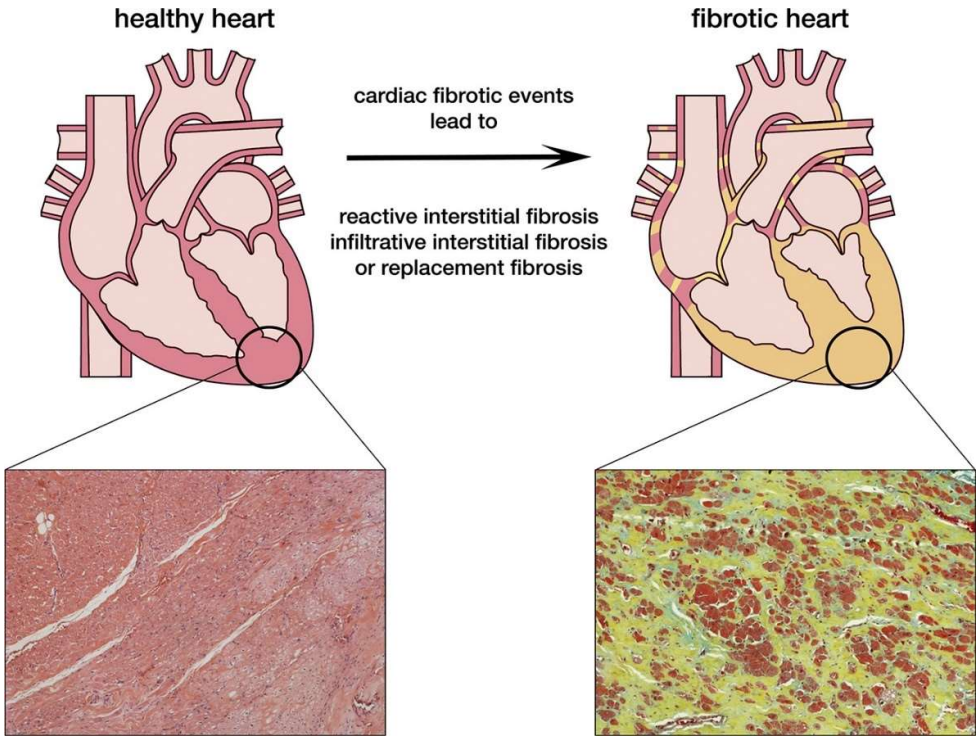

Fig 7: Cardiac wall stiffening due to extensive collagen deposition post-MI adapted from (Hinderer and Schenke-Layland, 2019). Muscle tissue is red and collagen is depicted in yellow.

2.7 LOX

The LOX family consists of copper-dependent enzymes that play a critical role in maintaining and remodeling the ECM. LOX enzymes primarily function by oxidizing the Lysyl and hydroxylysyl residues on the collagen and elastin chains, generating highly reactive aldehydes. These aldehydes then spontaneously react with neighboring amino groups and other aldehydes, forming covalent inter- and intra-chain cross-links that are essential for ECM stability and function (Rodríguez and Martínez-González, 2019). LOX is the primary member of a family of five closely related copper-

dependent enzymes, including LOX, and four LOX-like isoenzymes (LOXLs: LOXL1, LOXL2, LOXL3, and LOXL4) (Molnar et al., 2003). Despite being encoded by distinct genes, these isoenzymes share a highly conserved catalytic domain, although they differ significantly in other regions of their sequence. The expression profiles of LOX and LOXLs vary across tissues, with LOX being the most prevalent isoform in the heart. Most studies of cardiac function refer to this isoenzyme (Molnar et al., 2003). LOX was initially synthesized as a precursor protein of approximately 46 kDa. This precursor undergoes proteolytic processing to form an active enzyme of 32 kDa. Fibronectin plays a crucial role in proteolytic activation by binding to both LOX and BMP1, thereby modulating LOX's catalytic activity (Fogelgren et al., 2005).

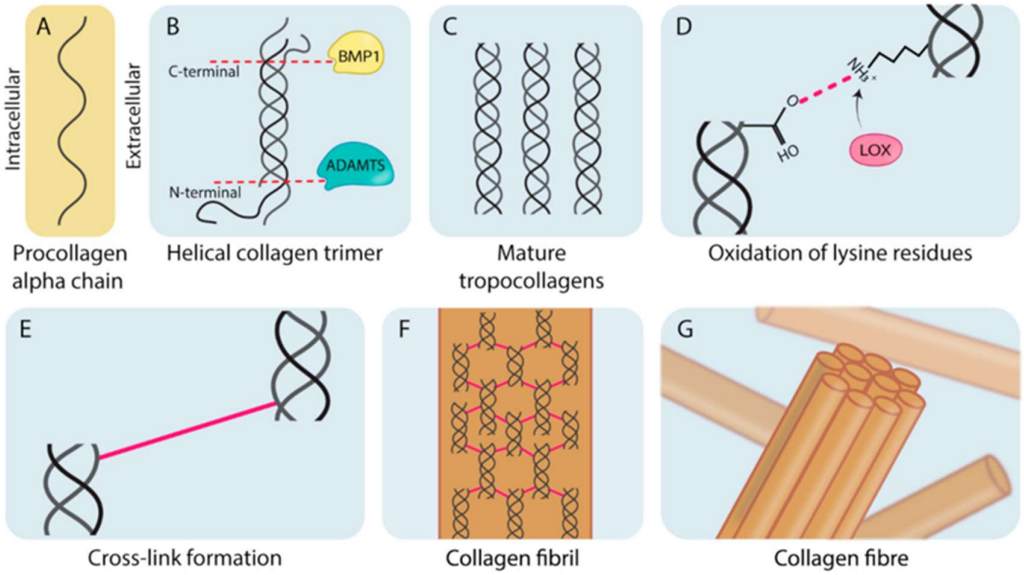

Fig 6: The role of LOX in collagen crosslinking. (A) Pro-collagen alpha-chain subunits are synthesized (B) These alpha chains are assembled into helical collagen trimers in the endoplasmic reticulum and then secreted into the extracellular space where they

undergo post-translational processing by bone morphogenetic protein 1 (BMP1) and a disintegrin and metalloproteinase with thrombospondin motifs (ADAMTS). (C) Cleavage resulted in the formation of mature tropocollagen. (D) LOX family members catalyze oxidative deamination of lysine residues on mature tropocollagen chains. (E) The deaminated residues on adjacent chains spontaneously condense, resulting in crosslinking. (F) Cross-linked tropocollagens organize to form collagen fibrils. (G) Collagen fibrils are further organized and assembled into collagen fibers. This figure is adapted from (Setargew et al., 2021).

2.7.1 LOX in cardiac remodelling

Most pathophysiological stimuli that trigger cardiac fibrosis modulate LOX, which plays a critical role in this process. During the final maturation phase of myocardial remodelling, LOX activity increases, promoting the formation and deposition of stiff collagen fibers (Lerman et al., 1983). The induction of LOX by TGF-β1 in cardiac fibroblasts requires activation of PI3K/Akt, Smad3, and MAPK signalling (Voloshenyuk et al., 2011)**.** Increased LOX mRNA and protein levels in the myocardium of patients with dilated cardiomyopathy and end-stage heart failure have also been linked to elevated TGF-β expression and collagen content (Sivakumar et al., 2008)**.** In patients with hypertension and stage C heart failure, collagen crosslinking rather than total collagen content was associated with elevated filling pressures. The study concluded that an excessive degree of collagen crosslinking contributes to increased left ventricular stiffness, which, in turn, results in higher filling pressures in these patients (López et al., 2012). Osteopontin (OPN), which upregulates LOX, also

contributes to higher collagen crosslinking and LV dysfunction (López et al., 2013), while miRNA-mediated regulation, such as that by miR-19b, inversely affects LOX levels (Beaumont et al., 2017), further highlighting LOX's role in fibrosis. Inhibiting LOX with agents such as BAPN reverses fibrosis and improves function, indicating therapeutic potential (Rosin et al., 2015), while LOX overexpression in transgenic models exacerbates cardiac hypertrophy, inflammation, oxidative stress, and fibroblast-to-myofibroblast transition (Galán et al., 2017). LOXL2 is also key to promoting interstitial fibrosis and heart failure, underscoring its role in fibrosis and cardiac dysfunction (Yang et al., 2016). Conversely, excessive LOX inhibition may impair scar maturation, as seen in AMPKα1 knockout models, where reduced LOX leads to poor scar contractility and LV dilation (Noppe et al., 2014).

2.8 Conduction abnormalities

Cardiac fibrosis plays a significant role in both atrial and ventricular conduction disturbances, by disrupting electrical signal propagation and altering myocyte connectivity. Normally, cardiac action potentials propagate through gap junction channels located primarily at intercalated discs in the mature myocardium, allowing end-to-end and side-to-side myocyte connections. However, cardiac fibrosis induces significant structural and functional changes in the myocardium, which contribute to arrhythmogenic mechanisms. The deposition of collagen disrupts the uniformity of cardiac tissue, creating heterogeneity that slows conduction and increases the risk of conduction block. Collagen bundles can electrically isolate myocytes, forcing electrical signals to navigate zigzag paths through the tissue, thereby altering the

propagation of action potentials. Additionally, fibrosis is associated with the remodelling of gap junctions, which reduces electrical coupling between myocytes and further impairs signal conduction. This remodelling also increases tissue anisotropy, amplifies directional differences in conduction velocity, and promotes slow conduction. The heterogeneous environment created by varying levels of fibrosis facilitates re-entry mechanisms, as the combination of slow and uneven conduction provides a substrate for the initiation and maintenance of arrhythmias. Alterations in connexin expression, particularly Cx43 and Cx40, further complicate the impact of fibrosis on conduction because changes in their distribution and quantity affect both atrial and ventricular conduction. Overall, targeting fibroblasts is a promising strategy for managing conduction abnormalities associated with fibrosis in the heart (Verheule and Schotten, 2021)**.**

2.9 Connexin 43 (Cx43)

Connexins are integral to the gap junction (GJ) channels in the heart. Each connexin subunit is comprised of four transmembrane α-helices, two extracellular domains (E1 and E2), and a cytoplasmic loop. Six connexin subunits assemble to form a hemichannel, with two hemichannel couplings to create a GJ channel, facilitating molecular exchange and ensuring electrical and metabolic connectivity between the cardiomyocytes. The conduction system of the heart relies on three main gap junction proteins: Cx40, Cx43, and Cx45. Cx43, the most abundant protein, is polarized at intercalated disks (IDs) between the atrial and ventricular myocytes.

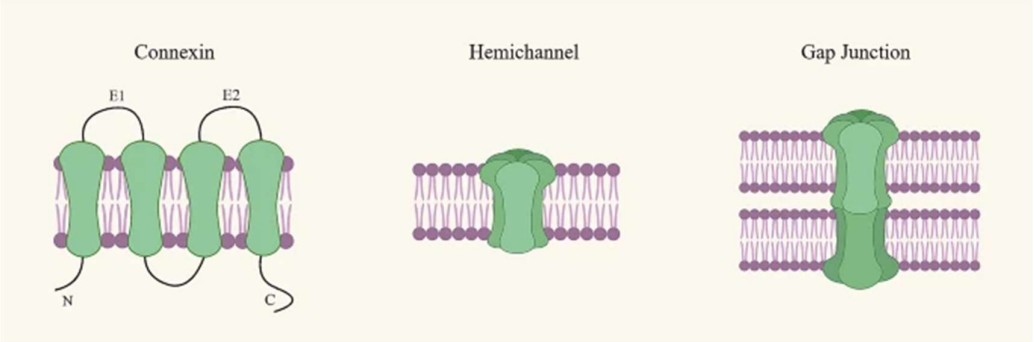

Fig 9: Molecular structure of Cx43. One connexin subunit consists of a cytoplasmic loop and two extracellular segments: E1 and E2. Six connexin subunits form a half-channel and two half-channels constitute a gap junction channel (Yang et al., 2024).

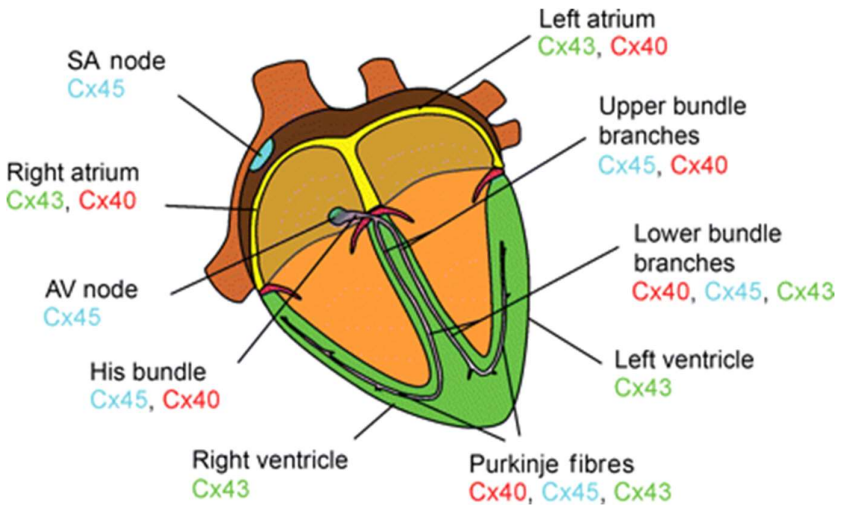

Fig 10: Expression patterns of different connexins in the heart. Adapted from (Desplantez, 2017)

2.9.1 Cx43 in cardiac remodelling

Cx43, the primary gap junction protein in ventricular cardiomyocytes, plays a crucial role in maintaining the electrical conduction homogeneity. Abnormalities in Cx43 expression and localization disrupt conduction velocity and orientation, leading to arrhythmia. Post-MI, Cx43 is frequently downregulated and redistributed from IDs to the lateral sides of cardiomyocytes, termed lateralization, resulting in exacerbation of conduction heterogeneity. Studies have demonstrated that ischemic conditions induce Cx43 dephosphorylation, reduce ID localization, and lateral redistribution, contributing to conduction abnormalities and arrhythmogenesis. In infarct border zones, Cx43 lateralization occurs early during post-MI remodelling, preceding the fibrotic changes. This is often accompanied by compensatory upregulation of Cx40 in endocardial regions, highlighting the dynamic changes in gap junction protein expression during cardiac injury and repair.

Aging and cardiac injury are both associated with the disrupted expression and distribution of Cx43. Following MI, cardiomyocytes exhibit decreased and redistributed Cx43 expression, which contributes to conduction abnormalities. In contrast, cardiac fibroblasts from infarcted hearts display increased Cx43 expression and enhanced coupling with cardiomyocytes, potentially compensating for impaired cardiomyocyte connectivity (Lajiness and Conway, 2012).

Cardiac fibroblasts (CFs) respond to elevated TGF-β levels following injury by upregulating Cx43 expression in vitro, thereby enabling them to influence the electrophysiological properties of co-cultured cardiomyocytes. In vivo mouse models

suggest that increased Cx43 expression in fibroblasts, coupled with decreased Cx43 in cardiomyocytes post-MI, creates an unstable electrical environment prone to arrhythmogenesis. Furthermore, disrupting Cx43-mediated signalling alters paracrine factors, increases TNF-α, and reduces IL-6 levels in fibroblast-cardiomyocyte cocultures.

The reduction in Cx43 expression and its non-uniform distribution on the cardiomyocyte surface contribute to electrical conduction anisotropy within the myocardial tissues. This leads to a decreased conduction velocity and impaired Cx43 functionality. Collectively, these alterations significantly increase the risk of arrhythmogenesis after MI. Therefore, understanding the molecular mechanisms underlying Cx43 remodelling post-MI is essential for developing strategies to mitigate the incidence of post-infarction ventricular arrhythmias.

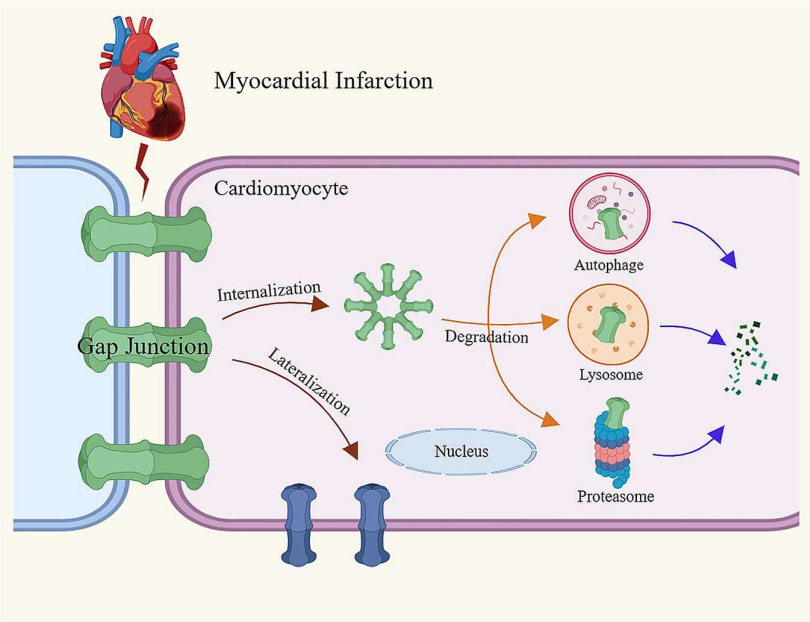

Fig 11: Reduced expression and redistribution of Cx43 in post-infarction cardiac tissue. Adapted from (Yang et al., 2024)

2.10 Matricellular proteins

Matricellular proteins represent a diverse group of extracellular macromolecules that, unlike structural matrix proteins, are not primarily involved in the maintenance of tissue architecture. Instead, they are upregulated in response to injury, where they modulate cell-cell and cell-matrix interactions. Upon release into the extracellular matrix, these proteins interact with growth factors, cytokines, and other bioactive molecules and bind to cell surface receptors, thereby initiating intracellular signalling cascades. In the context of cardiac injury and remodelling, matricellular proteins play pivotal roles in regulating the inflammatory, reparative, and fibrotic pathways (Frangogiannis, 2012).

Key members of this family, including thrombospondins (TSP-1, -2, and -4), tenascins (tenascin-C and -X), secreted protein acidic and rich in cysteine (SPARC), Osteopontin, POSTN, and CCN family members (e.g., CCN1 and CCN2/connective tissue growth factor), are implicated in various cardiac pathologies. These include myocardial infarction, cardiac hypertrophy and fibrosis, aging-associated myocardial remodelling, myocarditis, diabetic cardiomyopathy, and valvular disease (Murphy-Ullrich and Sage, 2014).

Despite their structural diversity, matricellular proteins share several defining characteristics:

a. Multifunctional interactions: Matricellular proteins bind to structural extracellular matrix components, cell surface receptors, cytokines, growth factors, and proteases, serving as integrative hubs for signalling pathways.
b. Regulation of adhesion: Unlike most extracellular matrix proteins that enhance cell adhesion, matricellular proteins often induce cellular "de-adhesion," promoting a state of intermediate adhesion. This state facilitates survival signalling and expression of genes associated with adaptation and repair.
c. Dynamic expression: The expression of matricellular proteins is typically low in normal adult tissues, but is significantly upregulated during development and in response to injury.
d. Role in injury response: In uninjured tissues, the absence of matricellular proteins typically results in minor phenotypic changes. However, their loss profoundly affects tissue repair and remodelling following injury, leading to a spectrum of functional alterations.

2.11 Periostin (POSTN)

POSTN, initially identified as a protein secreted by murine osteoblasts and originally named osteoblast-specific factor-2 (OSF-2), was first proposed to have a role in bone metabolism. To avoid confusion with a transcription factor bearing the same designation, its name was revised to “Periostin,” reflecting its high expression levels in the periosteum and periodontal ligament (Horiuchi et al., 1999). In recent years, increasing research on POSTN has revealed its involvement in diverse pathophysiological processes, including neoplasia, tissue repair, and cardiac injury.

Functional studies have established POSTN as a matricellular protein, characterized by its upregulation in injured and remodeled tissues. Rather than serving a structural role, POSTN interacts with extracellular matrix proteins and modulates cellular phenotypes and functions through integrin-mediated signalling (Norris et al., 2008).

2.11.1 Structure of POSTN

POSTN is structurally homologous to the insect protein fasciclin-1, which plays a role in axon guidance and cell adhesion. The POSTN protein comprises a signal sequence, four fasciclin-1-like repeat domains, an N-terminal cysteine-rich region, and a heparin-binding domain at the C-terminal end. Although the precise functions of these domains remain unclear, POSTN is part of a family of four mammalian genes, characterized by the presence of fasciclin domains. Among these, TGF-β-induced gene-human clone 3 (βigH3) encodes a secreted protein that shares 49% amino acid homology with POSTN, whereas stabilin-1 and stabilin-2 are transmembrane molecules that exhibit greater sequence divergence and are broadly expressed across various tissues (Duchamp de Lageneste and Colnot, 2019).

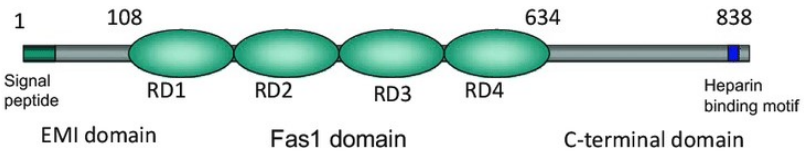

Fig 12: POSTN structure adapted from (Duchamp de Lageneste and Colnot, 2019)

2.11.2 POSTN expression in cardiac tissue

Under normal conditions, POSTN expression is typically negligible in most adult tissues. However, tissue injury, repair, and remodelling processes are associated with a significant upregulation of POSTN expression. This increase was largely attributed to the localized activation of TGF-β and Ang II. In vitro studies have demonstrated that TGF-β and Ang II are potent stimulators of POSTN expression in various cell types. Notably, Ang II has been shown to enhance POSTN expression in smooth muscle cells via a phosphoinositide 3-kinase (PI3K)-dependent mechanism (Li et al., 2006). Additionally, Ang II promotes POSTN expression in fibroblasts by activating the Erk1/2/TGF-β1 and Ras/p38 MAPK/CREB signalling pathways (Li et al., 2011).

POSTN expression in the normal myocardium is high during the neonatal period but subsequently falls to low levels. POSTN may play an important role in the maturation and differentiation of fibroblasts in the developing neonatal heart because of its known function in fibroblast differentiation and its high expression levels in the neonatal myocardium. Studies using POSTN-null mice have provided significant insights into the in vivo role of POSTN. After 3–4 weeks of age, POSTN-knockout mice exhibited notable growth retardation and remained consistently smaller than their wild-type littermates. Approximately 15% of the PostnlacZ/lacZ mutants died within 2–3 weeks after birth. While male PostnlacZ/lacZ mice are fertile, they are unable to conceive (Periostin Null Mice Exhibit Dwarfism, Incisor Enamel Defects, and an Early-Onset Periodontal Disease-Like Phenotype: Molecular and Cellular Biology: Vol 25, No 24, n.d.). Subsequent investigations revealed that early mortality in a subset of POSTN-

null animals can be attributed to cardiac defects. These findings underscore the essential requirement of POSTN in the development stages of conditional knockout models for studying the cardiac-specific effects of POSTN, as opposed to complete knockout models.

Recent research on POSTN conditional knockouts has yielded promising insights. A study investigating the timeline of POSTN expression following MI revealed that POSTN gene and protein levels peaked between days 2 and 7 post-MI, with the highest expression observed on day 7 post-MI. This finding highlights the critical timeframe for POSTN-targeted therapies to enhance cardiac repair while maintaining wall stability (Gil et al., 2022). Additionally, targeted ablation of POSTN-expressing activated fibroblasts has been shown to prevent adverse cardiac remodelling in mice (Kaur et al., 2016). Snider et al. demonstrated that POSTN is essential for maturation and ECM stabilization of non-cardiomyocyte lineages in the heart (Snider et al., 2008). Another study reported that age-related increases in POSTN expression in cardiac fibroblasts contributed to cardiomyocyte senescence (Li et al., 2014). Furthermore, POSTN has been identified as a key modulator of chronic cardiac remodelling following MI, underscoring its multifaceted role in cardiac health and disease (Minicucci et al., 2013).

2.11.3 POSTN and Collagen Crosslinking

POSTN-mediated collagen synthesis and crosslinking constitute a multistep process critical for maintaining the mechanical integrity of collagen-rich connective tissues. POSTN plays a critical role in modulating the biomechanical properties of connective

tissues by directly interacting with matrix proteins, such as type I and type V collagen, fibronectin, and tenascin-C, thereby regulating collagen fibril assembly. In POSTN-null mice, significant reductions in collagen fibril diameter within the dermis have been observed, accompanied by diminished levels of collagen cross-linking (Norris et al., 2007)**.** Notably, POSTN facilitates fibroblast migration by interacting with integrin αvβ3 and triggering downstream Akt and FAK phosphorylation, which supports tissue repair through the secretion of type I collagen by fibroblasts (Kii and Ito, 2017)**.** During the early phases, POSTN enhances collagen production; however, after the removal of its C-terminal domain, its function shifts to promoting collagen cross-linking. The EMI domain of POSTN is essential for its multimerization, which facilitates the formation of fibronectin and tenascin-C network, supporting collagen cross-linking (Qiao et al., 2024). This process is catalyzed by the active form of LOX, which is produced from its precursor by bone morphogenetic protein-1 (BMP-1). Fibronectin alignment is a key determinant of collagen crosslinking efficiency, implicating the POSTN-BMP-1-LOX axis as a fundamental pathway that regulates the mechanochemical properties of the collagen matrix (Maruhashi et al., 2010). Collectively, these findings underscore POSTN's central role of POSTN in collagen crosslinking.

2.11.4 POSTN as an emerging therapeutic strategy

POSTN, a matricellular protein, has emerged as a significant therapeutic target in various fibrotic and oncologic conditions owing to its multifaceted role in ECM remodelling, fibrosis, and tumor progression. Several strategies have been developed

to inhibit the pathological functions of POSTN, focusing on its interactions with integrins and downstream signalling pathways.

Blocking the POSTN function using antibodies, peptides, and aptamers has shown promise in preclinical models. Integrin blockade peptides effectively reduce fibrosis-related gene expression in vitro, while anti-POSTN polyclonal antibodies attenuate renal fibrosis by modulating TGF-β signalling and the inflammatory and apoptotic pathways (Hwang et al., 2017). Anti-POSTN peptides have been demonstrated to reverse chemoresistance, such as doxorubicin resistance, in breast cancer cells. These peptides target specific POSTN-integrin interactions, particularly in the αvβ3 integrin-binding region (Nakazawa et al., 2018).

Recent advancements include the development of POSTN-binding aptamers with improved affinity and specificity compared to those of conventional antibodies or small molecules. For example, intraperitoneal administration of these aptamers effectively inhibits peritoneal fibrosis and reduces profibrotic protein production and blood urea nitrogen levels in diabetic mice. Other innovative approaches include benzyl-d(U)TP-modified DNA aptamers that target POSTN in breast cancer. These therapies effectively suppress primary tumor growth, metastatic lesions, and bone degradation, thereby improving the survival rates in preclinical cancer models. (Nam et al., 2017). These findings highlight the potential of aptamers as a novel therapeutic approach for POSTN-mediated pathologies.

Anthocyanidins have also demonstrated efficacy in targeting POSTN-mediated epithelial-to-mesenchymal transition (EMT). In vitro studies have shown that

anthocyanidins reduce POSTN, fibronectin, and Snail expression induced by TGF-β, and inhibit Smad2 and Akt phosphorylation.

In cancer therapy, POSTN-specific antibodies have been engineered to target cancer. For instance, PN21-Ab, a functional blocking antibody, significantly suppresses tumor relapse in triple-negative breast cancer (TNBC) xenografts when combined with chemotherapy. This combination therapy reversed PTX-induced mesenchymal tumor cell proliferation and invasive phenotypes, demonstrating the potential of the antibody to overcome chemoresistance (Nakazawa et al., 2018). Other innovative approaches include two monoclonal antibodies, MPB4B1 and MPC5B4, which inhibit the POSTN-induced migration of human endothelial colony-forming cells in aggressive breast cancer (Field et al., 2016).

Overall, targeting POSTN using diverse therapeutic strategies offers a promising approach. Although preclinical data are encouraging, further in vivo and clinical studies are essential to establish the translational potential of these approaches.

CHAPTER 3

MATERIALS AND METHODS

CONSTITUENTS OF MEDIUM, BUFFERS AND REAGENTS

3.1 REAGENTS USED FOR CARDIAC FIBROBLAST ISOLATION AND CULTURE

3.1.1 Dissociation medium for cardiac fibroblast isolation (100ml)

Sodium chloride (0.68 g), HEPES (0.555 g), sodium dihydrogen phosphate (0.140 g), glucose (0.100 g), potassium chloride (0.04 g), magnesium sulfate (0.02 g), BSA (100 mg), and 10 µL of 1 mM CaCl2 were dissolved in 100 ml sterile double-distilled (DD) Milli-Q water. pH was adjusted to 7.4. An enzyme cocktail containing trypsin (70 mg), pancreatin (2 mg), and collagenase type IA (40 mg) (Sigma) was dissolved and syringe-filtered through a 0.22-micron filter. Penicillin (50 µg/ml), gentamycin (40 µg/ml) and amphotericin B (1mg/ml) were added at the time of usage. All the chemicals used in the dissociation medium were purchased from Sigma-Aldrich (USA).

3.1.2 Phosphate-buffered saline (PBS) (pH 7.4)

Sodium chloride (0.8 g), potassium chloride (0.02 g), disodium hydrogen phosphate (0.186 g), and potassium dihydrogen phosphate (0.02 g) were dissolved in 100 ml of deionized water and autoclaved before use.

3.1.3 Fibroblast growth medium (pH 7.4)

Cardiac fibroblasts were cultured in M199 with Earle's salts (Sigma) containing fetal bovine serum (FBS) (10%) (Thermofischer, USA), benzylpenicillin (50U/ml) and gentamycin (0.04 mg/ml)

3.1.4 Trypsin-EDTA solution (pH 7.4)

25 mg of trypsin (Sigma) and 3.8 mg of EDTA were dissolved in 10 ml PBS

3.2 REAGENTS USED FOR WESTERN BLOTTING

3.2.1 SDS gel-loading buffer/ Laemmli buffer (6X)

0.9g of SDS was added to 3.75 ml of stacking buffer (pH 6.8) and kept at 37°C overnight. To this solution, 5 ml of glycerol, 0.9 ml of β- mercaptoethanol and bromophenol blue (0.03%) were added. 6X stock was diluted to 1X before use.

3.2.2 Cell Lysis Buffer (1X)

Cell lysis buffer (Cell signalling Technology) (10X) was diluted with deionized water to get a 1X solution.

3.2.3 30% Acrylamide solution

29.2 g of acrylamide and 0.8 g of N, N'-Methylene bis-acrylamide (Sigma) were dissolved in 60 ml deionized water and kept at 37°C overnight. The total volume was made up to 100 ml on the next day.

3.2.4 Resolving gel buffer

An 18.165 g trizma base (Sigma) was dissolved in 70 ml of deionized water, and the pH was adjusted to 8.8 using concentrated HCl. The total volume was then made up to 100 ml.

3.2.5 Stacking gel buffer

An 18.165 g trizma base was dissolved in 70 ml of deionized water, and the pH was adjusted to 6.8 using concentrated HCl. The total volume is then made up to 100 ml.

3.2.6 Electrode buffer/ running buffer (pH 8.3)

Trizma base (1.5135 g), glycine (7.2 g), and SDS (0.5 g) were dissolved in 500 ml of deionized water.

3.2.7 Towbin's buffer (Transfer buffer)

1.5135 g of Trizma base, 7.2 g of glycine and 100 ml of methanol were mixed and made up to 500 ml with deionized water.

3.2.8 Tris-buffered saline (10X, pH 7.6)

24.2 g of Tris base and 80 g of sodium chloride were dissolved in water. After adjusting the pH to 7.4 using conc. HCl, and the solution was made up to 1 L with deionized water.

3.2.9 Tris-buffered saline with Tween-20 (TBST) [1X]

1X TBST was prepared by adding 0.1% Tween-20 to 10X TBS.

3.2.10 Blocking solution

5% (w/v) skim milk or BSA (Sigma) was dissolved in 1X TBST containing 0.1% Tween-20.

3.2.11 Resolving Gel for SDS – PAGE (10-12% depending upon the molecular weight of proteins to be resolved)

10 ml of resolving gel contains 3.3 ml of deionized water, 4 ml of 30% acrylamide, 2.5 ml of 1.5 M Tris (pH 8.8), 0.1 ml of 10% SDS, 0.1 ml of 10% ammonium persulfate and 4 µl TEMED.

3.2.12 Stacking gel for SDS – PAGE (5%)

0.670 ml of 30% acrylamide, 0.500 ml of 1 M Tris (pH 6.8), 0.04 ml of 10% SDS, 0.04 ml of 10% ammonium persulfate and 4 µl TEMED were added to 2.7 ml of deionized water.

3.3 REAGENTS USED FOR IMMUNOHISTOCHEMISTRY (IHC)

3.3.1 Paraformaldehyde (4%)

4 g paraformaldehyde was dissolved in 100 ml PBS at 60ºC. The pH was adjusted to 7.4 using 11N NaOH

3.3.2 10X Tris-EDTA buffer (Antigen retrieval buffer, pH 9)

To prepare the solution, 12.1 g of Tris base and 3.7 g of EDTA were dissolved in 1000 ml of distilled water. The pH of the solution was adjusted to 9. Subsequently, 5 ml of Tween 20 was added to the solution and mixed thoroughly. Prior to use, the solution was diluted to 1:10 with distilled water.

3.3.3 10X Wash buffer

The solution was prepared by dissolving 61 g Tris base and 90 g sodium chloride in 1000 ml of distilled water. The pH of the solution was adjusted to 8.4. Next, 5 mL

Tween 20 was added and mixed thoroughly. Before use, the solution was diluted 1:10 with distilled water.

3.3.4 Schott's solution for bluing

3.5 g of sodium bicarbonate and 20 g of magnesium sulphate were dissolved in 100 ml of tap water.

3.3.5 DAB substrate solution

DAB substrate was procured from (Thermo Fischer Scientific). 900 µl of solution A and 100 µl of solution B were mixed well

METHODS

3.4 Isolation of cardiac fibroblasts

Cardiac fibroblasts were isolated from young adult male Sprague-Dawley rats (1-3 months old), following standardized protocols (Sahadevan and Allen, 2022; Shivakumar and Kumaran, 2001). Animal handling and experimental procedures were conducted in accordance with Institutional Animal Ethics Committee approval (SCT/IAEC-298/JANUARY/2019/99). After euthanasia using intraperitoneal thiopentone sodium (5-10 mg/kg), the hearts were excised, atria were removed, and the ventricles were used for fibroblast isolation. Ventricular tissue was washed in PBS, minced into 1-3 mm pieces, and digested in a dissociation medium containing Collagenase type IA (0.5 mg/ml), Trypsin (0.7 mg/ml), and Pancreatin (0.020 mg/ml) with gentle shaking at 37°C. The supernatants were centrifuged at 1500 rpm for 10 minutes, and the resulting cell pellets were pooled, resuspended in M199 medium with

10% fetal bovine serum (FBS), and seeded onto one 60 mm culture dish. As cardiac fibroblasts exhibit preferential adherence to culture plates within 2.5 hours, the cells were collected after 2.5 hours following a brief wash post-initial plating to remove non-adherent cells. The adhered cells were cultured in M199 medium supplemented with 10% FBS and 1% antibiotic-antimycotic solution at 37°C in a humidified CO2 incubator (95% air, 5% CO2). After 24 hours, the cells were washed and cultured in M199 medium containing 10% FBS, at 37°C in a CO2 incubator.

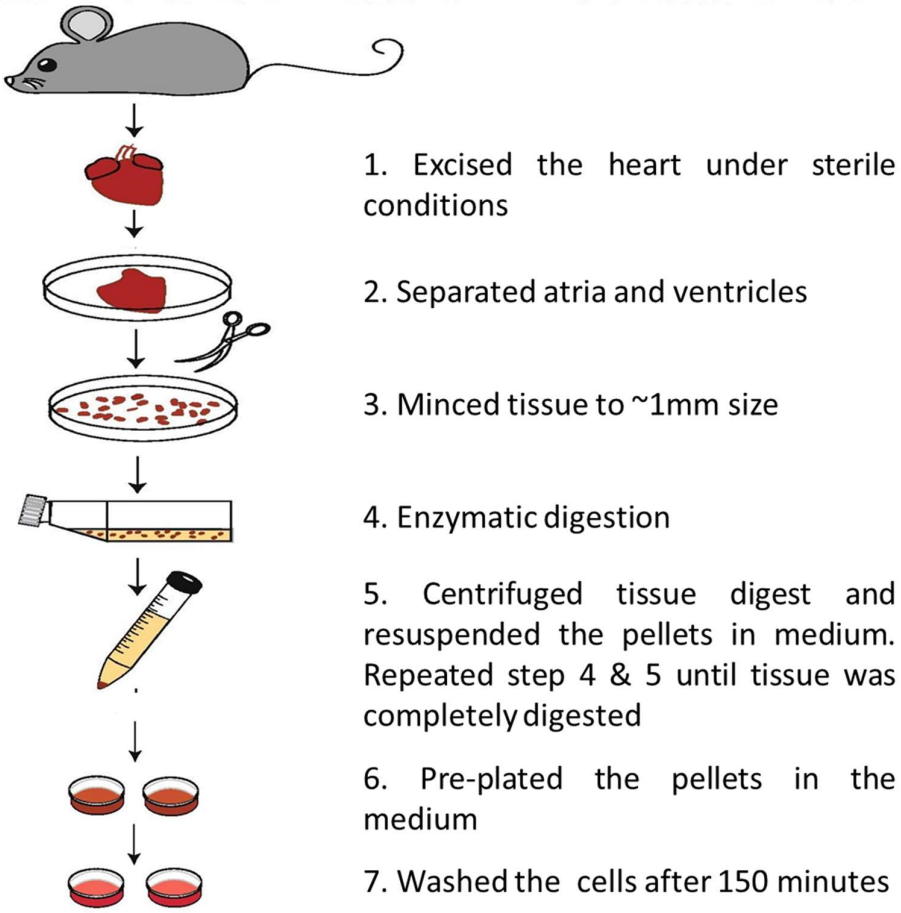

Fig 13: Schematic representation of the isolation of cardiac fibroblasts (Adapted from (Sahadevan and Allen, 2022)

3.5 Subculture and maintenance of cardiac fibroblasts

Cardiac fibroblasts were subcultured upon reaching confluency. The culture medium was aspirated, and the cells were washed with PBS. Trypsin-EDTA solution was added to detach the cells, which were subsequently neutralized with M199 containing 10% FBS. The detached cells were harvested by centrifugation and resuspended in fresh M199-FBS medium. Finally, the cells were seeded onto new culture dishes at a split ratio of 1:3 to ensure their continued growth and proliferation for further experiments.

3.6 Characterization of cardiac fibroblasts

The cells were characterized using comprehensive morphological and immunocytochemical analyses. Cells were examined under an inverted phase-contrast microscope to assess their characteristic spindle-shaped morphology, which is a hallmark of cardiac fibroblasts. Immunocytochemical staining for the specific fibroblast markers vimentin, DDR2, PDGRFα and Von Willebrand Factor (vWF) was conducted on cells at passage 2. After fixation with 4% paraformaldehyde for 20 minutes, the cells were washed thrice in PBS. Cells for vimentin staining were permeabilized using 0.25% Triton X100. All cells were subsequently blocked with 1% bovine serum albumin (BSA) for 30 minutes to prevent nonspecific binding and incubated with primary antibodies at room temperature for 1 hour. The primary antibodies used were DDR2 (Bioss) at 1:500 dilution, PDGFRα (CST) at 1:1000 dilution, vimentin (Abcam) at 1:1000 dilution, and Von Willebrand Factor (Abcam) at 1:1000 dilution. This was followed by incubation with anti-mouse or anti-rabbit Alexa Fluor 488-conjugated secondary antibodies (Abcam) for 1 hour at room temperature.

After thorough washing to remove unbound antibodies, nuclei were counterstained with Hoechst 33258 to visualize cell nuclei. Finally, the slides were mounted using Fluoromount (Abcam) and visualized using a fluorescence microscope (ZEISS AXIO Imager.A2.).

3.7 Effect of Ang II on POSTN and LOX

3.7.1 Expression of POSTN and LOX in Ang II-stimulated cardiac fibroblasts at different time points

Cardiac fibroblasts at passage 2 were treated with Ang II (Sigma) (1μM) for 6,12, 24, and 48 hours. POSTN and LOX expression was evaluated by western blot analysis. Untreated cells were used as controls.

3.7.2 Expression of POSTN and LOX in response to blocking Ang II receptor activity

Subconfluent cardiac fibroblasts (P2) were pretreated with 10 μM candesartan (an AT1 receptor antagonist) (Sigma) for 1 hour prior to incubation with 1μM Ang II for 24 hour in the experimental group. POSTN and LOX expression was evaluated by western blot analysis. Untreated cells were used as controls.

3.8 Study design/experiments to elucidate molecular mechanisms involved in the regulation of LOX

To elucidate the POSTN-mediated molecular mechanisms involved in the regulation of LOX in cardiac fibroblasts, the following experiments were performed:

- , mRNA and protein expression levels of LOX were probed in POSTN-silenced Ang II-treated cells.
- Furthermore, LOX activity was determined in POSTN-silenced Ang II-treated cells.
- To identify the pathway downstream of POSTN, ERK1/2 was probed in POSTN-silenced Ang II-treated cells.
- To further confirm the involvement of ERK1/2 pathway, ERK1/2 was silenced and LOX expression was probed.
- To identify the transcription factor involved in the regulation of LOX, the expression of SRF was probed in POSTN-silenced-and ERK1/2-silenced Ang II-treated cells.
- This was further confirmed by probing the expression of LOX in SRF-silenced Ang II-treated cells and SRF inhibition using CCG-1423. Appropriate controls were used for all experiments.
- Additionally, we investigated how POSTN regulates LOX in TGF-β1-stimulated cardiac fibroblasts. Furthermore, we investigated whether Ang II mediates LOX expression via TGF-β1.
- To confirm this, the expression of POSTN, ERK1/2, SRF, and LOX was probed in TGF-β1-silenced, Ang II-treated cells. This methodology is described in detail in the following sections.

3.9 Gene silencing

Subconfluent cultures of cardiac fibroblasts at passage 2 were transiently transfected with POSTN (50nM), ERK (100nM), SRF (25nM) and TGF-β1 (50nM) siRNA (Eurogentec) in Opti-MEM medium with lipofectamine 2000 (8 µl) (Thermo Fischer Scientific) as the transfection reagent according to the manufacturer's protocol. Control cells were treated with scrambled siRNAs at equimolar concentrations. After 24 hours of serum deprivation (1%), the cells were stimulated with Ang II (1µM)or TGF-β1 (10ng/ml) for 24 hours. Cell lysates were prepared in 1X RIPA lysis buffer and stored at -80ºC until use. The relative expression levels of POSTN, ERK, SRF, and LOX in the knockdown samples were assessed by real-time PCR analysis.

3.10 Real-time PCR analysis

The relative expression levels of POSTN, ERK, SRF, and LOX in the knockdown samples were assessed by real-time PCR analysis. Briefly, total RNA was isolated using TRIzol reagent (Invitrogen), followed by DNase I treatment. Subsequently, 500ng of total RNA was reverse-transcribed to cDNA using the Prime Script RT Reagent Kit (Takara). PCR was performed using POSTN, LOX, ERK, and SRF-specific primers (Integrated DNA Technologies) and TB Green Premix Ex Taq II (Tli RNase H Plus) (Takara), and amplified using the ABI Prism 7500 Sequence Detection System (Applied Biosystems, CA). The primers used in this study are listed in Table 1. PCR amplifications were performed under the following conditions: initial denaturation at 95°C for 10 min, followed by 40 cycles of denaturation at 95°C for 15 seconds and annealing/extension at 60°C for 1 minute. Ct values were determined. β-

Actin served as the endogenous control. Amplicon integrity was confirmed by agarose gel electrophoresis. The relative fold-change in target mRNA levels between treated and control samples was determined using the $2^{-\Delta\Delta Ct}$ method. The data are depicted graphically as fold-changes in mRNA expression.

Table 2 Primer sequences used for Real-Time - PCR analysis

Genes	Primer sequence
POSTN	FORWARD- 5' ACCCGGGAAGAAGCCATCAT 3' REVERSE- 5' TCTTTGCAGGTGTGTCTTTTTGC 3'
ERK	FORWARD- 5' TACCTGGACCAGCTCAACCACATT 3' REVERSE- 5' AGCAGGTCAAGAGCTTTGGAGTCA 3'
SRF	FORWARD- 5' GATGGAGTTCATCGACAACAAGCTG 3' REVERSE- 5' CCCTGTCAGCGTGGACAGCTCATA 3'
LOX	FORWARD- 5' CTGCTGCTGCGTGACAAC 3' REVERSE- 5' GACGGCGAGAAACCAACT 3'
β-Actin	FORWARD- 5' GTACTCTGTGTGGATCGGTGG 3' REVERSE- 5' GGTGTAAAACGCAGCTCAGTAA 3'

3.11 Western blot analysis

Western blot analysis was performed to quantitatively assess the protein expression levels following standard protocols. Cardiac fibroblasts were subjected to the indicated treatments and lysed in the Laemmli buffer. Protein lysates were denatured by incubation with 2X SDS-gel loading buffer at 95°C for 5 minutes. A total of 35 µg of protein was separated by electrophoresis on 10% SDS-PAGE gels at 80 V and transferred to PVDF membranes (Millipore) at 25 V for 16 hours. Membranes were blocked for 1 hour with 5% skim milk or BSA (for phosphoproteins) and incubated overnight at 4°C with primary antibodies (1:1000 dilution in 5% BSA in 1X TBST) with gentle shaking. The unbound primary antibody was removed by washing thrice

for 10 minutes each with 1X TBST. The membranes were then incubated with HRP-conjugated anti-mouse or anti-rabbit secondary antibodies (1:10,000 dilution in 5% skim milk in TBST) (Sigma) for 1 hour. Excess secondary antibody was washed off with three 10-minute washes in TBST. Proteins were detected using an enhanced chemiluminescence reagent (SuperSignal West Femto; Thermo Scientific). β-actin, α-tubulin or GAPDH were used as the loading control. Relative band intensities were calculated using ImageJ software (NIH, USA) and normalized to loading control. The primary antibodies used were TGF-β (1:1000), POSTN (1:5000), SRF (1:500), LOX (1:500), phospho-ERK 1/2 (1:1000), ERK ½ (1:1000), pFAK (1:1000), FAK (1:1000), α-tubulin (1:5000), β-actin (1:1000) and GAPDH (1:1000). The details of the antibodies are mentioned in table 2.

3.12 Detection of LOX activity using LOX assay kit

Sub-confluent cultures of cardiac fibroblasts at passage 2 were treated with POSTN siRNA or scrambled siRNA as explained in section 3.10. The cells were then treated with Ang II (1μM) for 24 hours. To detect LOX activity, the cell culture medium from each condition was collected, and LOX activity was measured using the LOX Activity Fluorometric Assay Kit (Abcam, Cambridge, UK) according to the manufacturer's instructions. Briefly, the supernatant was collected and centrifuged at 13,000× g for 5 min at 4◦C. 50 μL of the supernatant was distributed in triplicate into a black-bottom 96-well plate with 50 μL of assay buffer serving as the blank. Next, 50 μL of LOX reaction mix was added to each well. The plates were then incubated for 40 minutes at 37°C in the dark. The fluorescence was monitored using a microplate reader (BioTek) at Ex/Em = 560/590 nm. The data are represented as relative LOX activity.

3.13 Study design/experiments to elucidate molecular mechanisms involved in the regulation of Cx43

To investigate the expression of POSTN and Cx43 in Ang II- and TGF-β1-stimulated cardiac fibroblasts, the cells were serum-deprived for 24 hours and subsequently treated with 1μM Ang II (Sigma) and 10ng/ml TGF-β1 (Invitrogen). Untreated cells served as controls. To elucidate the molecular mechanisms involved in the POSTN-mediated regulation of Cx43 in response to TGF-β1, the following experiments were performed.

- The expression of Cx43 was further analyzed in POSTN-silenced cardiac fibroblasts following TGF-β1 treatment. Additionally, the functional activity of Cx43 was assessed in POSTN-silenced, TGF-β1-treated cells.
- To elucidate the downstream signaling pathway of POSTN, ERK1/2 activation was assessed in POSTN-silenced, TGF-β1-treated cells.
- To confirm the involvement of ERK1/2, ERK1/2 was silenced, and the expression of Cx43 was examined.
- The transcriptional regulation of Cx43 was explored by analyzing the expression of SRF in POSTN-silenced and ERK1/2-silenced TGF-β1-treated cells.
- This was further validated by probing Cx43 expression in SRF-silenced, TGF-β1-treated cells. Untreated cells served as controls. Detailed methodologies are described in the following sections.

3.14 Effect of Ang II on POSTN and Cx43

Cardiac fibroblasts at passage 2 were treated with Ang II (1μM) for 24 hours. POSTN and Cx43 expression was evaluated by western blot analysis. Untreated cells were used as controls.

3.15 Effect of TGF-β1 on POSTN and CX43

Cardiac fibroblasts at passage 2 were treated with TGF-β1 (10ng/ml) for 24 hours. POSTN and Cx43 expression was evaluated by western blot analysis. Untreated cells were used as controls.

3.16 Immunostaining of Cx43 in POSTN-silenced cells

POSTN-silenced cardiac fibroblasts following TGF-β1 treatment for 24 hours were fixed with 4% paraformaldehyde for 20 minutes. The cells were permeabilized with 0.25% Triton X-100 and subsequently blocked with 1% bovine serum albumin (BSA) for 30 minutes to minimize non-specific antibody binding. Cells were then incubated with a primary antibody against Cx43 (Abcam,1:1000 dilution) at room temperature for 1 hour. Following primary antibody incubation, cells were treated with Alexa Fluor 488-conjugated anti-rabbit secondary antibody (Abcam) for 1 hour at room temperature. The nuclei were counterstained with Hoechst 33258. The slides were mounted with Fluoromount (Abcam) and visualized under a fluorescence microscope (ZEISS AXIO Imager.A2).

3.17 Dye transfer assay for functional analysis of Cx43 Activity

Cardiac fibroblasts at passage 2 were treated with POSTN siRNA or scrambled siRNA. The cells were then treated with TGF-β1(10 ng/ml) for 24 hours. The medium was discarded, and the cells were rinsed gently with Ca-Mg-PBS (pH 7.2). Dilithium salt of Lucifer Yellow hydrazine (LY, 1 mg/mL in PBS) (Thermo Fischer Scientific) was introduced by scraping a monolayer of cells. The dish was incubated for 5–6 min at room temperature to allow the LY dye to travel through adjacent cell layers. The LY-dye solution from the plate was removed, and the cells were rinsed three times with CaMg-PBS to remove all the extracellular dye. Dye transfer was monitored using a fluorescent microscope. The cells were imaged using a fluorescence microscope (ZEISS AXIO Imager.A2)) with excitation at 428 nm and emission at 536 nm. For image quantification using ImageJ, five distinct fields were analyzed for each of the five independent samples. The data are represented as the distance travelled by the dye (measured in μm).

3.18 *In vivo* study design

Animal experiments were carried out following approval from the Institutional Animal Ethics Committee (SCT/IAEC-360/JULY/2020/106). The expressions of POSTN, LOX, and Cx43 were correlated in a rat model of MI. The study included two groups: the MI group (n=6) and sham group (n=3). A schematic representation illustrates the overall study design, including the time points for the procedures, ECG, and ECHO assessments, as well as tissue analysis performed at the 4-week endpoint. In the MI

and sham groups, the heart was retrieved at the 4-week endpoint and subjected to histological evaluation, immunohistochemistry, and western blot analysis.

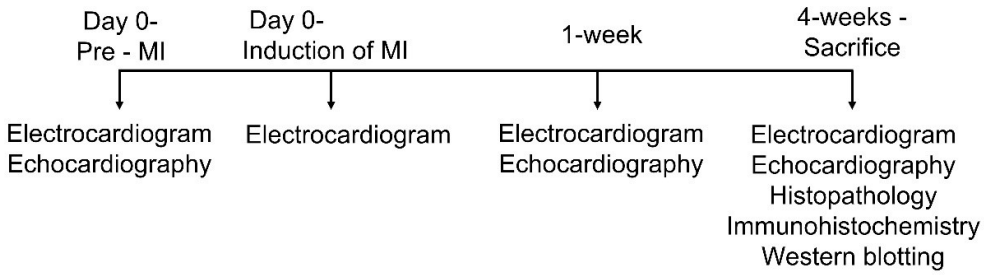

Fig 14: Schematic representation of the in vivo experimental design. MI was induced in Wistar rats by coronary artery ligation. ECG and echocardiography were performed at the following time points: prior to MI to establish the baseline measurements, at the MI procedure to confirm the successful induction of MI, and post-1-week and 4-weeks to assess cardiac function. The rats were euthanized at 4-weeks and histopathology, immunohistochemistry, and western blotting were performed to evaluate the underlying pathological mechanisms and to correlate the expression of POSTN, LOX, and Cx43 within the collagen-rich scar.

3.19 Induction of MI in Rats

MI was induced in adult male Wistar rats (n=6), aged 10-12 weeks, by ligation of the left anterior descending (LAD) coronary artery. Prior to the surgical procedure, the rats were anesthetized with a combination of ketamine and xylazine, and anesthesia for subsequent steps was maintained using 1.5% isoflurane. A left parasternal thoracotomy was then performed, and an alm self-retaining retractor was used to provide optimal exposure of the left ventricle. Permanent occlusion of the LAD

coronary artery was achieved by ligation using a 7-0 prolene suture. Successful induction of myocardial ischemia was confirmed by blanching of the left ventricular myocardium, along with the rapid onset of akinesia and observable changes in electrocardiogram (ECG) readings. Following the procedure, the chest cavity and skin were sutured and anesthesia was gradually withdrawn. The rats were extubated upon return of spontaneous breathing. Postoperative care involved the administration of ceftriaxone at a dose of 25 mg/kg body weight and meloxicam at 0.5 mg/kg body weight for five days. As a control, a group of rats (n=3) underwent the same surgical procedure, including thoracotomy, but without ligation of the LAD coronary artery, serving as the sham-operated group.

3.20 ECG

The rats were anesthetized with a combination of ketamine (80 mg/kg body weight) and xylazine (10 mg/kg body weight) prior to ECG recordings. ECG data for the MI group were acquired using an ADInstruments system (ADInstruments, New Zealand) and recorded at four distinct time points: pre-MI (to obtain baseline values), at the time of MI induction, 1-week post-MI, and 4 weeks post-MI. Post-MI ECG recordings were compared to baseline values. Following stabilization of the animals, ECG signals were continuously recorded in lead II for a minimum duration of 15 minutes. Data acquisition and analysis were conducted using LabChart software (ADInstruments, New Zealand). A representative ECG is presented in the results section.

3.21 Echocardiography

Rats were anesthetized using a combination of ketamine (80 mg/kg body weight) and xylazine (10 mg/kg body weight) prior to the echocardiographic recordings. Transthoracic echocardiography was performed in MI rats using the Mindray echocardiographic system (Mindray, China) with an L14-6NE transducer probe. Echocardiography was taken at three different time points: prior to MI (pre-MI for baseline values), 1-week post-MI and 4-weeks post-MI. M-mode echocardiography images at the parasternal long axis and short axis were captured using DC 70 vet software. Measurements included the interventricular septum (IVS), left ventricular internal diameter (LVID), left ventricular posterior wall (LVPW) thickness during systole and diastole, as well as end-diastolic volume (EDV), end-systolic volume (ESV), and stroke volume (SV). The values were taken as the average of three recordings (n=6). The results are represented as the change in ejection fraction with standard deviation.

3.22 Morphological analysis of retrieved heart

Four weeks after MI, the rats were euthanized, their hearts were carefully excised, washed in cold phosphate-buffered saline (PBS) to remove blood residues, and blotted dry. Furthermore, gross lesions were noted in the heart. Morphological analysis was conducted to assess structural changes associated with cardiac injury and remodelling. The heart was then bisected transversely at the mid-ventricular level to expose the left and right ventricular walls and septum. The sections were visually inspected for infarcted regions, fibrosis, or other abnormalities. Photographs were taken for

documentation, and tissue samples from ventricular areas that were infarcted and remodelled were preserved in 10% neutral-buffered formalin for histological analysis or collected in RIPA buffer for western blotting analysis.

3.23 Processing of samples for histology and western blotting

For histological analysis, the hearts were excised and immediately fixed in 10% neutral-buffered formalin to preserve the tissue architecture. Transverse sections of the ventricles were obtained from formalin-fixed hearts and processed for paraffin embedding. Serial sections (5 μm thick) from both sham and MI samples were deparaffinized in xylene for 10 min with two changes. The sections were then rehydrated through a series of descending isopropanol concentrations (100% for 3 minutes, 90% for 3 minutes, 70% for 3 minutes, 50% for 3 minutes, and 30% for 3 minutes), followed by a 3-minute wash in distilled water and stained with hematoxylin and eosin (H&E) to visualize the changes in the noninfarcted heart and fibrotic scar tissue. Additionally, sections were stained with Picrosirius Red (Sigma) to assess collagen deposition and evaluate the extent of fibrosis. Furthermore, the expression of POSTN, LOX, Cx43, Collagen type I, and alpha SMA was probed in the tissue sections by immunohistochemistry. A detailed methodology is described in the following sections.

For protein analysis via western blotting, a portion of the infarcted left ventricle (LV) was dissected from MI samples (n=6) and healthy ventricles from sham rats (n=3) prior to formalin fixation and homogenized in RIPA buffer for protein extraction. The protein concentration was determined using the Pierce BCA Protein Assay Kit

(Thermo Scientific). The assay involved preparing protein standards and tissue lysates in a 96-well plate with the working reagent following the manufacturer's protocol. After incubation at 37°C for 30 minutes, the absorbance was measured. A standard curve generated from known protein concentrations was used to calculate protein concentrations in the tissue samples. Equal concentrations of proteins were loaded into the gel for western blot analysis.

3.24 Haematoxylin and Eosin staining for assessing the injury site

Formalin-fixed, paraffin-embedded tissue sections of rat hearts were stained to analyze the site of injury induced by myocardial ischemia. For haematoxylin and eosin (H&E) staining, the rehydrated sections were stained with Harris's haematoxylin for 7 minutes and subsequently washed in tap water for 5 minutes. Differentiation was performed using 1% acid-alcohol with 1–2 quick dips, followed by another 5-minute wash in tap water. The sections were then treated with Schott's solution for 1 minute for bluing and dipped in 70% ethanol for 1 minute. Counterstaining was performed with eosin Y for 15–30 seconds. Following staining, the tissue sections were dehydrated in isopropanol (95% for 5 minutes) and two changes of 100% ethanol (5 minutes each), cleared in xylene (two changes, 10 minutes each), and mounted in DPX. The stained sections and images were captured using an upright microscope (Olympus BX43).

3.25 Picrosirius red staining

The extent of myocardial fibrosis, and collagen deposition, were determined in formalin-fixed paraffin-embedded sections of sham and MI samples by Picrosirius red staining. Briefly, the sections were deparaffinized, rehydrated, rinsed in distilled water,

and stained with 0.1% Sirius red in a saturated aqueous solution of picric acid for 60 minutes, followed by a wash with two changes of acidified water. Tissue sections were dehydrated in isopropanol (2 changes in 100% ethanol for 5 minutes each), cleared in xylene (2 changes, 5 min each), mounted in DPX, and viewed under an upright light microscope (Olympus BX43). Positive staining was indicated by red colouration and quantified using ImageJ software (NIH, USA) with the Colour Deconvolution 2 ImageJ plugin (Ruifrok and Johnston, 2001). Quantification was performed using five random images of the infarct zone from each MI sample and five random images of the left ventricle from each sham sample. The results are graphically represented as the collagen content in percentage for the MI (n=6) and sham (n=3) samples.

Sirius Red-stained sections were examined using an upright Olympus microscope equipped with a polarizer to visualize the birefringence of collagen fibers in both the infarcted scar and healthy ventricular tissue. Representative images of collagen birefringence were captured for analysis.

3.26 Immunohistochemistry

Formalin-fixed paraffin-embedded sections from sham and MI samples were deparaffinized, rehydrated, rinsed in distilled water, and subjected to antigen retrieval using Tris-EDTA buffer (pH 9). Immunostaining was performed using the Super Sensitive Polymer-HRP IHC Detection System (BioGenex, USA) following the manufacturer's protocol. In brief, after antigen retrieval, the sections were washed with distilled water for 3 minutes and incubated with Peroxide Block for 5 minutes to inhibit endogenous peroxidase activity. After another wash with IHC wash buffer (TBST, pH

8.4), the sections were treated with Power Block™ for 5 minutes to reduce nonspecific binding. Following blocking, the sections were incubated with a primary antibody specific to the target protein. Negative controls were treated with an antibody diluent without the primary antibody. After washing with the IHC buffer, the sections were incubated with Super Enhancer™ for 20 minutes, followed by incubation with Poly-HRP reagent for 30 minutes. The immunostaining signal was developed using 3,3'-diaminobenzidine (DAB) substrate solution, applied for 5-10 minutes, resulting in a brown-colored precipitate at the site of positive antigen expression. The sections were then washed with distilled water for 5 minutes. For counterstaining, the sections were treated with hematoxylin for 1 minute, washed with tap water, dehydrated using a graded series of isopropanol, cleared in xylene, and mounted using DPX mounting medium. The stained sections were visualized using an Olympus BX43 upright brightfield microscope at 40x magnification, and images were captured using the QCapture Pro 7 imaging software (Q Imaging). For negative control staining, sections underwent the same staining procedure, except that they were incubated with an antibody diluent without the primary antibody. Positive staining was indicated by brown colouration and quantified using ImageJ software (NIH, USA) with the Colour Deconvolution 2 ImageJ plugin (Ruifrok and Johnston, 2001). Quantification was performed using five random images of the infarct zone from each MI sample and five random images of the left ventricle from each sham sample. The results are graphically represented as the percentage area of positive staining for MI (n=6) and sham (n=3) samples. The primary antibodies used were POSTN (1:500), LOX (1:500), Cx43

(1:1000), collagen type I (1:1000), and α-Smooth Muscle Actin (α-SMA) (1:1000). (Antibody details are provided in Table 2 provided below)

3.27 Western blotting of tissue sample

Initially, the tissues were homogenized in RIPA lysis buffer containing protease and phosphatase inhibitors to prevent protein degradation and maintain phosphorylation states. The lysates were then centrifuged to remove cellular debris, and protein concentrations were quantified using the BCA method. Equal amounts of protein were denatured by boiling in a lysis buffer. The samples were separated by SDS-PAGE, transferred onto a PVDF membrane, and subjected to the protocol detailed in section 3.12. The expression of POSTN (1:5000), LOX (1:500), TGF-β (1:1000), p-ERK1/2 (1:1000), ERK1/2 (1:1000), SRF (1:500), collagen type 1 (1:1000), and α-SMA (1:2000), Cx43 (1:1000) was analyzed by western blotting. α-Tubulin or GAPDH was used as a loading control. (Antibody details are provided in the table 2 provided below)

3.28 Statistical analysis

All *in vitro* data included in this study are representative of three or more independent experiments and are presented as mean ± SD. Graphical representations and statistical analyses were conducted using the GraphPad Prism 8 software. For comparisons between two groups, an unpaired two-tailed Student's t-test was used. For analyses involving more than two groups with two variables, a two-way analysis of variance (ANOVA) was performed, followed by Tukey's multiple comparison test. A p-value of less than 0.05 ($P < 0.05$) was considered statistically significant.

Table 3 – Details of chemicals, reagents and antibodies used in this study

Sl No:	Reagents/Antibody	Brand	Catalogue No:
1.	Collagenase	Sigma	C9891
2.	Trypsin	Sigma	T4799
3.	M199 medium	Sigma	M2520
4.	Angiotensin II (1μM)	Sigma	A9525
5.	TGF-β1 recombinant	Thermo Fisher Scientific	PHG9214
6.	Scrambled siRNA/ Control siRNA duplexes negative control.	Eurogentec	SR-CL000-005
7.	POSTN siRNA (50nM)	Eurogentec (Custom designed)	Sense: GCAUCUCCAUUAACGGAAU
8.	ERK siRNA (100nM)	Eurogentec (Custom designed)	Sense: GUACUAUGAUCCGACAGAU
9.	SRF siRNA (25nM)	Eurogentec (Custom designed)	Since: GAUGGAGUUCAUCGACAAC
10.	TGF-β1 Silencer Select pre-designed siRNA (50nM)	Ambion	4390771
11.	CCG-1423 (SRF Inhibitor) (10μM)	Sigma	SML0987

12.	Anti-Mouse IgG Peroxidase antibody (1:10000)	Sigma	A9044
13.	Anti-Rabbit IgG Peroxidase antibody (1:10000)	Sigma	A0545
14.	Periostin Polyclonal antibody (1:5000 for WB, 1:500 for IHC)	Invitrogen	PA5-79850
15.	Phospho-ERK 1/2 antibody (1:1000)	CST	9101
16.	ERK ½ antibody (1:1000)	CST	9102
17.	Phospho-FAK antibody (1:1000)	Abcam	ab81298
18.	FAK antibody (1:1000)	Abcam	Ab40794
19.	SRF antibody (1:500)	CST	5147
20.	LOX antibody (1:500) CX43	Abcam	ab174316
21.	Cx43 antibody (1:1000)	Abcam	ab11370
22.	α-tubulin antibody (1:5000)	Abcam	ab7291
23.	β-actin antibody (1:1000)	Sigma	A5316
24.	α-SMA (1:2000 for WB, 1:1000 for IHC)	CST	19245
25.	Collagen type 1 (1:1000 for WB&IHC)	Invitrogen	PA5-95137
26.	TGF-β antibody (1:1000)	CST	3711S
27.	GAPDH antibody	CST	2118

28.	PDGFRα antibody	CST	3174
29.	Vimentin	Abcam	ab92547
30.	DDR2	Bioss	bs-4194R
31.	vWF	Abcam	ab 6994
32.	Anti-Rabbit IgG (Alexa Fluor® 488)	Abcam	ab150081
33.	Anti-Mouse IgG (Alexa Fluor® 488)	Abcam	ab150117
34.	Picrosirius red/ direct red	Sigma	365548
35.	Pierce BCA protein assay kit	Thermo Scientific	23225
36.	Super Signal West Femto	Thermo Scientific	34095
37.	RIPA lysis and extraction buffer	Rockland	MB-030-0050
38.	Immunohistochemistry Kit	Biogenex	QD400-60KE
39.	LOX Assay Kit	Abcam	ab112139
40.	SYBR green Master Mix	Takara	RR420
41.	Trizol	Invitrogen	15596026

CHAPTER 4

RESULTS

4.1 Characterization of adult rat cardiac fibroblasts

4.1.1 Morphological analysis

Cardiac fibroblasts were isolated from the ventricular tissue of 1–3-month-old adult male rats and cultured according to the protocol described in the methods section. A pre-plating step of 150 minutes post-isolation facilitated the selective adhesion of fibroblasts, which constituted over 99% of the cultured cells. The cells displayed a spindle-shaped appearance at 24 hours. Upon reaching confluence, the cultures exhibited a characteristic monolayer pattern (Figure 15). The absence of 'cobblestone' or 'hill and valley' morphologies excluded the possibility of contamination by endothelial cells (ECs) and vascular smooth muscle cells (VSMCs), respectively. Cells from passage 2 were used for subsequent experiments.

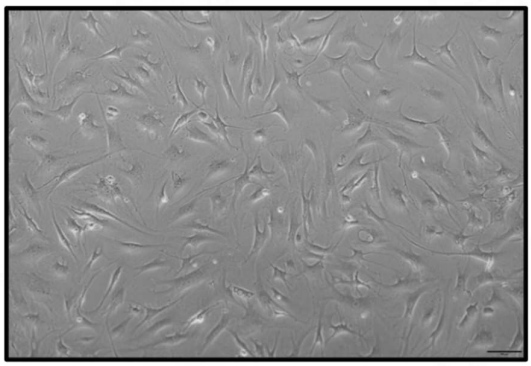

Fig 15: Phase contrast image of adult rat cardiac fibroblasts at passage 2 (scale bar 100μm)

4.1.2 Characterization of cardiac fibroblast cultures using immunocytochemistry

The cells were positive for cardiac fibroblast markers, such as DDR2, PDGFRα, and vimentin, and negative for the endothelial marker vWF (Figure 16).

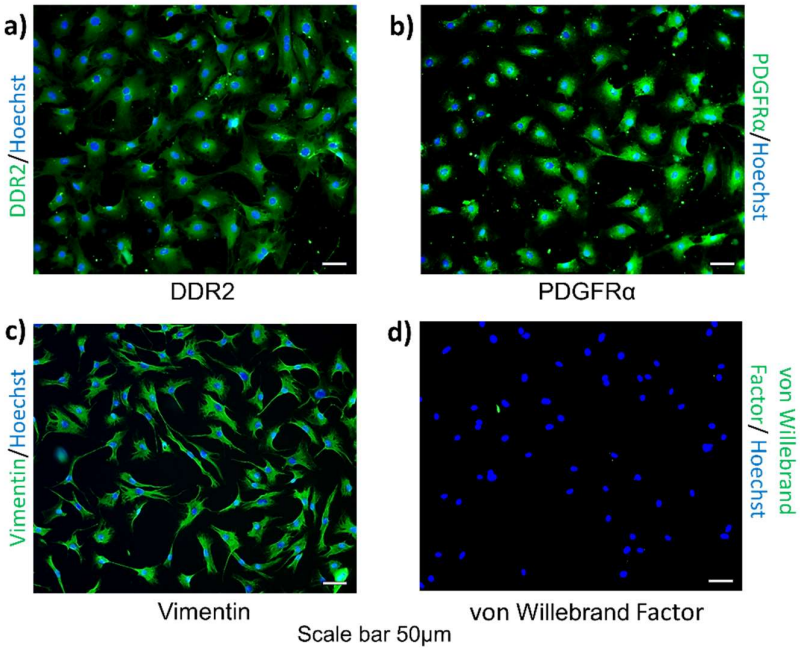

Fig 16: Characterization of cardiac fibroblasts: Cardiac fibroblasts at passage 2 are positive for (a) DDR2, (b) PDGFRα, and (c) Vimentin and negative for (d) vWF. Positive staining is indicated by green fluorescence. The nuclei were counterstained with Hoechst dye (blue).

Morphological analysis and immunocytochemical staining confirmed the fibroblastic identity of the cells.

OBJECTIVE 1

Delineating the molecular basis of the regulation of LOX expression

4.2 Ang II upregulates the expression of LOX

The effect of Ang II on LOX expression was investigated by treating cardiac fibroblasts of passage 2 with 1 μM Ang II for varying durations of 6, 12, 24, and 48

hours. LOX expression was analyzed by western blotting. As shown in Figure 17, Ang II treatment resulted in a significant upregulation of LOX expression at the 24- and 48-hour time points.

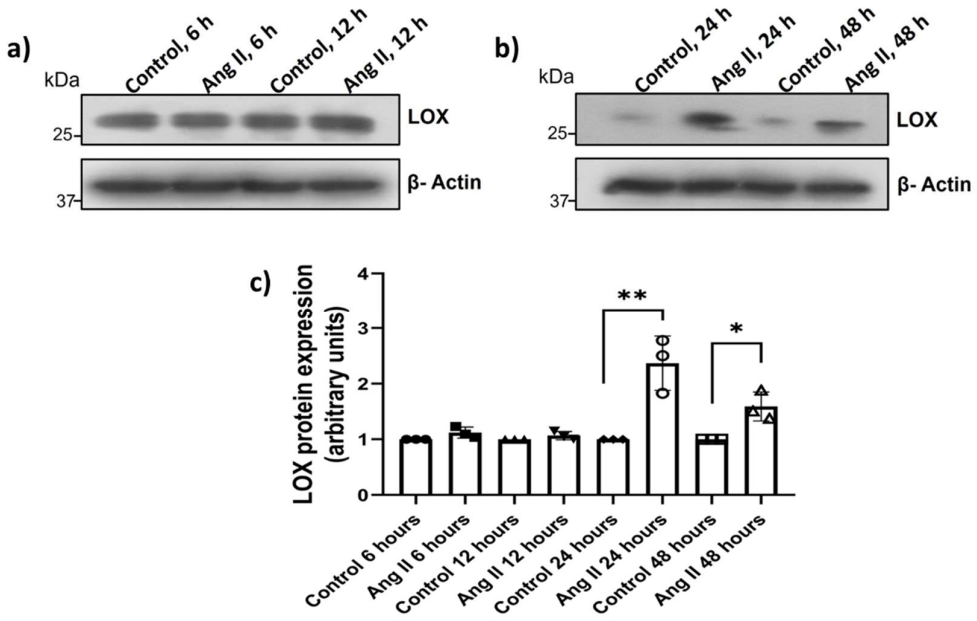

Fig 17: (a, b) Expression of LOX in Ang II-stimulated cardiac fibroblasts at 6, 12, 24, and 48 hours. (c) Graphical representation of changes in the expression levels for LOX at 6,12, 24 and 48 hours. β- Actin was used as the loading control. Significance was determined by Student's t-test, * represents $p<0.05$ and ** represents $p<0.01$. Data are representative of three independent experiments (n=3, Mean $\pm$ SD).

4.3 Ang II upregulates the expression of POSTN

POSTN expression was probed in cardiac fibroblasts treated with 1 μM Ang II for 6, 12, 24, and 48 hours. As illustrated in Figure 18, Ang II treatment upregulated POSTN expression at 24- and 48-hour time points, with the most pronounced upregulation

observed at the 24-hour time point. So, 24-hour time point was chosen for subsequent studies.

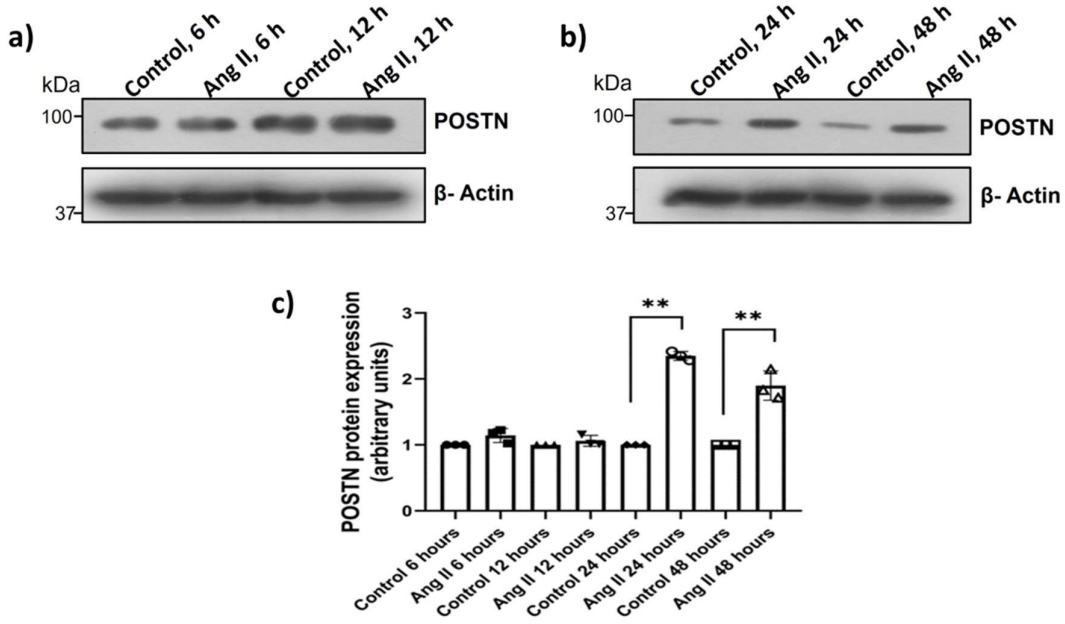

Fig 18: (a, b) Expression of POSTN in Ang II-stimulated cardiac fibroblasts at 6, 12, 24, and 48 hours. (c) Graphical representation of changes in the expression levels for POSTN at 6,12, 24 and 48 hours. β-Actin was used as the loading control. Significance was determined by Student's t-test, ** represents $p<0.01$. Data are representative of three independent experiments (n=3, Mean $\pm$ SD).

4.4 Ang II mediates POSTN and LOX expression via AT1 receptor

To determine whether Ang II exerts its effects via the AT1 receptor, cardiac fibroblasts were pretreated with 10 μM AT1 receptor blocker, candesartan for 1 hour before incubation with 1 μM Ang II for 24 hours. Western blot analysis revealed a significant upregulation of both POSTN and LOX at 24 hours in Ang II-treated cells. However,

candesartan abolished the Ang II-induced increase in LOX expression, indicating that Ang II-mediated LOX expression via the AT1 receptor (Figure 19).

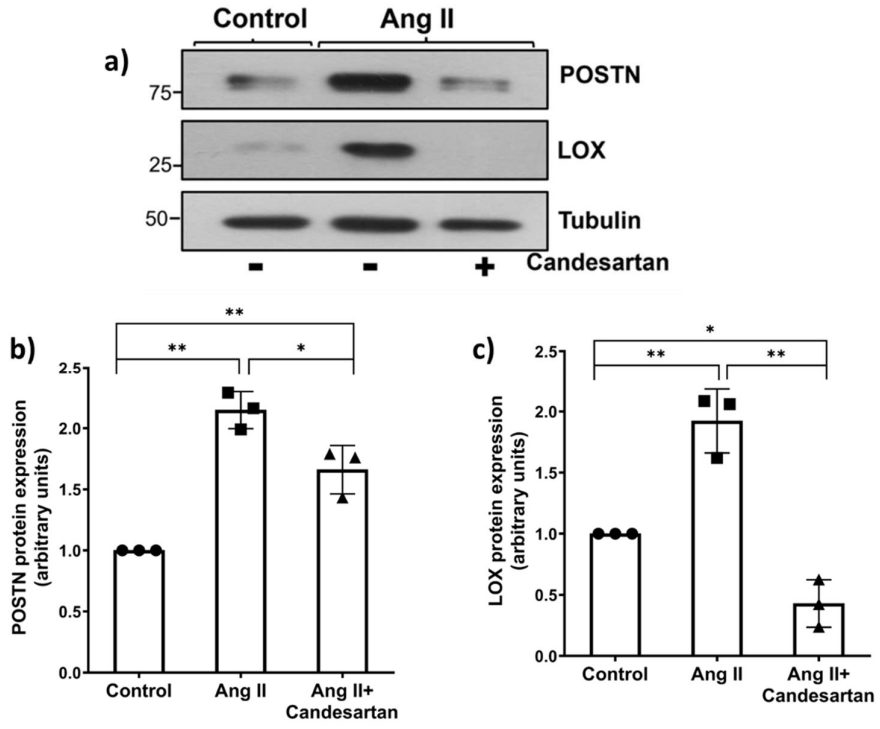

Fig 19: (a) Expression of POSTN and LOX in Candesartan-treated Ang II-stimulated cardiac fibroblasts. (b, c) Graphical representation of changes in the expression levels for POSTN and LOX respectively. α-Tubulin was used as the loading control. Significance was determined using one-way ANOVA with Tukey's multiple comparison test. * represents $p<0.05$ and ** represents $p<0.01$. Data are representative of three independent experiments (n=3, Mean $\pm$ SD).

4.5 POSTN is required for Ang II-mediated LOX expression

The role of Ang II-induced POSTN in mediating LOX expression in cardiac fibroblasts was investigated. siRNA-mediated knockdown of POSTN using POSTN siRNA (50 nM) significantly attenuated Ang II-induced LOX mRNA and protein expression (Figure 20).

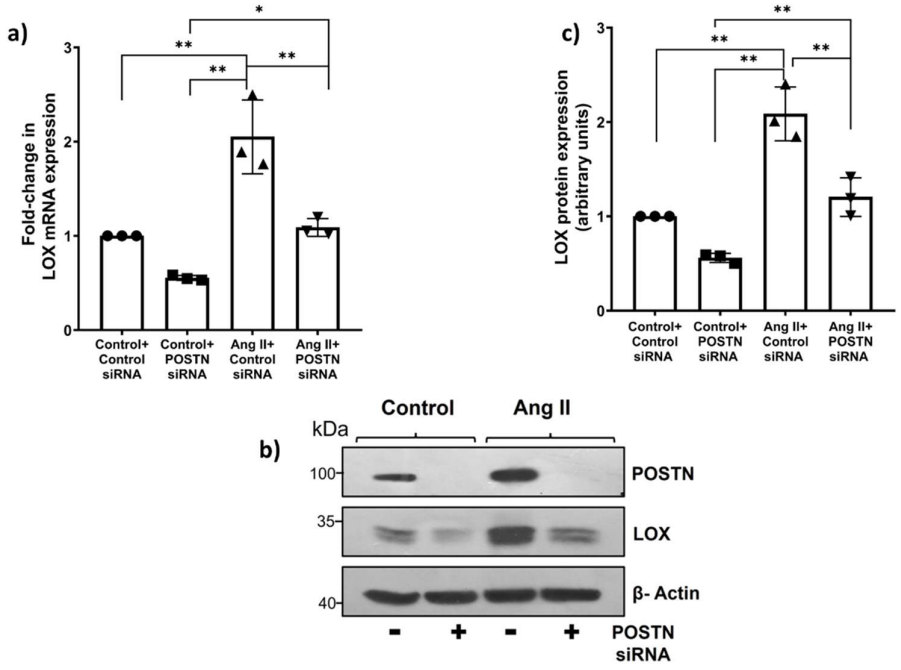

Fig 20: (a) LOX mRNA expression in POSTN-silenced Ang II-treated cells. (b) LOX protein expression in POSTN-silenced Ang II-treated cells. (c) Graphical representation of changes in LOX protein expression levels in POSTN-silenced Ang II-treated cells. β-Actin was used as the loading control. Significance was determined using two-way ANOVA with Tukey's multiple comparison test. * represents $p<0.05$ and **represents $p<0.01$. Data are representative of three independent experiments (n=3, Mean± SD).

4.6 POSTN has a role in modulating Ang II-mediated LOX activity

To further confirm that LOX activity was suppressed following POSTN silencing, functional assays were performed using a commercially available LOX activity assay kit. The results showed that cardiac fibroblasts stimulated with Ang II exhibited significantly elevated LOX enzymatic activity, which was markedly reduced upon POSTN silencing, indicating a clear reduction in LOX activity (Figure 21).

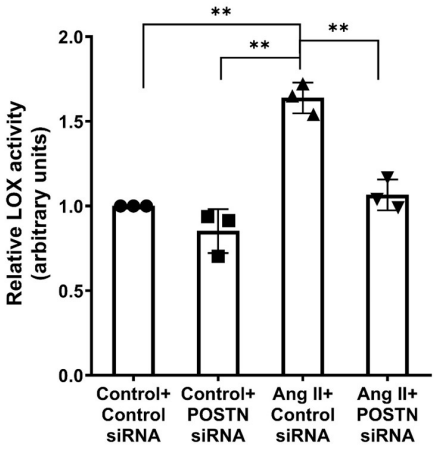

Fig 21: Relative LOX activity in POSTN-silenced Ang II-stimulated cardiac fibroblasts. Significance was determined using two-way ANOVA with Tukey's multiple comparison test. ** represents $p<0.01$. Data are representative of three independent experiments (n=3, Mean $\pm$ SD).

4.7 POSTN knockdown does not affect FAK phosphorylation in Ang II-stimulated cardiac fibroblasts

To investigate the downstream signalling effectors involved in POSTN-mediated regulation of LOX expression in cardiac fibroblasts exposed to Ang II, we examined

the role of FAK, which has been reported to be activated downstream of POSTN (Chuanyu et al., 2017; Ma et al., 2020). Specifically, we explored whether POSTN-dependent activation of FAK contributes to the regulation of LOX expression. Our results indicated that siRNA-mediated silencing of POSTN did not alter Ang II-induced phosphorylation of FAK indicating that FAK is not involved in the regulation of LOX expression in response to Ang II in cardiac fibroblast (Figure 22)

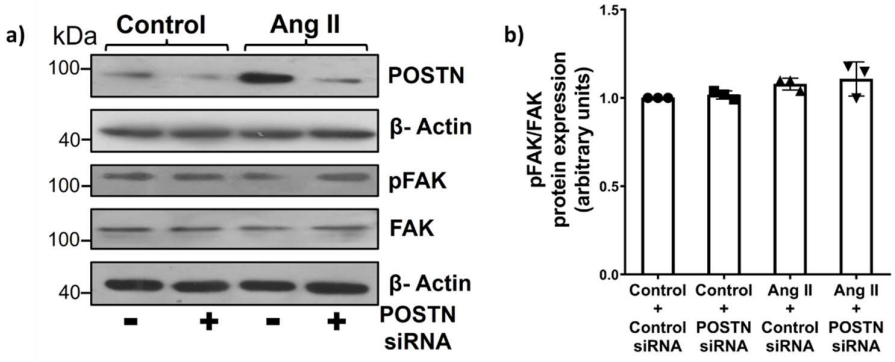

Fig 22: (a) FAK phosphorylation (pFAK) and total FAK in POSTN-silenced Ang II-stimulated cardiac fibroblasts. b) Graphical representation of FAK phosphorylation (pFAK). β-Actin was used as the loading control. Significance was determined using two-way ANOVA with Tukey's multiple comparison test. Data are representative of three independent experiments (n=3, Mean± SD).

4.8 POSTN acts via ERK 1/2 MAPK to upregulate LOX expression in cardiac fibroblasts exposed to Ang II

4.8.1 POSTN regulates ERK 1/2 MAPK activation

Given that FAK is not involved, we next investigated the potential involvement of ERK 1/2 MAPK in mediating LOX expression. Previous studies have reported that

POSTN exerts its downstream effects through activation of ERK 1/2 MAPK (Chen et al., 2019; Liu et al., 2016; Wu et al., 2023). Notably, siRNA-mediated silencing of POSTN decreased Ang II-induced phosphorylation of ERK1/2, indicating that POSTN regulates ERK1/2 MAPK activation (Figure 23).

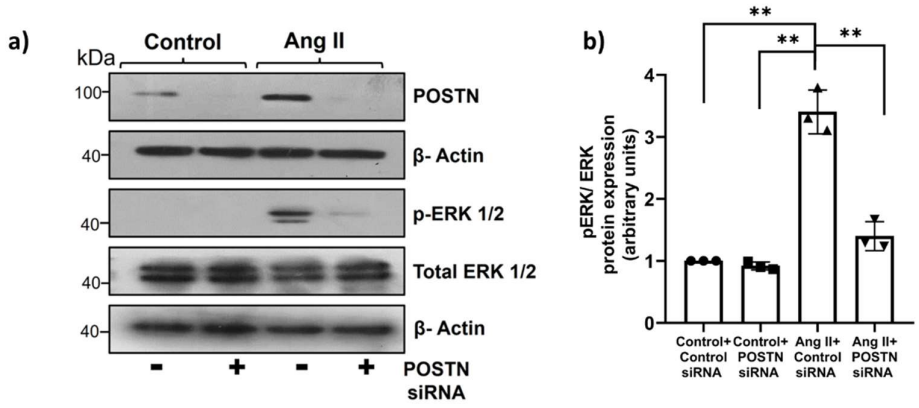

Fig 23: (a) Phosphorylation of ERK 1/2 (pERK 1/2) and total ERK 1/2 in POSTN-silenced Ang II-stimulated cardiac fibroblasts. b) Graphical representation of ERK1/2 phosphorylation (pERK 1/2). β-Actin was used as the loading control. Significance was determined using two-way ANOVA with Tukey's multiple comparison test. **represents $p<0.01$. Data are representative of three independent experiments (n=3, Mean $\pm$ SD).

4.8.2 Knockdown of ERK 1/2 MAPK reduced LOX expression

To further validate that POSTN-dependent activation of ERK 1/2 regulates LOX expression, ERK 1/2 MAPK was silenced and LOX expression was subsequently probed. Knockdown of ERK 1/2 significantly attenuated the Ang II-induced increase in both LOX mRNA and protein levels. Together, these findings demonstrate the involvement of POSTN-dependent activation of the ERK 1/2 MAPK signalling

pathway in the regulation of LOX expression in response to Ang II in cardiac fibroblasts (Figure 24).

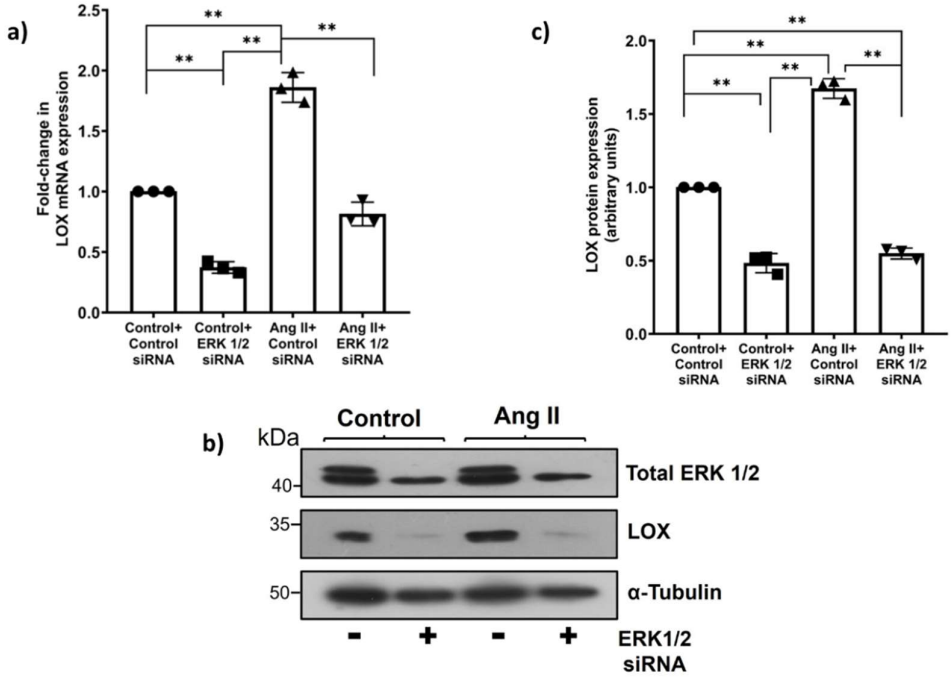

Fig 24: (a) LOX mRNA expression in ERK 1/2 MAPK-silenced Ang II-treated cells. (b) LOX expression in ERK 1/2 MAPK-silenced Ang II-treated cells. (c) Graphical representation of changes in LOX expression levels in ERK 1/2 MAPK-silenced Ang II-treated cells. α-Tubulin was used as the loading control. Significance was determined using two-way ANOVA with Tukey's multiple comparison test. **represents $p<0.01$. Data are representative of three independent experiments (n=3, Mean $\pm$ SD).

4.9 SRF-mediates transcriptional regulation of LOX via POSTN-dependent ERK1/2-MAPK signalling in Ang II-Stimulated Cardiac Fibroblasts

4.9.1 POSTN regulates SRF expression

Bioinformatics analysis using ALGGEN PROMO identified 2 binding sites for the transcription factor SRF (CC(A/T)6GG) at 298 and 2196 base pairs upstream of the transcription start site in the promoter region of the LOX gene. Additionally, previous studies (Santos et al., 2019; Titus et al., 2020) demonstrated that SRF acts downstream of Ang II to modulate myofibroblast function. Therefore, the role of SRF in the POSTN-dependent regulation of LOX was investigated. Our data revealed that siRNA-mediated silencing of POSTN abolished the Ang II-induced upregulation of SRF, confirming that POSTN regulates SRF expression in Ang II-stimulated cardiac fibroblasts (Figure 25).

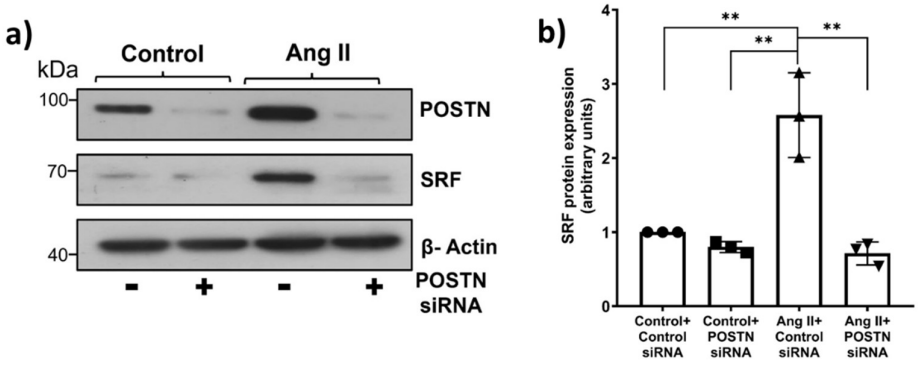

Fig 25: (a) Expression of SRF in POSTN-silenced Ang II-treated cells. (b) Graphical representation of changes in the expression levels of SRF in POSTN-silenced Ang II-treated cells. β-Actin was used as the loading control. Significance was determined

using two-way ANOVA with Tukey's multiple comparison test. **represents p<0.01. Data are representative of three independent experiments (n=3, Mean ± SD).

4.9.2 SRF acts downstream of ERK 1/2 MAPK

To determine whether SRF acts downstream of ERK1/2 MAPK, ERK1/2 was silenced using specific siRNA and the expression of SRF was probed. The knockdown of ERK 1/2 reduced SRF expression indicating that SRF acts downstream of ERK 1/2 MAPK signaling cascade (Figure 26).

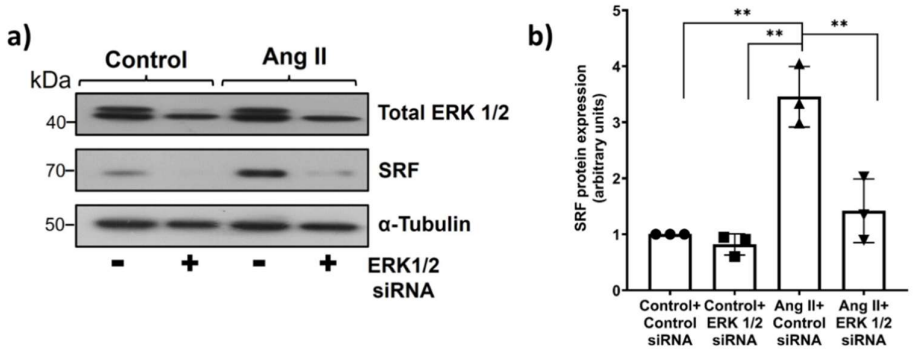

Fig 26: (a) Expression of SRF in ERK 1/2 MAPK-silenced Ang II-treated cells. (b) Graphical representation of changes in the expression levels of SRF in ERK 1/2 MAPK-silenced Ang II-treated cells. α-Tubulin was used as the loading control. Significance was determined using two-way ANOVA with Tukey's multiple comparison test. **represents p<0.01. Data are representative of three independent experiments (n=3, Mean ± SD).

4.9.3 SRF inhibition using CCG-1423 reduced Ang II-mediated LOX expression

To investigate the role of SRF in the regulation of Ang II-mediated LOX expression, the SRF inhibitor CCG-1423 was used. Treatment with CCG-1423 significantly

reduced the expression of LOX in cardiac fibroblasts exposed to Ang II, suggesting that SRF is a critical mediator of LOX transcription in response to Ang II stimulation (Figure 27).

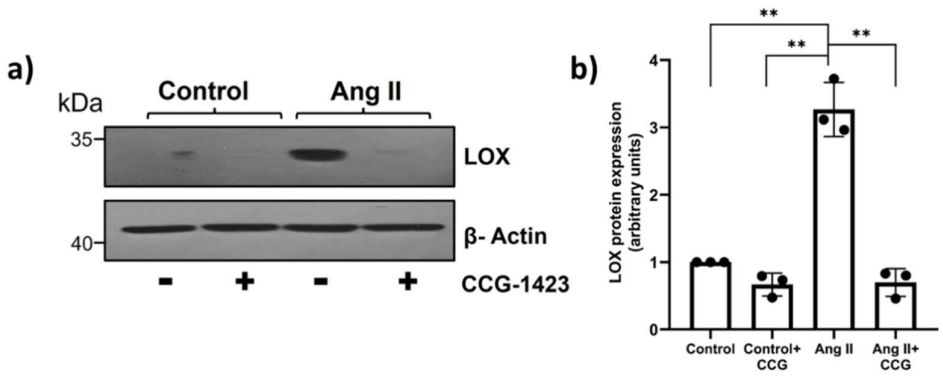

Fig 27: (a) Expression of LOX in CCG-1423-treated Ang II-stimulated cells. (b) Graphical representation of changes in the expression levels of LOX in CCG-1423-treated Ang II-stimulated cells. β-Actin was used as the loading control. Significance was determined using two-way ANOVA with Tukey's multiple comparison test. **represents $p<0.01$. Data are representative of three independent experiments (n=3, Mean $\pm$ SD).

4.9.4 SRF knockdown reduced Ang II-mediated LOX expression

The involvement of SRF in LOX regulation was further confirmed by probing the expression of LOX in SRF-silenced Ang II-treated cells. SRF knockdown markedly diminished Ang II-induced elevation of both LOX mRNA and protein levels (Figure 28).

Collectively, these results demonstrate that POSTN-dependent transcriptional regulation of SRF plays a critical role in regulating LOX expression in response to Ang II in cardiac fibroblasts.

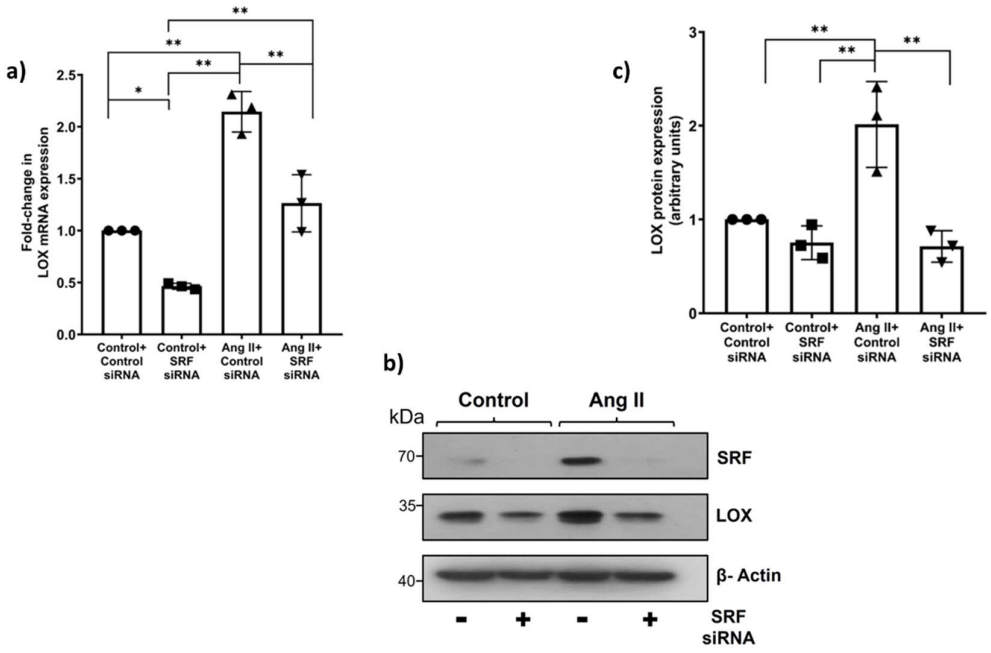

Fig 28: (a) LOX mRNA expression in SRF-silenced Ang II-treated cells. (b) LOX expression in SRF-silenced Ang II-treated cells. (c) Graphical representation of changes in the expression levels of LOX in SRF-silenced Ang II-treated cells. β-Actin was used as the loading control. Significance was determined using two-way ANOVA with Tukey's multiple comparison test. **represents $p<0.01$. Data are representative of three independent experiments (n=3, Mean $\pm$ SD).

4.10 POSTN also mediates the TGF-β1-stimulated expression of LOX in cardiac fibroblasts

4.10.1 TGF-β1 enhances the expression of POSTN and LOX

TGF-β1 is a key growth factor that promotes fibrosis and plays a critical role in the activation of cardiac fibroblasts (Dobaczewski et al., 2011; Györfi et al., 2018). Additionally, our previous studies have shown that Ang II induces TGF-β1 expression in cardiac fibroblasts (V et al., 2019). To investigate the potential involvement of TGF-β1 in the Ang II-dependent regulation of POSTN and LOX expression, we first checked whether TGF-β1 enhanced the expression of POSTN and LOX. Our results indicated that TGF-β1 treatment for 24 hours enhanced the expression of both POSTN and LOX (Figure 29).

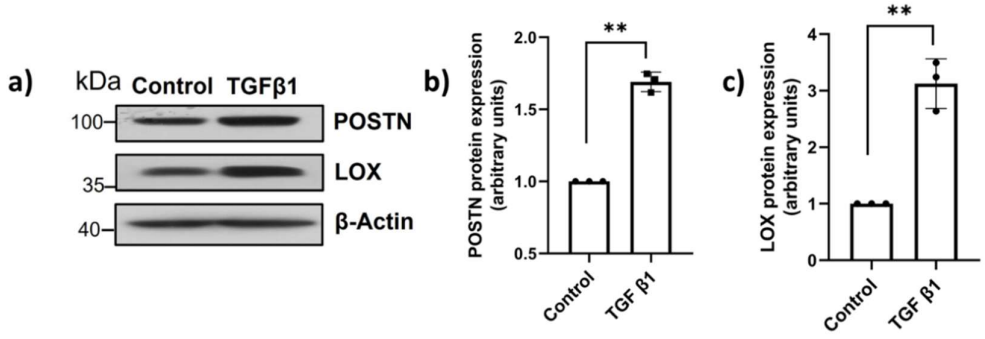

Fig 29: (a) Expression of POSTN and LOX in TGF-β1-stimulated cardiac fibroblasts at 24 hours. (b) Graphical representation of change in expression levels for POSTN in TGF-β1-stimulated cardiac fibroblasts. (c) Graphical representation of change in expression levels for LOX in TGF-β1-stimulated cardiac fibroblasts. β-Actin was used

as the loading control. Significance was determined by Student's t-test, ** represents $p<0.01$. Data are representative of three independent experiments (n=3, Mean $\pm$ SD).

4.10.2 Ang II regulates LOX via TGF-β1

Furthermore, we silenced TGF-β1 using specific siRNA in the presence of Ang II and examined POSTN and LOX expression levels. Our findings revealed that TGFβ1 silencing in Ang II-stimulated samples abolished POSTN and LOX expression, confirming that Ang II regulates LOX via TGF-β1 (Figure 30).

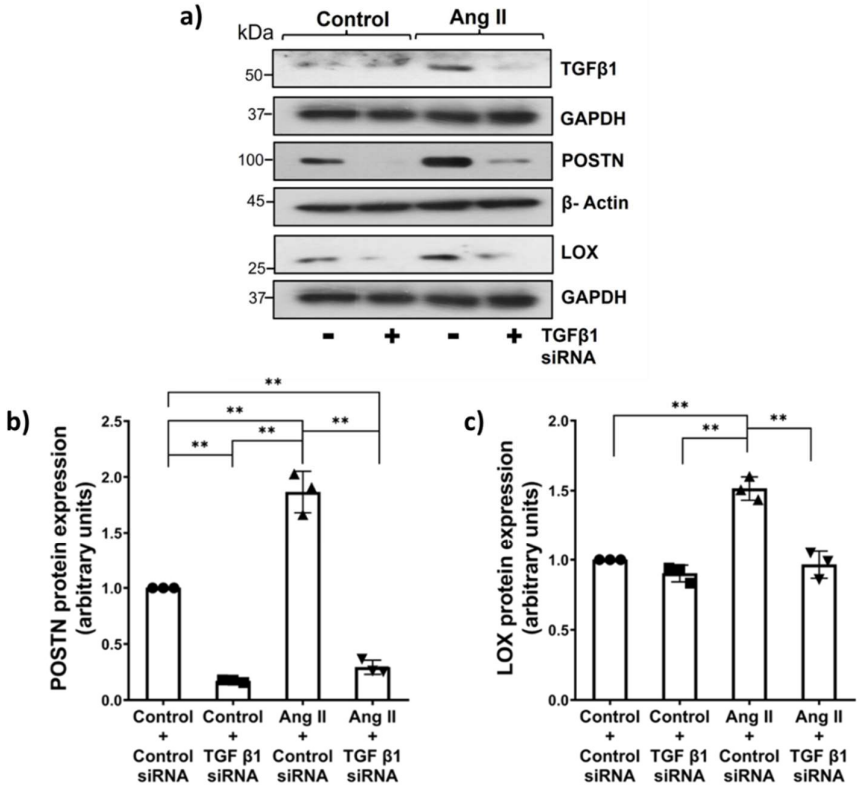

Fig 30: (a) Expression of POSTN and LOX in TGF-β1-silenced Ang II-treated cells. (b) Graphical representation of changes in the expression levels of POSTN in TGF-β1-silenced Ang II-treated cells. (b) Graphical representation of changes in the

expression levels of LOX in TGF-β1-silenced Ang II-treated cells. β-Actin and GAPDH were used as the loading control. Significance was determined using two-way ANOVA with Tukey's multiple comparison test. **represents $p<0.01$. Data are representative of three independent experiments (n=3, Mean ± SD).

4.10.3 POSTN mediates the TGF-β1 effect on LOX via ERK 1/2 and SRF

Furthermore, we explored whether POSTN silencing in TGF-β1-stimulated cells affects LOX expression. POSTN knockdown led to reduced LOX expression in TGF-β1-stimulated cells, suggesting that POSTN may regulate LOX expression in the presence of TGF-β1. Interestingly, POSTN silencing in TGFβ1-stimulated cardiac fibroblasts also decreased the expression of pERK 1/2 and SRF (Figure 31).

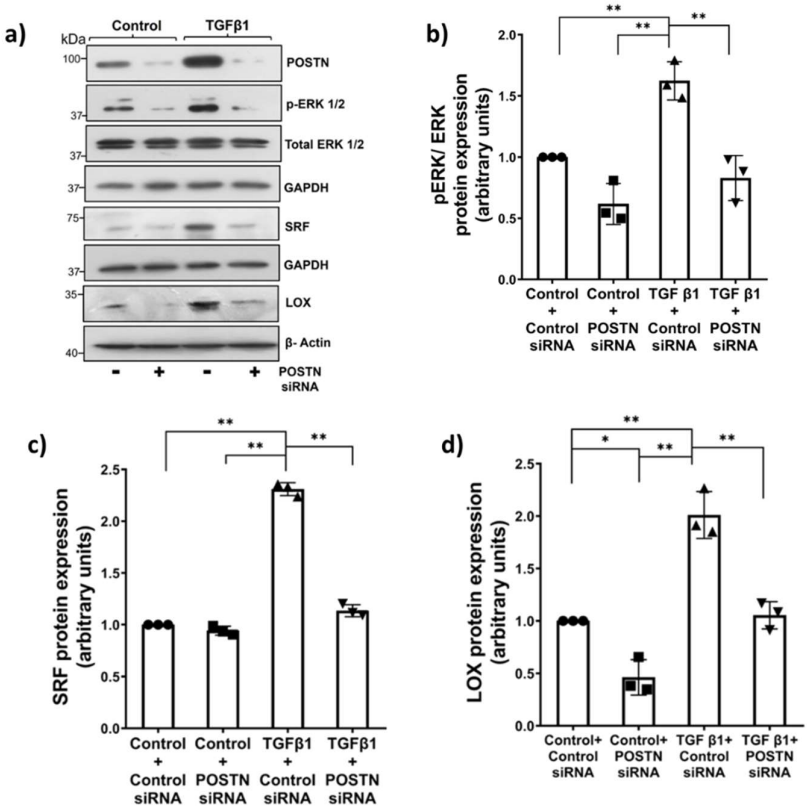

Fig 31: (a) Expression of pERK 1/2, SRF, and LOX in POSTN-silenced, TGFβ1-stimulated cardiac fibroblasts. (b) Graphical representation of change in expression levels of pERK 1/2 in POSTN-silenced, TGF-β1-stimulated cardiac fibroblasts. (c) Graphical representation of changes in SRF expression levels in POSTN-silenced, TGF-β1-stimulated cardiac fibroblasts. (d) Graphical representation of change in expression levels for LOX in POSTN-silenced, TGF-β1-stimulated cardiac fibroblasts. β-Actin and GAPDH were used as the loading control. Significance was determined using two-way ANOVA with Tukey's multiple comparison test. **represents $p<0.01$. Data are representative of three independent experiments (n=3, Mean ± SD).

Schematic diagram based on the findings presented above

Based on the findings presented, POSTN has an obligate role in Ang II- and TGF-β1-stimulated upregulation of LOX expression (Figure 32)

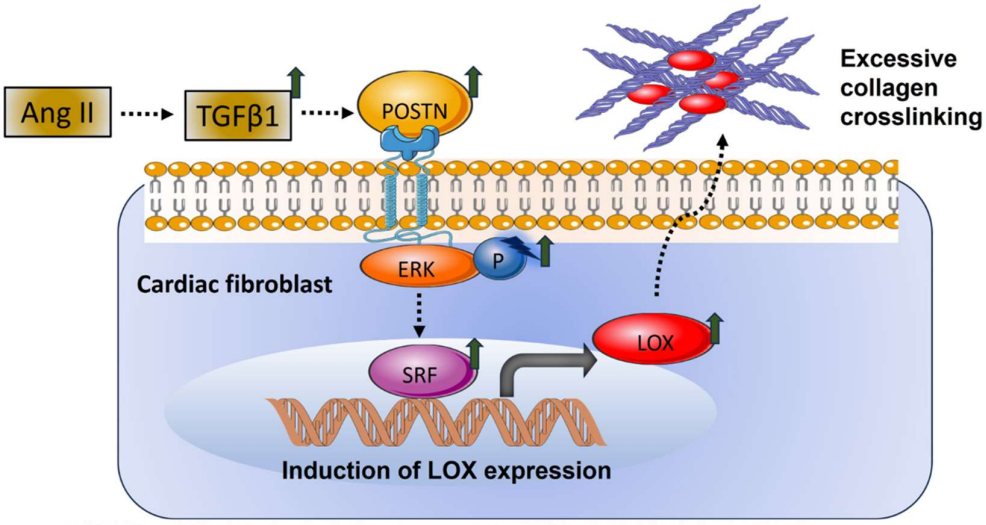

Fig 32: Schematic representation of POSTN-mediated regulation of LOX in response to Ang II and TGF-β1

OBJECTIVE 2

Delineating the molecular basis of the regulation of Cx43 expression

The second phase of this study focuses on elucidating the molecular mechanisms underlying the regulation of Cx43 gene expression

4.11 Ang II upregulates the expression of Cx43

Cx43 expression was probed in cardiac fibroblasts after treatment with 1 μM Ang II for 24 hours. Following treatment with Ang II, Cx43 expression was significantly upregulated in cardiac fibroblasts (Figure 33).

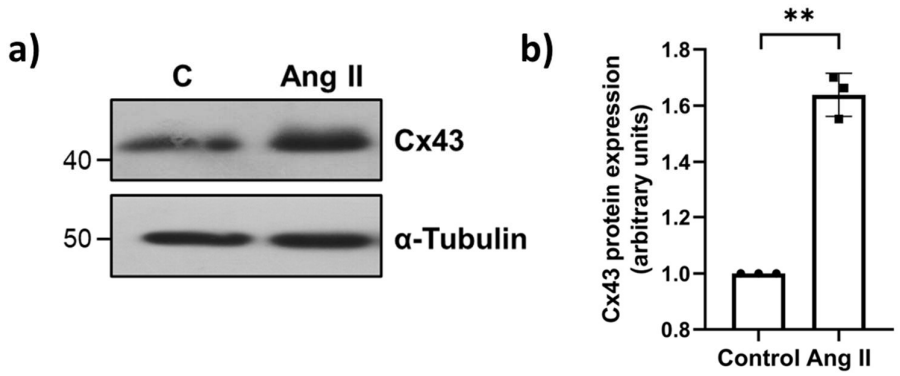

Fig 33: (a) Expression of Cx43 in Ang II-stimulated cardiac fibroblasts (b) Graphical representation of changes in expression levels of Cx43 in Ang II-stimulated cardiac fibroblasts. α-Tubulin was used as the loading control. Significance was determined by Student's t-test, ** represents $p<0.01$. Data are representative of three independent experiments (n=3, Mean $\pm$ SD).

4.12 TGF-β1 upregulates the expression of Cx43

Cx43 expression was probed following treatment of cardiac fibroblasts with TGF-β1(10ng/ml) for 24 hours. TGF-β1treatment for 24 hours resulted in a significant upregulation of Cx43 expression (Figure 34). As the Ang II effect is mediated by TGF-β1, as evident from our previous data, TGF-β1 was used as a profibrotic stimulus in subsequent experiments.

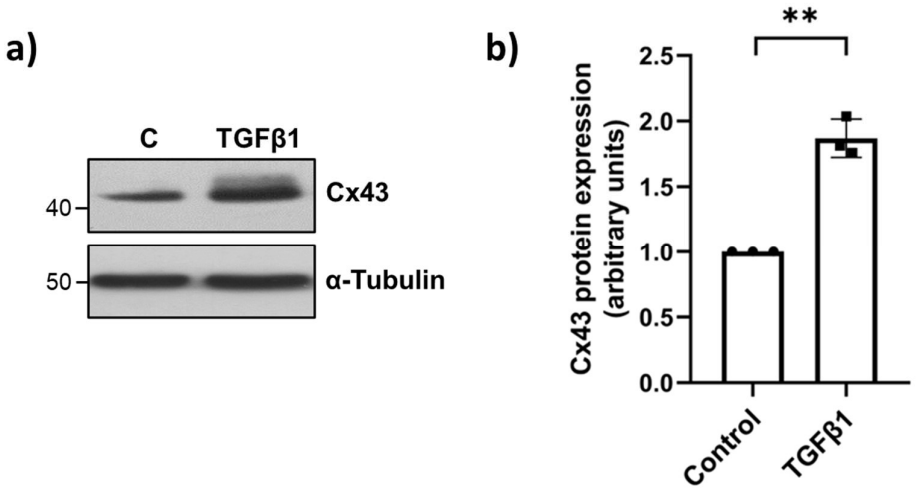

Fig 34: (a) Expression of Cx43 in TGF-β1-stimulated cardiac fibroblasts (b) Graphical representation of changes in expression levels of Cx43 in TGF-β1-stimulated cardiac fibroblasts. α-Tubulin was used as loading control Significance was determined by Student's t-test, ** represents $p<0.01$. Data are representative of three independent experiments (n=3, Mean $\pm$ SD).

4.13 POSTN-mediates TGF-β1-stimulated upregulation of Cx43

We examined whether POSTN silencing in the presence of TGF-β1 affects Cx43 expression. Our findings revealed that POSTN knockdown led to reduced Cx43

expression in TGF-β1-stimulated cells, suggesting that POSTN may regulate Cx43 expression independently of TGF-β1 stimulation. This conclusion was further supported by immunofluorescence staining data, which corroborated the observed decrease in Cx43 expression upon POSTN knockdown (Figure 35).

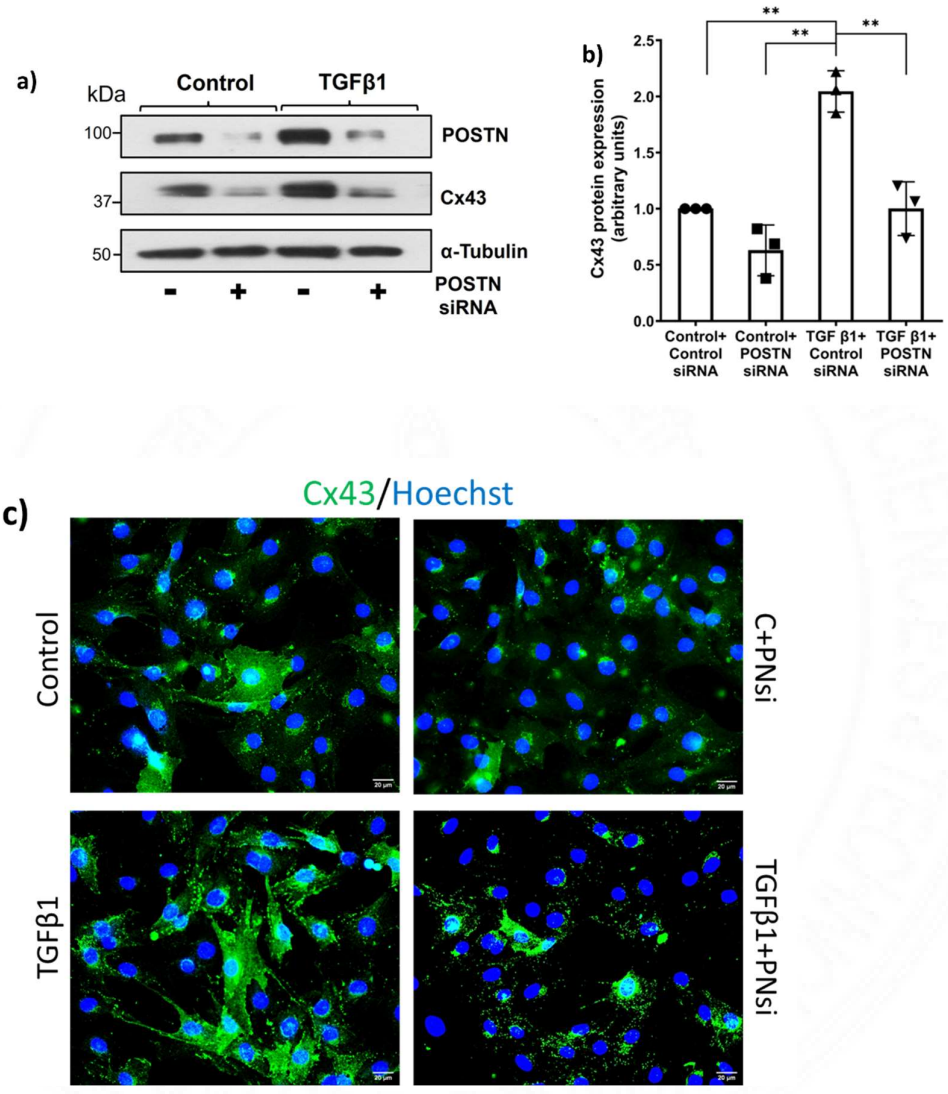

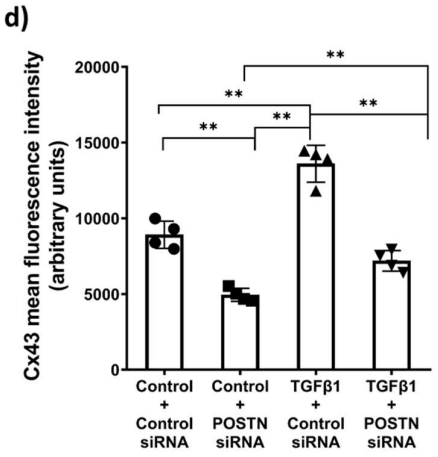

Fig 35: (a) Expression of Cx43 in POSTN-silenced TGF-β1-stimulated cardiac fibroblasts. (b) Graphical representation of changes in expression levels of Cx43 in POSTN-silenced TGF-β1-stimulated cardiac fibroblasts. α-Tubulin was used as the loading control. **represents $p<0.01$. Data are representative of three independent experiments (n=3; Mean $\pm$ SD). (c) Immunofluorescence staining of Cx43 in POSTN-silenced TGF-β1-stimulated cardiac fibroblasts. Cx43 was stained green with Alexa Fluor 488 and the nuclei were counterstained with Hoechst dye (blue). Scale bar 20μm. (d) Graphical representation of the change in Cx43 mean fluorescence intensity in POSTN-silenced TGF-β1-stimulated cardiac fibroblasts. Five different fields from each of the four different samples were used for the quantification of the immunofluorescence images. Significance was determined using two-way ANOVA with Tukey's multiple comparison test. **represents $p<0.01$. Data are representative of four independent experiments, (n=4, Mean $\pm$ SD).

4.14 POSTN has a role in modulating Cx43 activity

To further confirm that Cx43 activity was attenuated following POSTN silencing, functional assays were conducted using the Lucifer Yellow dye transfer activity assay. The results demonstrated a significant increase in the distance travelled by the dye in cardiac fibroblasts stimulated with TGF-β1, which was substantially diminished upon POSTN silencing, indicating a marked reduction in Cx43 activity (Figure 36).

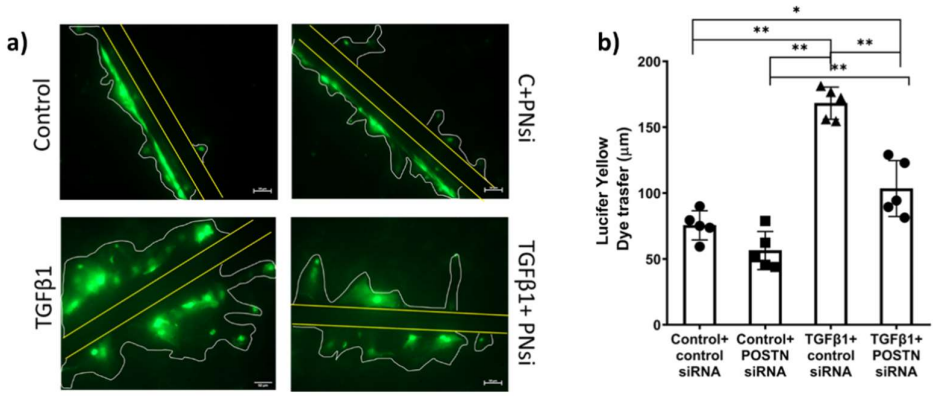

Fig 36: (a) Lucifer Yellow dye transfer activity assay in POSTN-silenced TGFβ1-stimulated cardiac fibroblasts. The straight line represents the scraped region where Lucifer Yellow dye was introduced. The curved line indicates the trajectory of the dye movement. The green coloration denotes the transfer of Lucifer Yellow dye through gap junctions. Scale bar 50µm. (b) Graphical representation of the distance travelled by the dye in POSTN-silenced TGF-β1-stimulated cardiac fibroblasts. Significance was determined using two-way ANOVA with Tukey's multiple comparison test. * represents $p<0.05$ and ** represents $p<0.01$. Data are representative of five independent experiments (n=5, Mean ± SD).

4.15 POSTN-mediates Cx43 via ERK 1/2 MAPK

To investigate the mechanisms mediating POSTN-dependent Cx43 expression, the role of ERK1/2 MAPK was analysed. Given the earlier observation that ERK1/2 MAPK is activated downstream of POSTN in response to TGF-β1, its involvement in Cx43 regulation was explored further. siRNA-mediated knockdown of POSTN resulted in a significant reduction in pERK 1/2 in TGF-β1-stimulated cardiac fibroblasts, suggesting that POSTN mediates ERK 1/2 activation. Additionally, silencing of ERK1/2 using a specific siRNA led to a marked decrease in Cx43 expression, indicating that ERK1/2 MAPK acts downstream of POSTN in the regulation of Cx43 expression in response to TGF-β1 stimulation (Figure 37).

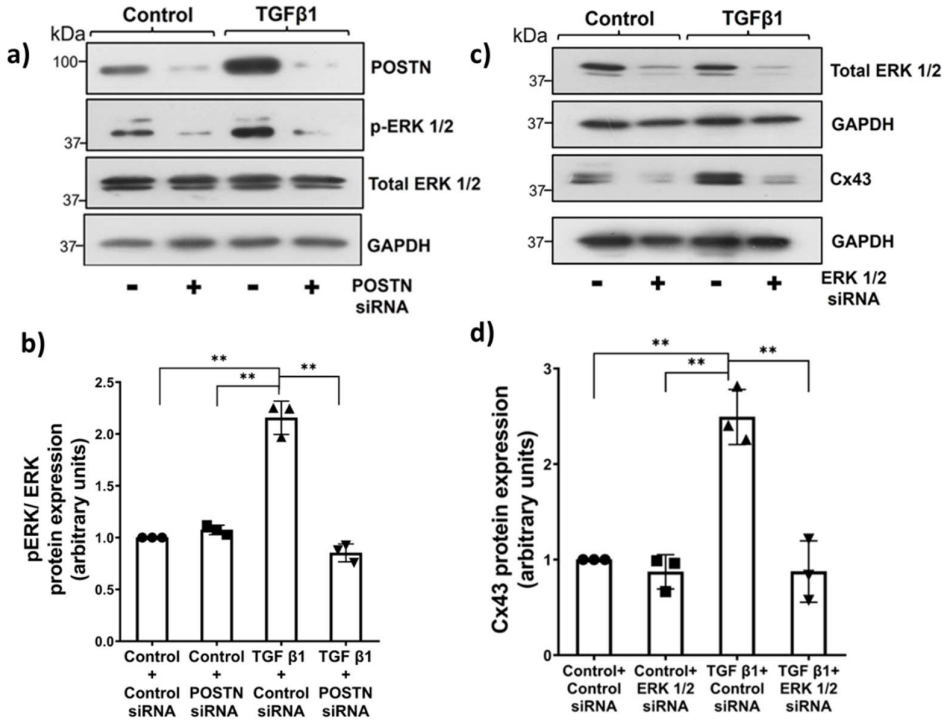

Fig 37: (a) Expression of pERK 1/2 in POSTN-silenced TGF-β1-stimulated cardiac fibroblasts. (b) Graphical representation of the changes in pERK 1/2 expression in POSTN-silenced TGF-β1-stimulated cardiac fibroblasts. (c) Expression of Cx43 in ERK1/2 MAPK-silenced TGFβ1-stimulated cardiac fibroblasts. (d) Graphical representation of changes in Cx43 expression in ERK1/2 MAPK-silenced TGF-β1-stimulated cardiac fibroblasts. GAPDH was used as a loading control, and significance was determined using two-way ANOVA with Tukey's multiple comparison test. ** represents $p<0.01$. Data are representative of three independent experiments (n=3, Mean $\pm$ SD).

4.16 SRF mediates the transcriptional regulation of Cx43

Based on the earlier observation that SRF are activated downstream of POSTN, the involvement of SRF in Cx43 regulation was investigated. In addition, bioinformatics analysis using ALGGEN PROMO identified 1 binding site for the transcription factor SRF (CC(A/T)6GG) in the 550 base pair upstream of the transcription start site in the promoter region of the Cx43 gene. Our data indicated that POSTN silencing in TGFβ1-stimulated cardiac fibroblasts reduced SRF expression, whereas SRF knockdown resulted in the reduction of TGF-β1-stimulated elevation of Cx43 expression (Figure 38).

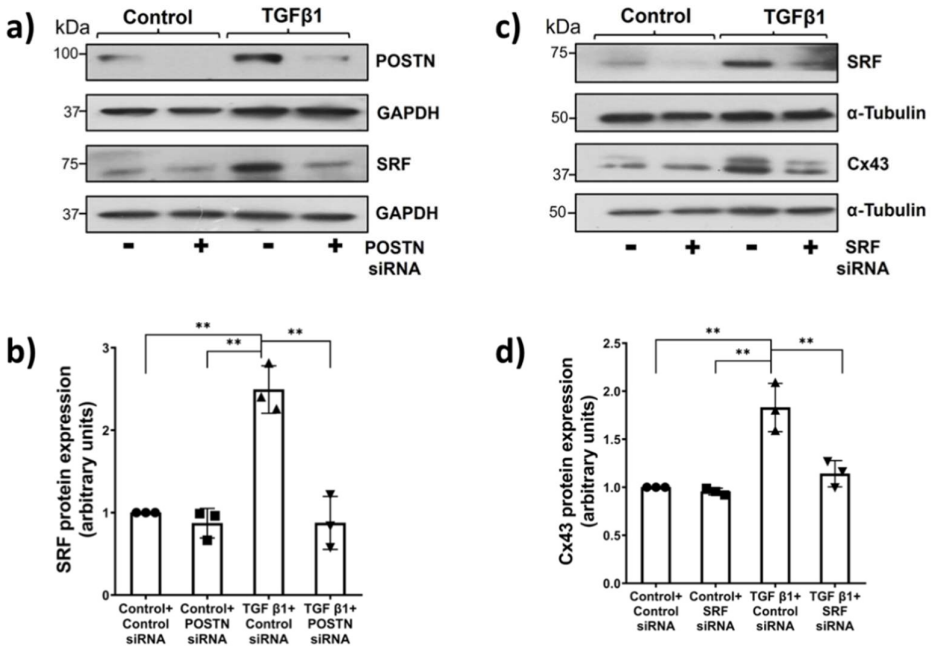

Fig 38: (a) Expression of SRF in POSTN-silenced TGF-β1-stimulated cardiac fibroblasts. (b) Graphical representation of the changes in SRF expression in POSTN-silenced TGF-β1-stimulated cardiac fibroblasts. (c) Expression of Cx43 in SRF-silenced TGF-β1-stimulated cardiac fibroblasts. (d) Graphical representation of changes in Cx43 expression in SRF-silenced TGF-β1-stimulated cardiac fibroblasts. α-Tubulin and GAPDH were used as loading control. Significance was determined using two-way ANOVA with Tukey's multiple comparison test. ** represents $p<0.01$. Data are representative of three independent experiments (n=3, Mean $\pm$ SD).

Schematic diagram based on the findings presented above

Based on the findings presented, POSTN has an obligate role in TGF-β1-stimulated upregulation of Cx43 expression (Figure 39)

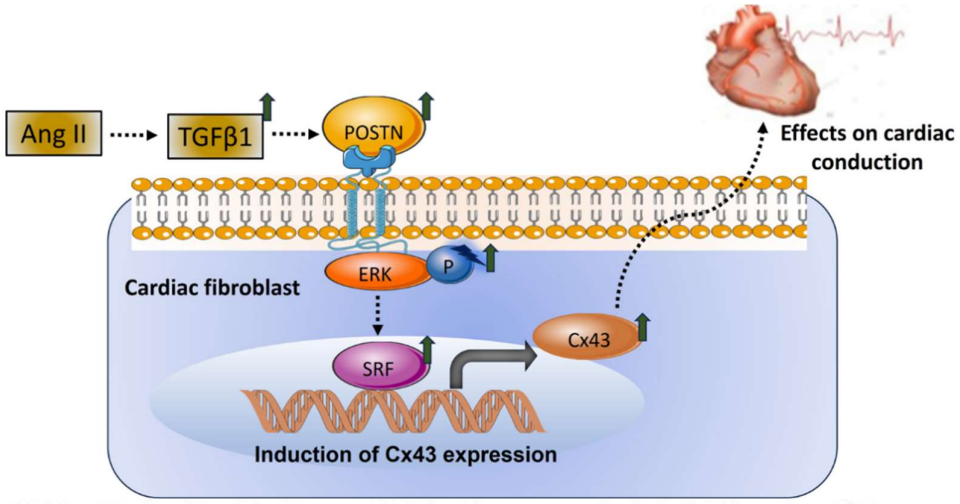

Fig 39: Schematic representation of POSTN-mediated regulation of Cx43 in response to Ang II and TGF-β1

OBJECTIVE 3

Correlating the levels of POSTN, LOX, and Cx43 in a rat model of myocardial infarction

The third objective of the study was to demonstrate the correlation between POSTN, LOX, and Cx43 expression in a rat model of myocardial infarction.

4.17 Induction of MI in Rats

Male Wistar rats (10-12 weeks old) were anesthetized for surgical procedures. Electrocardiography (ECG) (Figure 40a) and Echocardiography (Echo) (Figure 40b) were conducted to assess baseline cardiac function. Tracheostomy was then performed (Figure 40c-e) to facilitate mechanical ventilation. MI was induced surgically via parasternal thoracotomy (Figure 40f) by ligating the LAD coronary artery (Figure 40g-h). Successful induction of MI was confirmed visually by observing myocardial

blanching distal to the ligation site (Figure 40i). After completing the procedure, the chest wall was closed (Figure 40j) and the animals were ventilated until spontaneous breathing was restored.

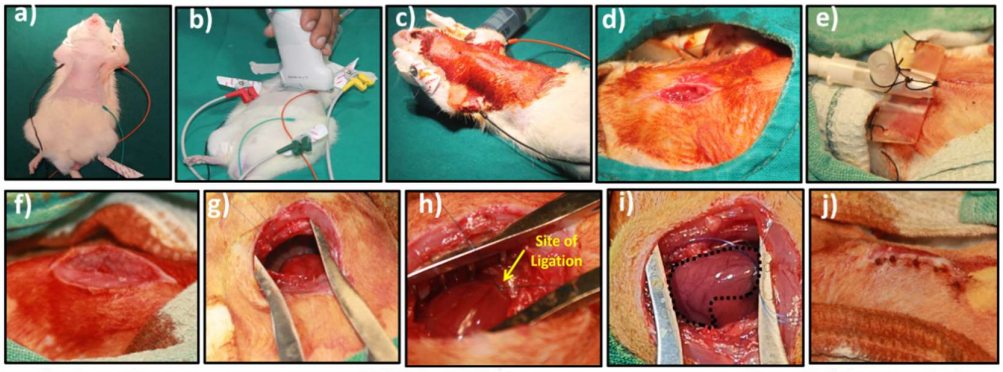

Fig 40: Experimental procedure for myocardial infarction induction (a) ECG) was performed to assess baseline cardiac electrical activity (b) Echo was conducted to evaluate baseline cardiac structure and function (c-e) Tracheostomy was performed to enable mechanical ventilation during the procedure (f) MI was surgically induced via a parasternal thoracotomy (g-h) LAD coronary artery was ligated to occlude blood flow (i) The development of MI was visually confirmed by myocardial blanching (j) The chest wall was closed following the procedure.

4.18 Morphological analysis of retrieved heart

The rats were euthanized and gross lesions were examined after 4 weeks of MI induction. Gross morphology of the MI heart revealed the presence of an infarct scar. The affected tissue was characterized by a fibrotic and pale-yellow appearance. Cardiac wall thinning was evident in the MI region compared with the surrounding

healthy myocardium, indicative of tissue remodelling and scar formation following ischemic injury.

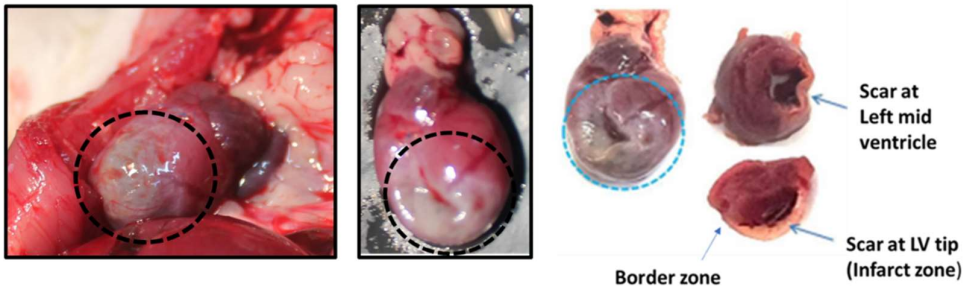

Fig 41: Representative photograph of the heart collected four weeks after MI induction, highlighting the gross morphological changes associated with infarct formation and remodelling. The first two were fresh images of the retrieved heart soon after autopsy. The third and fourth images of a formalin-fixed MI heart display cross-sections of the ventricle, highlighting structural changes associated with infarct formation, characterized by a prominent white scar and subsequent remodeling.

4.19 ECG and Echocardiographic recordings exhibited pathological remodelling post-MI with a reduction in wall movement and ejection fraction

MI was confirmed by variations in ECG and echocardiographic recordings. A representative ECG from an MI rat showing Baseline ECG recordings, ECG at MI, post 1-week and at 4-weeks is shown in Figure 41a-d. Sinus rhythm was observed in ECG readings at baseline (Figure 42a). At MI, ECG recordings showed bradycardia and atrial fibrillation with complete AV block. A pathological Q wave was also detected. This result confirmed the induction of MI (Figure 42b). ECG recording at 1-week post-MI demonstrated a Qr pattern. Sinus tachycardia with ST elevation was also

observed (Figure 42c). The 4-week post-MI ECG readings showed sinus rhythm with a Qr pattern and T-inversion, indicating evolved MI (Figure 42d). Baseline M-mode echocardiogram, M-mode echocardiogram post-1-week and at 4-weeks are represented in Figure 42e-g.

The baseline echocardiographic results showed normal contractility with good LV function (Figure 42e). At 1-week post-MI, mild LV dysfunction was evident, which became severe at the end of 4-weeks. Increased left ventricular wall movement was observed in the 1-week echocardiographic data, confirming tachycardia (Figure 42f). An increase in left ventricular internal diameter at end-diastole (LVIDd) and left ventricular internal diameter at end-systole (LVIDs) with a reduction in left ventricular wall movement was observed at 4-weeks post-MI (Figure 42g) compared to the baseline condition. Post-MI echocardiographic data showed that the change in ejection fraction from pre-MI to post-MI was 36.9%+15.5, and the change in fractional shortening was 23.94%+5.3 at 4-weeks.

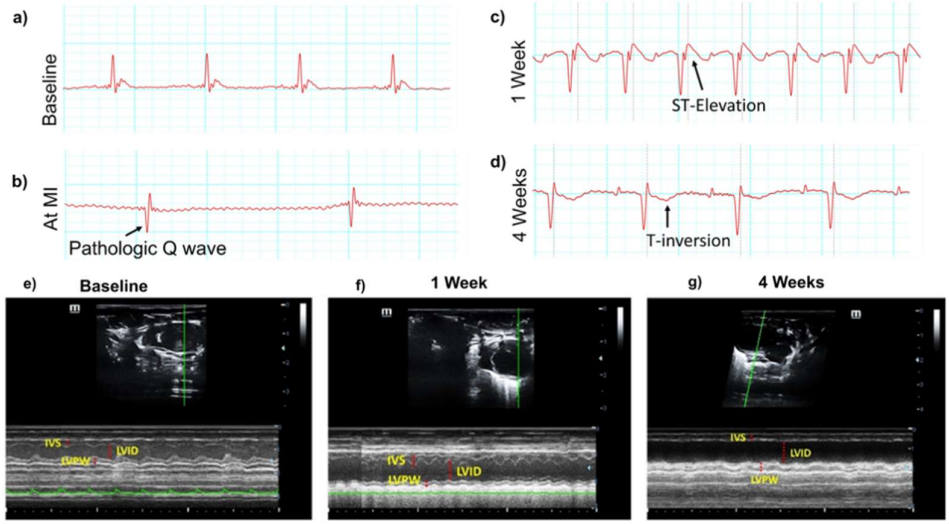

Fig 42: Representative ECG and Echo recordings at Baseline and Post-MI. (a) Representative ECG at baseline (b) at MI (c) 1 week after MI (d) 4-weeks after MI. Representative baseline M-mode echocardiogram in parasternal long-axis view (e) prior to MI (f) at 1-week post-MI and (g) at 4-weeks post-MI. IVS -interventricular septum, LVID- Left ventricle internal diameter and LVPW- Left ventricle posterior wall

4.20 Post-MI histology demonstrated a progressive worsening in LV remodelling

H&E staining of infarcted rat heart tissues at 4-weeks demonstrated LV wall thinning with extensive myocyte damage, interstitial edema, and vasculitis. Infiltration of spindle-shaped cardiac fibroblasts involved in the repair process was observed as depicted with black arrows (Figure 43a). Excessive collagen deposition was apparent in picrosirius red staining in the infarct area and border zone. Almost the entire infarct scar was found to accumulate collagen, and quantitative analysis of picrosirius red staining indicated a 25% increase in collagen in the MI samples compared to the control (Figure 43b-c). Collagen visualization by picrosirius red staining under polarized light showed the presence of long and highly aligned mature collagen bundles that appeared birefringent in reddish-orange color within the scar tissue and at the border zone, in contrast to the control tissue with no infarct that did not display any birefringence (Figure 43d).

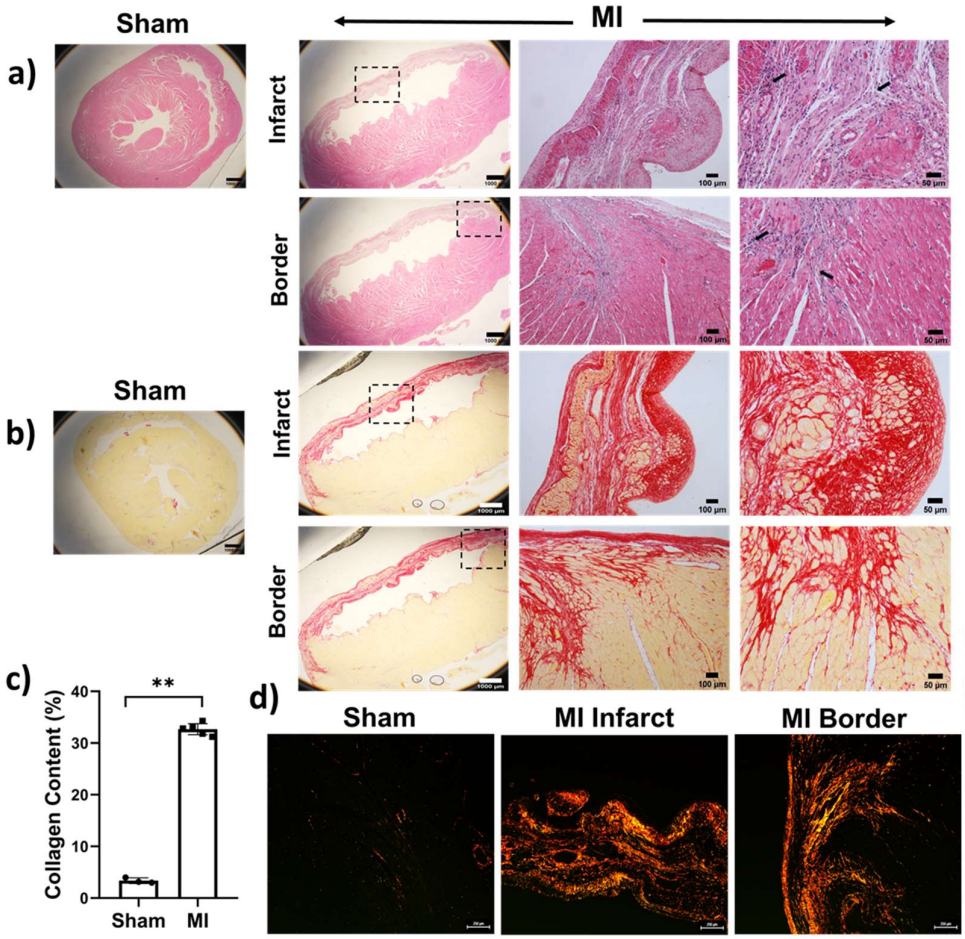

Fig 43: Histology of heart sections from control and MI rats at 4 weeks post-MI. (a) Representative images of H&E staining of control and MI rats at 4 weeks indicated ventricular wall thinning and the presence of spindle-shaped cardiac fibroblasts in the scar tissue. The arrows indicate infiltrating spindle-shaped cardiac fibroblasts involved in myocardial repair. Representative picrosirius red staining of the heart taken in bright-field mode showing collagen deposition in red. The second and third panel images of MI indicate higher magnifications of the region of interest in the infarct zone, denoted by dotted squares. Scale bars indicate 1000, 100 and 50µm. (c) Graphical representation of percentage collagen content from quantitative analysis of

picrosirius red staining using ImageJ in control and MI rats. (d) Picrosirius red staining under polarized light for birefringence detection indicated by a reddish-orange color, showing the presence of mature aligned collagen fibers in the scar of MI rats at 4 weeks. Significance was determined by Student's t-test; ** represents $p<0.01$, Mean ± SD (n=3 for sham, n=6 for MI).

4.21 POSTN and LOX expression was upregulated within the collagen-rich scar tissue at the infarct zone

Immunohistochemical analysis of ventricular tissue sections using an anti-POSTN antibody demonstrated a significant increase in POSTN expression, specifically within the collagen-rich scar tissue of MI-rat. Notably, LOX expression was also higher in infarcted scars. The expression of both POSTN and LOX was negligible in control samples. Following the above observation, profibrotic markers such as α-SMA and collagen type I were found to be elevated in the infarct LV of MI rats. α-SMA was observed around vessels in the control sample, however in the MI sample it was observed both in the infarct zone and around blood vessels. Prominent CX43 positive staining was observed in the ID disc at the cell junctions between myocytes in the control. However, total Cx43 staining was reduced within the scar in the MI group due to loss/ damage of cardiomyocytes following MI. However, Cx43 staining was seen localized mainly to areas with high cardiac fibroblast density in the MI group (Figure 44).

Western blot analysis of ventricular tissue from an in vivo rat model of MI revealed a significant elevation in the protein expression of both POSTN and LOX. Concomitant

with the above observation, profibrotic factors such as collagen Type I and α-SMA were elevated in the infarct LV area. TGF-β, pERK, and SRF were also increased in the infarcted LV (Figure 45). These findings implicate a possible association between POSTN, LOX, and Cx43 in post-MI pathological remodeling.

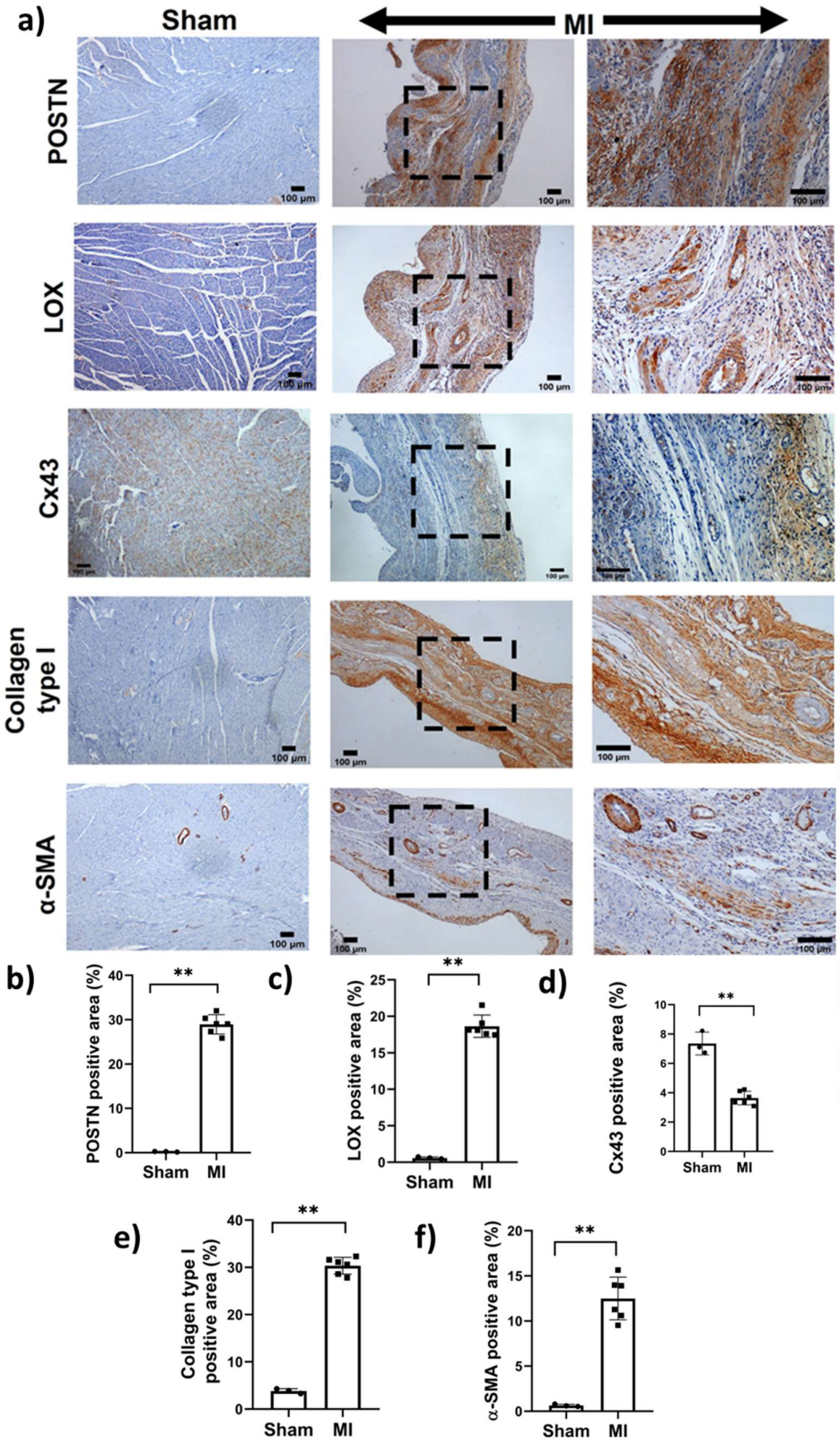
a)
Sham
MI
POSTN
LOX
Cx43
Collagen type I
α-SMA
100 µm
b)
POSTN positive area (%)
c)
LOX positive area (%)
d)
Cx43 positive area (%)
e)
Collagen type I positive area (%)
f)
α-SMA positive area (%)
**
Sham
MI

Fig 44: Immunostaining of ventricular sections of control and MI rat hearts at 4 weeks post-MI. (a) Representative Images of immunostaining for POSTN, LOX, Cx43, Collagen type I, and α-SMA present in the ventricle of control and ventricular scars of MI rats at 4 weeks. The positive region is indicated by the brown color of the DAB staining. The second and third panels of the MI images indicate higher magnifications of the region of interest in the infarct zone, denoted by a dotted square. Scale bar is 100 μm. (b-e) Graphical representation of the percentage of POSTN, LOX, Cx43, Collagen type I, and α-SMA from quantitative analysis of immunostaining in control and MI rats. Significance was determined by Student's t-test; ** represents $p<0.01$, mean $\pm$ SD (n=3 for sham, n=6 for MI).

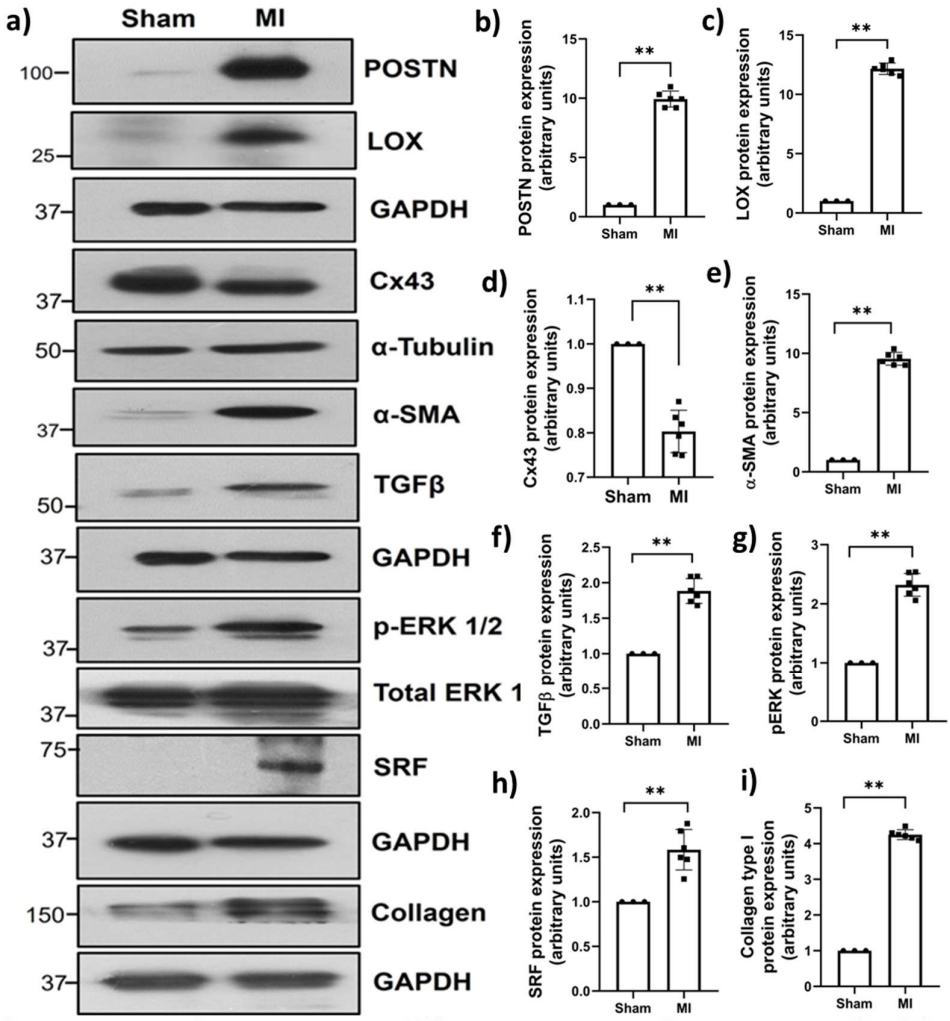

Fig 45: (a) Protein expression of POSTN, LOX, Cx43, Collagen type I, TGF-β, pERK1/2, ERK1/2, α-SMA and SRF at 4 weeks. (b-i) Graphical representation of changes in the expression levels for POSTN, LOX, Cx43, Collagen type I, TGF-β, pERK1/2, ERK1/2, α-SMA and SRF. α-Tubulin and GAPDH were used as loading control. Significance was determined by Student's t-test; ** represents $p<0.01$, mean $\pm$ SD (n=3 for sham, n=6 for MI).

CHAPTER 5

DISCUSSION

Myocardial injury refers to damage to the cardiac muscle, often resulting from ischemia and an inadequate supply of oxygen and nutrients due to reduced or obstructed blood flow. Following myocardial injury, a series of intricate cellular responses are triggered, particularly within cardiomyocytes and cardiac fibroblasts, leading to myocardial remodelling (Tallquist and Molkentin, 2017). Cardiomyocytes typically respond to stress or injury via hypertrophy or apoptosis.

In contrast, cardiac fibroblasts, which are normally phenotypically quiescent, are activated in response to injury and undergo phenotypic transformation into myofibroblasts. Over time, myofibroblasts resist apoptosis and persist at the site of injury, leading to excessive collagen deposition and the development of cardiac fibrosis. Although, initial fibroblast activation, proliferation, and collagen deposition generates scar tissue that protects the cardiac wall from rupture, their persistent activation in the scar, excessive collagen deposition, and crosslinking are overwhelmingly pathological (Frangogiannis, 2021). Cardiac wall stiffening and conduction abnormalities are two major long-term consequences of cardiac fibrosis that result in heart failure.

Currently, one of the main approaches for treating adverse myocardial remodelling following MI is to inhibit the action of Ang II (Nakamura et al., 2003). Ang II has been implicated as a significant contributor in cardiac remodelling, exerting pleiotropic effects on cardiac fibroblasts. It is a key regulator of activation (Porter and Turner, 2009), migration (Siddesha et al., 2013), and collagen secretion (Gao et al., 2009; Lijnen et al., 2001) in cardiac fibroblasts. However, the effectiveness of Ang II inhibition is limited (Iwanami et al., 2009). Therefore, it is necessary to explore the

molecular basis of cardiac fibrosis and identify other alternate therapeutic targets for the treatment of cardiac fibrosis.

Excessive crosslinking of the collagen leads to stiffening of the ventricular wall, compromising its ability to contract effectively. Hence, modulation of collagen crosslinking would be a favourable approach in the treatment of cardiac fibrosis. Although the expression of collagen type I, which is the primary extracellular matrix protein in the heart and a crucial component in scar tissue formation after injury, has been extensively studied (Goldstein and Frishman, 2021; López et al., 2006; Querejeta et al., 2004), the role of collagen crosslinking, particularly in the context of elevated levels of LOX in the development of heart failure, has not been explored (López et al., 2012, 2016).

The upregulation of Cx43 in cardiac fibroblasts following myocardial injury plays a critical role in the development of conduction abnormalities. Cx43 facilitates intercellular communication between cardiomyocytes, ensuring coordinated electrical signalling throughout the myocardium. However, the excessive expression of Cx43 in activated cardiac fibroblasts can disrupt normal conduction pathways, leading to arrhythmias and impaired electrical conduction (Fontes et al., 2012). Although the association between Cx43 expression and intercellular communication has been widely studied (Fontes et al., 2012; Zhang et al., 2010), the specific mechanisms by which altered Cx43 expression in cardiac fibroblasts post-MI contributes to the progression of conduction abnormalities in heart failure remain inadequately explored.

Admittedly, understanding the mechanisms that regulate LOX and Cx43 expression in fibroblasts following injury could identify potential therapeutic targets for managing fibrotic disease progression. While prior studies have implicated POSTN in collagen cross-linking within the bone and skin, they have primarily emphasized its role as a scaffolding protein that facilitates BMP-1 recruitment to a fibronectin-rich matrix, thereby catalytically activating LOX (Maruhashi et al., 2010; Norris et al., 2007; Snider et al., 2008). Little is explored on the role of POSTN in the transcriptional regulation of LOX and in the regulation of Cx43 protein expression in cardiac fibroblasts and the exact underlying mechanisms remain largely obscure. Hence, we investigated the relationship between POSTN, LOX, and Cx43 and their implications in cardiac wall stiffening and conduction abnormalities.

Cardiac fibroblasts isolated from young adult rats demonstrated preferential adherence to culture plates within 2.5 hours, a characteristic property commonly used to distinguish fibroblasts from other cardiac cell types, such as endothelial cells and cardiomyocytes. These cells exhibited characteristic spindle-shaped morphology and were positively stained for key markers, including the cytoskeletal and mesenchymal protein vimentin, the collagen receptor DDR2, and PDGFRα, a well-recognized marker for resident cardiac fibroblasts. This expression profile strongly supports their identity as cardiac fibroblasts. The potential contamination of endothelial cells at passage 0 was eliminated through serial passaging, which facilitated enrichment of a pure population of cardiac fibroblasts. The absence of von Willebrand factor (VWF), an endothelial cell marker, in passage 2 cells further confirmed the lack of endothelial contamination, ensuring a relatively pure culture.

Initially, we investigated whether Ang II, a potent pro-fibrotic stimulus known to be upregulated following myocardial injury, contributes to the enhanced expression of POSTN and LOX. To address this, a time-course study was conducted using 1 μM Ang II at intervals of 6, 12, 24, and 48 hours. The results revealed that both POSTN and LOX expression levels were significantly elevated at 24 and 48 hours, with the most pronounced upregulation observed at 24 hours. Based on these findings, the 24-hour time point was selected for subsequent experiments to investigate the regulatory role of POSTN in LOX expression. Similar observations have been reported for the upregulation of POSTN and LOX in cardiac fibroblasts and rat kidney tubule epithelial cells (Li et al., 2011; Zhang et al., 2022). In addition, previous studies from our laboratory (George et al., 2016; V et al., 2019) and others (Li et al., 2011) have demonstrated that Ang II at 1uM concentration is optimal for investigating profibrotic gene expression. Based on this evidence, we selected this concentration for the present study.

Ang II acts via its receptor AT1 to activate most of its profibrotic effects (Higuchi et al., 2007). Inhibiting the activity of AT1 using candesartan, a potent inhibitor of the AT1 receptor, decreased both POSTN and LOX expression, confirming that Ang II-mediated upregulation occurs through its receptor AT1.

To further elucidate the regulatory role of POSTN in LOX expression in Ang II-stimulated cardiac fibroblasts, we investigated changes in the expression levels of both LOX mRNA and protein. Silencing of POSTN resulted in a significant reduction in LOX mRNA expression, demonstrating that POSTN regulates LOX at the transcriptional level. It is pertinent to note that the LOX protein exists in two forms:

an unprocessed precursor (~47 kDa) and a mature, enzymatically active form (~32 kDa). In this study, we focused on the mature form of LOX (approximately 32 kDa). POSTN silencing led to a decrease in LOX protein expression, specifically its mature, enzymatically active, and processed form, with a molecular weight of approximately 32 kDa. Thus, the observed reduction in both LOX mRNA and mature LOX protein conclusively highlights the obligatory role of POSTN in regulating LOX expression in Ang II-mediated cardiac fibroblasts.

In tandem with the observed decrease in the mature, enzymatically active form of the LOX protein upon POSTN silencing, our study also detected a significant reduction in LOX enzymatic activity in POSTN-silenced cardiac fibroblasts. This decrease in LOX activity underscores the critical role of POSTN in facilitating collagen crosslinking in Ang II-mediated cardiac fibroblasts. While we acknowledge that direct measurements of crosslinked collagen were not performed, this limitation arises from the challenge of detecting crosslinked collagen content in Ang II-treated or POSTN-silenced cells within a 24-hour time frame. Collagen crosslinking typically requires prolonged culture duration, which is beyond the scope of the current experimental design.

Previous studies from our lab have demonstrated that TGF-β1 acts downstream of Ang II in cardiac fibroblasts. Hence, we investigated whether TGF-β1, a potent pro-fibrotic stimulus, also influences the expression of POSTN and LOX. Our results revealed that TGF-β1 significantly upregulated both POSTN and LOX at 24 hours. To determine whether the effects of Ang II on POSTN and LOX are mediated via TGF-β1, we silenced TGF-β1 in Ang II-stimulated cardiac fibroblasts. Silencing of TGF-β1 led to a marked reduction in the expression of both POSTN and LOX, confirming that TGF-

β1 functions downstream of Ang II in the regulation of LOX by POSTN. Supporting these findings, Carrasco et al. reported that losartan reduced LOX expression via TGF-β1 and CTGF in an experimental model of hypertension with myocardial fibrosis, further highlighting the critical role of this signaling axis in profibrotic pathways. Carrasco et al (Miguel-Carrasco et al., 2017) have shown that Losartan metabolite reduces the expression of LOX via TGF-β1 and CTGF in an experimental model of hypertension with myocardial fibrosis.

Next, we investigated whether Ang II and TGF-β1 enhance Cx43 expression. Our findings demonstrated that both Ang II and TGF-β1 significantly upregulated Cx43 expression in cardiac fibroblasts at 24 hours. Given that Ang II exerts its effects through TGF-β1 as evident from our previous data, TGF-β1 was used as profibrotic stimulus in subsequent experiments. Previous reports have also emphasized the pivotal role of TGF-β1 in Cx43 expression. *Zhang et al.,* have observed that TGF-β1 induced an increase in Cx43 expression in cardiac fibroblasts (Zhang et al., 2010). Our findings are also consistent with those of *Salvarani et al.,* who reported a 5-fold enhancement in gap junctional coupling between TGF-β1-depolarized cardiomyocytes and coupled myofibroblasts, as reflected by increased Cx43 expression (Salvarani et al., 2017). Interestingly, POSTN knockdown abolished TGF-β1-stimulated upregulation of Cx43, as evidenced by decreased Cx43 expression. This observation was further corroborated by immunostaining, which revealed a decrease in the total fluorescence intensity of Cx43 in POSTN-silenced cells, confirming the reduced Cx43 expression.

Consistent with the observed reduction in Cx43 expression, POSTN silencing abolished gap junctional coupling mediated by Cx43 in TGF-β1-stimulated cardiac

fibroblasts. Gap junctional coupling capacity was assessed using a dye transfer assay, which relies on the passage of Dilithium salt of Lucifer Yellow hydrazine. Given its impermeability to the cell membrane and low molecular weight (457 Da), Lucifer Yellow can only transfer from dye-loaded cells into adjacent cells through functional gap junctional channels. Upon POSTN silencing, a decrease in the distance of Lucifer Yellow dye transfer was observed, indicating reduced gap junctional coupling, which is indicative of decreased Cx43 activity. Collectively, these results strongly support a crucial regulatory role of POSTN in both Cx43 expression and functional activity.

Having established that POSTN mediates LOX and Cx43 expression in cardiac fibroblasts, we delved into the underlying molecular mechanisms. Myocardial injury triggers the activation of various signalling pathways that orchestrate collagen remodelling. Although POSTN has been implicated in modulating collagen remodelling through pathways such as SMAD2/3, FAK, and AKT (Kumar et al., 2018; Ma et al., 2020; Shimazaki et al., 2008), our results indicate that FAK is not activated downstream of POSTN. Activation of LOX by TGF-β1 through the Smad2/3 signalling pathway has been previously reported (Lu et al., 2019). Considering that TGF-β1 acts downstream of Ang II, we investigated the involvement of the non-canonical TGF-β1-activated pathways. The ERK1/2 MAPK pathway, a key downstream effector of TGF-β1, has been implicated in the progression of cardiac fibrosis (Kong et al., 2014). Notably, TGF-β1 is capable of activating all three major MAPK pathways: extracellular signal-regulated kinase (ERK), p38 mitogen-activated protein kinase (p38 MAPK), and c-Jun N-terminal kinase (JNK). Signalling through these pathways can exert both Smad-dependent and Smad-independent effects in

mediating TGF-β1 response (Biernacka et al., 2011). Our findings showed that downstream of POSTN, the ERK1/2 MAPK pathway was activated, which facilitated the enhanced expression of both LOX and CX43 in cardiac fibroblasts. In addition, ERK1/2 silencing abolished Ang II- and TGF-β1-induced expression of LOX and Cx43. This indicates the vital role of ERK1/2 in mediating collagen crosslinking and cardiac conduction, confirming that the ability of Ang II and TGF-β1 to induce LOX and Cx43 expression was dependent on ERK signalling. These observations need to be considered in tandem with a previous report showing that LOX is regulated by the β-arrestin-ERK-STAT3 pathway in renal fibrosis (Zhang et al., 2022). However, in this study, the critical role of POSTN in regulating ERK was not investigated. To the best of our knowledge, the present study is the first to demonstrate an obligate regulatory role of POSTN in mediating the expression of LOX and Cx43, thereby influencing collagen crosslinking and cardiac conduction within cardiac fibroblasts.

Probing further downstream into the regulatory mechanisms of POSTN, we found that POSTN activates SRF downstream of the ERK1/2 MAPK pathway to enhance the expression of LOX and Cx43. The significance of SRF in promoting myofibroblast differentiation and consequent tissue fibrosis has been well established (Chai et al., 2007; Small, 2012). Additionally, bioinformatic analysis revealed two putative binding sites for SRF (CC(A/T)6GG) within the LOX promoter and one within the Cx43 promoter, located upstream of their respective transcription start sites. Our results showed that SRF was decreased upon POSTN and ERK1/2 silencing, indicating that SRF acts downstream of the POSTN and ERK1/2 MAPK pathways. Consequent downregulation of SRF by either inhibiting with CCG-1423 or silencing

with specific siRNA reduced the expression of LOX and Cx43. Together, these results demonstrate the role of SRF in the transcriptional regulation of LOX and CX43 in cardiac fibroblasts. Previous studies have corroborated our finding that SRF functions as a transcription factor for both LOX (Santos et al., 2019) and Cx43 (Hirschi et al., 2003; Li et al., 2017). However, this study did not provide conclusive experimental evidence for SRF-promoter interactions for LOX and Cx43 using chromatin immunoprecipitation (ChIP) assays.

Having established the regulatory relationship between POSTN, LOX, and Cx43 in Ang II-and TGF-β1-stimulated cardiac fibroblasts, we further evaluated their functional significance in a rat model of MI. Specifically, we attempted to correlate the expressions of POSTN, LOX, and Cx43 in collagen-rich infarct scar MI rats. ECG and Echocardiography data indicated MI and cardiac remodelling in MI rats. 1-week and 4-weeks post-MI demonstrated Qr pattern, sinus tachycardia with persistent ST elevation. Persistent ST elevation at 1-week suggested LV remodelling. ST elevation was not marked at MI induction, possibly because of the rhythm being an escape rhythm due to a complete heart block. Furthermore, post-MI echocardiographic recordings exhibited a dilated ventricle cavity, reduced LV wall movement, ejection fraction, and fractional shortening, indicating a progressive worsening of LV function. Besides the above observation, pathological remodelling was also evident in H&E and picrosirius red staining which demonstrated, myocyte damage, infiltration of cardiac fibroblasts and extensive collagen deposition. Collagen birefringence in orange-red under the Polarizer analyser confirmed that the infarct scar is accumulated with

crosslinked collagen bundles. Collectively, these findings confirmed the occurrence of pathological remodelling in a rat model of MI.

Consistent with the above observation, our immunohistochemistry and western blot data indicated increased expression of POSTN and LOX in the collagen-rich infarct scar. This observation was also positively correlated with increased levels of myofibroblast proteins, such as Collag en type-I and α-SMA, in the infarcted ventricular wall. A surge in the levels of POSTN and LOX at the site of infarction was also evident in the border zone. However, total Cx43 expression was decreased in the western blot and was reduced within the collagen-rich scar tissue at the infarct zone in the IHC analyses. In healthy cardiac tissues, Cx43 is predominantly expressed in the cardiomyocytes. Following MI, the loss of cardiomyocytes within the infarct zone leads to a reduction in the total Cx43 expression in the tissue, as evidenced by western blot analysis. However, Cx43 expression was primarily confined to areas enriched with cardiac fibroblasts. Interestingly, Cx43 staining was mainly localized in areas with high cardiac fibroblast density in the MI group. Furthermore, western blot analysis of the infarct scar tissue demonstrated the role of TGF-β1, ERK, and SRF in mediating collagen crosslinking and cardiac conduction, as evidenced by the increased expression in the infarct zone. These findings also validate our in-vitro observation. Therefore, we speculate that POSTN regulates LOX and Cx43 by activating ERK 1/2 MAPK and SRF, which in turn leads to extensive crosslinking and impairs proper conduction in the heart.

5.1 Significance of the study

This study provides compelling evidence of an obligate role for POSTN in regulating LOX and Cx43 in Ang II- and TGF-β1-stimulated cardiac fibroblasts, which are major determinants of collagen crosslinking and cardiac conduction. These findings also shed light on the mechanistic coupling of two distinct pathological remodeling processes involving cardiac wall stiffening and conduction abnormalities following cardiac injury. The demonstration that POSTN regulates LOX and Cx43 expression in cardiac fibroblasts via ERK 1/2 MAPK and SRF pathway offers significant insights into the complex regulatory mechanisms underlying cardiac wall stiffening and conduction abnormalities post-myocardial injury.

While this study elucidated alterations in the expression of POSTN, LOX, and Cx43 and their underlying molecular mechanisms, it did not establish an in vivo role for POSTN in the pathogenesis of cardiac fibrosis. Demonstrating this would require loss-of-function studies within an in vivo disease model, specifically using cardiac fibroblast-specific POSTN knockout in a myocardial injury context, to definitively assess the roles of LOX and Cx43 in collagen crosslinking and cardiac conduction. Although this study identified POSTN's regulatory effect of POSTN on LOX expression in response to Ang II and TGF-β1, changes in tissue stiffness following POSTN silencing could not be evaluated. Detecting stiffness variations attributable to collagen crosslinking would necessitate long-term culture conditions, while our study employed a transient transfection approach to silence POSTN for 72 hours, which may not provide a sufficient timeframe to capture such changes. Furthermore, the study did not investigate potential changes in conduction properties resulting from Cx43

downregulation in cardiac fibroblasts, as electrophysiological assessments such as patch-clamp analyses were beyond the scope of this study.

CHAPTER 6

SUMMARY AND CONCLUSION

Myocardial injury triggers maladaptive remodelling within the heart, which is characterized by significant alterations in collagen deposition and crosslinking. These disturbances in collagen homeostasis contribute to accelerated progression of cardiac fibrosis, which subsequently leads to increased myocardial stiffness. Excessive collagen deposition and changes in Cx43 expression in cardiac fibroblasts also contribute to the development of conduction abnormalities (Cowling et al., 2019). Consequently, investigating the signalling pathways and cellular responses that govern collagen dysregulation and changes in CX43 expression in fibroblasts under stress or injury conditions could offer new avenues for therapeutic strategies to preserve ventricular function and improve long-term cardiac outcomes in patients with myocardial injury.

In this context, LOX and Cx43 have increasingly been implicated in structural and functional remodelling of the heart. It is noteworthy that complete inhibition of LOX or Cx43 may interfere with the initial wound-healing phase of myocardial injury. While the initial conduction of electrical impulses via Cx43 is essential for electrically linking infarct and non-infarct regions, adequate crosslinking via lOX is required for the formation of a stable scar. Hence, any intervention that modulates collagen crosslinking and cardiac conduction may require an intense understanding of the underlying mechanisms regulating LOX and Cx43 post-myocardial injury.

This study provides compelling evidence supporting the crucial role of POSTN in the transcriptional regulation of LOX and Cx43 post-myocardial injury. Although it is plausible that additional signaling pathways may contribute to LOX and Cx43 regulation or intersect with the pathways identified here, this study validates that

POSTN modulates both LOX and Cx43 through a common regulatory pathway. This pathway involves the activation of ERK1/2 MAPK and SRF in Ang II- and TGF-β1-stimulated cardiac fibroblasts, thereby advancing our understanding of the intricate mechanisms underlying collagen crosslinking and cardiac conduction.

Furthermore, POSTN-mediated regulation of Cx43 expression in cardiac fibroblasts possibly represents a mechanism by which cardiac fibroblasts may directly impact cardiac conduction. In contrast, POSTN-mediated regulation of cardiac wall stiffening via LOX regulation possibly represents a mechanism by which cardiac fibroblasts may indirectly impact cardiac conduction. Therefore, this study offers valuable insights into the molecular basis of cardiac wall stiffening and conduction abnormalities, paving the way for a potential drug target to mitigate adverse structural and functional alterations in the heart post-MI.

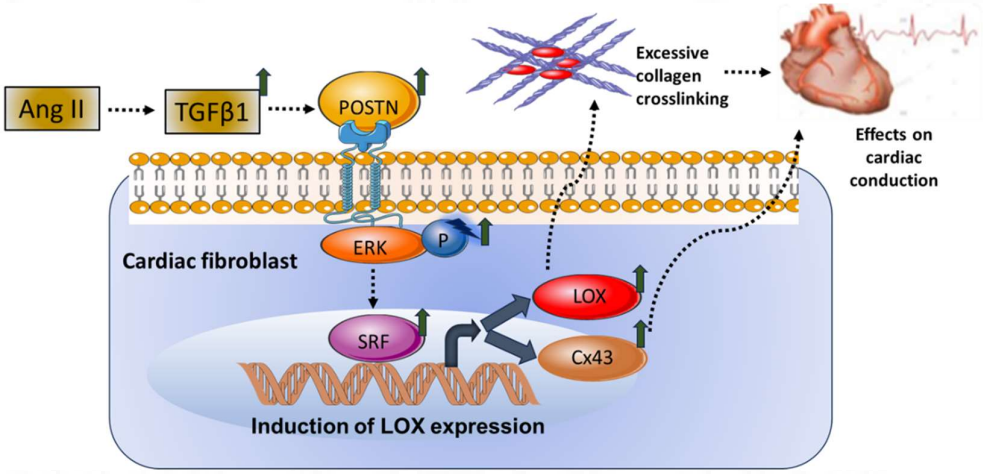

Fig 46: Schematic representation of POSTN in regulating cardiac wall stiffening and conduction abnormalities.

6.1 Major findings of the study

- Ang II enhances the expression of POSTN and LOX
- POSTN mediates Ang II-stimulated LOX expression
- POSTN has a role in modulating Ang II-mediated LOX activity
- POSTN-dependent activation of SRF via the ERK1/2 MAPK- pathway transcriptionally enhances LOX expression in Ang II-stimulated cardiac fibroblasts
- POSTN also mediates TGF-β1-stimulated expression of LOX in cardiac fibroblasts
- POSTN mediates the TGF-β1 effect on LOX via ERK 1/2 and SRF
- POSTN-mediates TGF-β1-stimulated upregulation of Cx43
- POSTN has a role in modulating Cx43 activity
- POSTN regulates Cx43 through ERK 1/2 MAPK-dependent SRF in TGF-β1-stimulated cardiac fibroblasts
- POSTN, and LOX levels correlated within the collagen-rich scar in a rat model of myocardial infarction
- Cx43 expression was localized within collagen-rich scars in areas where cells involved in repair and remodelling were present.

6.2 Future studies

Further research is needed to validate the establishment of regulation between POSTN and LOX, and POST and CX43 in myocardial injury models with POSTN silenced or inhibited in cardiac fibroblasts at specific time point during myocardial repair.

CHAPTER 7

REFERENCES

Barnes LA, Marshall CD, Leavitt T, et al. (2018) Mechanical Forces in Cutaneous Wound Healing: Emerging Therapies to Minimize Scar Formation. *Advances in Wound Care* 7(2). Mary Ann Liebert, Inc., publishers: 47–56.

Beaumont J, López B, Ravassa S, et al. (2017) MicroRNA-19b is a potential biomarker of increased myocardial collagen cross-linking in patients with aortic stenosis and heart failure. *Scientific Reports* 7(1). Nature Publishing Group: 40696.

Benjamin EJ, Muntner P, Alonso A, et al. (2019) Heart Disease and Stroke Statistics—2019 Update: A Report From the American Heart Association. *Circulation* 139(10). American Heart Association: e56–e528.

Biernacka A, Dobaczewski M and Frangogiannis NG (2011) TGF-β signaling in fibrosis. *Growth Factors (Chur, Switzerland)* 29(5): 196–202.

Bujak M, Ren G, Kweon HJ, et al. (2007) Essential Role of Smad3 in Infarct Healing and in the Pathogenesis of Cardiac Remodeling. *Circulation* 116(19). American Heart Association: 2127–2138.

Camelliti P, Borg T and Kohl P (2005) Structural and functional characterisation of cardiac fibroblasts. *Cardiovascular Research* 65(1): 40–51.

Campbell SE and Katwa LC (1997) Angiotensin II stimulated expression of transforming growth factor-beta1 in cardiac fibroblasts and myofibroblasts. *Journal of Molecular and Cellular Cardiology* 29(7): 1947–1958.

Chai J, Norng M, Tarnawski AS, et al. (2007) A critical role of serum response factor in myofibroblast differentiation during experimental oesophageal ulcer healing in rats. *Gut* 56(5): 621–630.

Chen L, Tian X, Gong W, et al. (2019) Periostin mediates epithelial-mesenchymal transition through the MAPK/ERK pathway in hepatoblastoma. *Cancer Biology & Medicine* 16(1): 89–100.

Chuanyu S, Yuqing Z, Chong X, et al. (2017) Periostin promotes migration and invasion of renal cell carcinoma through the integrin/focal adhesion kinase/c-Jun N-terminal kinase pathway. *Tumor Biology* 39(4). SAGE Publications Ltd STM: 1010428317694549.

Conway SJ and Molkentin JD (2008) Periostin as a heterofunctional regulator of cardiac development and disease. *Current Genomics* 9(8): 548–555.

Cowling RT, Kupsky D, Kahn AM, et al. (2019) Mechanisms of cardiac collagen deposition in experimental models and human disease. *Translational research : the journal of laboratory and clinical medicine* 209: 138.

Desplantez T (2017) Cardiac Cx43, Cx40 and Cx45 co-assembling: involvement of connexins epitopes in formation of hemichannels and Gap junction channels. *BMC Cell Biology* 18(1): 3.

Dobaczewski M, Chen W and Frangogiannis NG (2011) Transforming growth factor (TGF)-β signaling in cardiac remodeling. *Journal of Molecular and Cellular Cardiology* 51(4). Key Signaling Molecules in Hypertrophy and Heart Failure: 600–606.

Doppler SA, Carvalho C, Lahm H, et al. (2017) Cardiac fibroblasts: more than mechanical support. *Journal of Thoracic Disease* 9(Suppl 1). AME Publishing Company.

Duchamp de Lageneste O and Colnot C (2019) Periostin in Bone Regeneration. *Advances in Experimental Medicine and Biology* 1132: 49–61.

Fernandes I, Funakoshi S, Hamidzada H, et al. (2023) Modeling cardiac fibroblast heterogeneity from human pluripotent stem cell-derived epicardial cells. *Nature Communications* 14(1). Nature Publishing Group: 8183.

Field S, Uyttenhove C, Stroobant V, et al. (2016) Novel highly specific anti-periostin antibodies uncover the functional importance of the fascilin 1-1 domain and highlight preferential expression of periostin in aggressive breast cancer. *International Journal of Cancer* 138(8): 1959–1970.

Fogelgren B, Polgár N, Szauter KM, et al. (2005) Cellular Fibronectin Binds to Lysyl Oxidase with High Affinity and Is Critical for Its Proteolytic Activation *. *Journal of Biological Chemistry* 280(26). Elsevier: 24690–24697.

Fontes MSC, van Veen TAB, de Bakker JMT, et al. (2012) Functional consequences of abnormal Cx43 expression in the heart. *Biochimica et Biophysica Acta (BBA) - Biomembranes* 1818(8). The Communicating junctions, composition, structure and characteristics Part 1: 2020–2029.

Frangogiannis NG (2012) Matricellular Proteins in Cardiac Adaptation and Disease. *Physiological Reviews* 92(2). American Physiological Society: 635–688.

Frangogiannis NG (2017) The extracellular matrix in myocardial injury, repair, and remodeling. *The Journal of Clinical Investigation* 127(5): 1600–1612.

Frangogiannis NG (2019) Cardiac fibrosis: Cell biological mechanisms, molecular pathways and therapeutic opportunities. *Molecular Aspects of Medicine* 65: 70–99.

Frangogiannis NG (2021) Cardiac fibrosis. *Cardiovascular Research* 117(6): 1450–1488.

Frantz C, Stewart KM and Weaver VM (2010) The extracellular matrix at a glance. *Journal of Cell Science* 123(24): 4195–4200.

Fu X, Khalil H, Kanisicak O, et al. (2018) Specialized fibroblast differentiated states underlie scar formation in the infarcted mouse heart. *The Journal of Clinical Investigation* 128(5). American Society for Clinical Investigation: 2127–2143.

Fu X, Liu Q, Li C, et al. (2020) Cardiac Fibrosis and Cardiac Fibroblast Lineage-Tracing: Recent Advances. *Frontiers in Physiology* 11. Frontiers.

Galán M, Varona S, Guadall A, et al. (2017) Lysyl oxidase overexpression accelerates cardiac remodeling and aggravates angiotensin II–induced hypertrophy. *The FASEB Journal* 31(9): 3787–3799.

Gao X, He X, Luo B, et al. (2009) Angiotensin II increases collagen I expression via transforming growth factor-beta1 and extracellular signal-regulated kinase in cardiac fibroblasts. *European Journal of Pharmacology* 606(1): 115–120.

George M, Vijayakumar A, Dhanesh SB, et al. (2016) Molecular basis and functional significance of Angiotensin II-induced increase in Discoidin Domain Receptor 2 gene expression in cardiac fibroblasts. *Journal of Molecular and Cellular Cardiology* 90: 59–69.

Gil H, Goldshtein M, Etzion S, et al. (2022) Defining the timeline of periostin upregulation in cardiac fibrosis following acute myocardial infarction in mice. *Scientific Reports* 12(1). Nature Publishing Group: 21863.

Goldstein D and Frishman WH (2021) Diastolic Heart Failure: A Review of Current and Future Treatment Options. *Cardiology in Review* 29(2): 82–88.

González A, López B, Ravassa S, et al. (2019) The complex dynamics of myocardial interstitial fibrosis in heart failure. Focus on collagen cross-linking. *Biochimica Et Biophysica Acta. Molecular Cell Research* 1866(9): 1421–1432.

Gurantz D, Cowling RT, Varki N, et al. (2005) IL-1beta and TNF-alpha upregulate angiotensin II type 1 (AT1) receptors on cardiac fibroblasts and are associated with increased AT1 density in the post-MI heart. *Journal of Molecular and Cellular Cardiology* 38(3): 505–515.

Györfi AH, Matei A-E and Distler JHW (2018) Targeting TGF-β signaling for the treatment of fibrosis. *Matrix Biology* 68–69. SI : Fibrosis – Mechanisms and Translational Aspects: 8–27.

He L, Huang X, Kanisicak O, et al. (2017) Preexisting endothelial cells mediate cardiac neovascularization after injury. *The Journal of Clinical Investigation* 127(8). American Society for Clinical Investigation: 2968–2981.

Higuchi S, Ohtsu H, Suzuki H, et al. (2007) Angiotensin II signal transduction through the AT1 receptor: novel insights into mechanisms and pathophysiology. *Clinical Science* 112(8): 417–428.

Hinderer S and Schenke-Layland K (2019) Cardiac fibrosis – A short review of causes and therapeutic strategies. *Advanced Drug Delivery Reviews* 146. Wound healing and fibrosis – State of play: 77–82.

Hirschi KK, Burt JM, Hirschi KD, et al. (2003) Gap Junction Communication Mediates Transforming Growth Factor-β Activation and Endothelial-Induced Mural Cell Differentiation. *Circulation Research* 93(5). American Heart Association: 429–437.

Horiuchi K, Amizuka N, Takeshita S, et al. (1999) Identification and Characterization of a Novel Protein, Periostin, with Restricted Expression to Periosteum and Periodontal Ligament and Increased Expression by Transforming Growth Factor β. *Journal of Bone and Mineral Research* 14(7): 1239–1249.

Hwang JH, Yang SH, Kim YC, et al. (2017) Experimental Inhibition of Periostin Attenuates Kidney Fibrosis. *American Journal of Nephrology* 46(6): 501–517.

Ieda M, Tsuchihashi T, Ivey KN, et al. (2009) Cardiac Fibroblasts Regulate Myocardial Proliferation through β1 Integrin Signaling. *Developmental Cell* 16(2): 233–244.

Iwanami J, Mogi M, Iwai M, et al. (2009) Inhibition of the renin–angiotensin system and target organ protection. *Hypertension Research* 32(4). Nature Publishing Group: 229–237.

Johnson RD and Camelliti P (2018) Role of Non-Myocyte Gap Junctions and Connexin Hemichannels in Cardiovascular Health and Disease: Novel Therapeutic Targets? *International Journal of Molecular Sciences* 19(3). 3. Multidisciplinary Digital Publishing Institute: 866.

Kaur H, Takefuji M, Ngai C y., et al. (2016) Targeted Ablation of Periostin-Expressing Activated Fibroblasts Prevents Adverse Cardiac Remodeling in Mice. *Circulation Research* 118(12). American Heart Association: 1906–1917.

Kii I and Ito H (2017) Periostin and its interacting proteins in the construction of extracellular architectures. *Cellular and Molecular Life Sciences* 74(23): 4269–4277.

Kong P, Christia P and Frangogiannis NG (2014) The pathogenesis of cardiac fibrosis. *Cellular and molecular life sciences: CMLS* 71(4): 549–574.

Kubiczkova L, Sedlarikova L, Hajek R, et al. (2012) TGF-β – an excellent servant but a bad master. *Journal of Translational Medicine* 10(1): 183.

Kumar P, Smith T, Raeman R, et al. (2018) Periostin promotes liver fibrogenesis by activating lysyl oxidase in hepatic stellate cells. *Journal of Biological Chemistry* 293(33). Elsevier: 12781–12792.

Kurisu S, Ozono R, Oshima T, et al. (2003) Cardiac angiotensin II type 2 receptor activates the kinin/NO system and inhibits fibrosis. *Hypertension (Dallas, Tex.: 1979)* 41(1): 99–107.

Laczko R and Csiszar K (2020) Lysyl Oxidase (LOX): Functional Contributions to Signaling Pathways. *Biomolecules* 10(8): 1093.

Lajiness JD and Conway SJ (2012) The Dynamic Role of Cardiac Fibroblasts in Development and Disease. *Journal of Cardiovascular Translational Research* 5(6): 739–748.

Lajiness JD and Conway SJ (2014) Origin, development, and differentiation of cardiac fibroblasts. *Journal of Molecular and Cellular Cardiology* 70: 2–8.

Lerman RH, Apstein CS, Kagan HM, et al. (1983) Myocardial healing and repair after experimental infarction in the rabbit. *Circulation Research* 53(3). American Heart Association: 378–388.

Li C, Sun X-N, Zeng M-R, et al. (2017) Mineralocorticoid Receptor Deficiency in T Cells Attenuates Pressure Overload–Induced Cardiac Hypertrophy and Dysfunction Through Modulating T-Cell Activation. *Hypertension* 70(1). American Heart Association: 137–147.

Li G, Oparil S, Sanders JM, et al. (2006) Phosphatidylinositol-3-kinase signaling mediates vascular smooth muscle cell expression of periostin in vivo and in vitro. *Atherosclerosis* 188(2): 292–300.

Li H, Xiang Y, Fan L-J, et al. (2017) Myocardin inhibited the gap protein connexin 43 via promoted miR-206 to regulate vascular smooth muscle cell phenotypic switch. *Gene* 616: 22–30.

Li L, Fan D, Wang C, et al. (2011) Angiotensin II increases periostin expression via Ras/p38 MAPK/CREB and ERK1/2/TGF-β1 pathways in cardiac fibroblasts. *Cardiovascular Research* 91(1): 80–89.

Li L, Zhao Q and Kong W (2018) Extracellular matrix remodeling and cardiac fibrosis. *Matrix Biology* 68–69. SI : Fibrosis – Mechanisms and Translational Aspects: 490–506.

Li Q, Liu X and Wei J (2014) Ageing related periostin expression increase from cardiac fibroblasts promotes cardiomyocytes senescent. *Biochemical and Biophysical Research Communications* 452(3): 497–502.

Lijnen PJ, Petrov VV and Fagard RH (2001) Angiotensin II-induced stimulation of collagen secretion and production in cardiac fibroblasts is mediated via angiotensin II subtype 1 receptors. *Journal of the Renin-Angiotensin-Aldosterone System* 2(2). SAGE Publications Ltd STM: 117–122.

Liu Y, Li F, Gao F, et al. (2016) Periostin promotes tumor angiogenesis in pancreatic cancer via Erk/VEGF signaling. *Oncotarget* 7(26). Impact Journals: 40148–40159.

López B, González A, Querejeta R, et al. (2006) Alterations in the pattern of collagen deposition may contribute to the deterioration of systolic function in hypertensive patients with heart failure. *Journal of the American College of Cardiology* 48(1): 89–96.

López B, González A, Hermida N, et al. (2010) Role of lysyl oxidase in myocardial fibrosis: from basic science to clinical aspects. *American Journal of Physiology-Heart and Circulatory Physiology* 299(1). American Physiological Society: H1–H9.

López B, Querejeta R, González A, et al. (2012) Collagen Cross-Linking But Not Collagen Amount Associates With Elevated Filling Pressures in Hypertensive Patients With Stage C Heart Failure. *Hypertension* 60(3). American Heart Association: 677–683.

López B, González A, Lindner D, et al. (2013) Osteopontin-mediated myocardial fibrosis in heart failure: a role for lysyl oxidase? *Cardiovascular Research* 99(1): 111–120.

López B, Ravassa S, González A, et al. (2016) Myocardial Collagen Cross-Linking Is Associated With Heart Failure Hospitalization in Patients With Hypertensive Heart Failure. *Journal of the American College of Cardiology* 67(3): 251–260.

Lother A and Kohl P (2023) The heterocellular heart: identities, interactions, and implications for cardiology. *Basic Research in Cardiology* 118(1): 30.

Lu M, Qin Q, Yao J, et al. (2019) Induction of LOX by TGF-β1/Smad/AP-1 signaling aggravates rat myocardial fibrosis and heart failure. *IUBMB Life* 71(11). John Wiley & Sons, Ltd: 1729–1739.

Ma H, Wang J, Zhao X, et al. (2020) Periostin Promotes Colorectal Tumorigenesis through Integrin-FAK-Src Pathway-Mediated YAP/TAZ Activation. *Cell Reports* 30(3): 793-806.e6.

Maruhashi T, Kii I, Saito M, et al. (2010) Interaction between Periostin and BMP-1 Promotes Proteolytic Activation of Lysyl Oxidase *. *Journal of Biological Chemistry* 285(17). Elsevier: 13294–13303.

Miguel-Carrasco JL, Beaumont J, San José G, et al. (2017) Mechanisms underlying the cardiac antifibrotic effects of losartan metabolites. *Scientific Reports* 7: 41865.

Minicucci MF, Santos PP dos, Rafacho BPM, et al. (2013) Periostin as a modulator of chronic cardiac remodeling after myocardial infarction. *Clinics (Sao Paulo, Brazil)* 68(10): 1344–1349.

Molkentin JD, Bugg D, Ghearing N, et al. (2017) Fibroblast-Specific Genetic Manipulation of p38 Mitogen-Activated Protein Kinase In Vivo Reveals Its Central Regulatory Role in Fibrosis. *Circulation* 136(6). American Heart Association: 549–561.

Molnar J, Fong KSK, He QP, et al. (2003) Structural and functional diversity of lysyl oxidase and the LOX-like proteins. *Biochimica et Biophysica Acta (BBA) - Proteins and Proteomics* 1647(1). 3rd International Symposium on Vitamin B6, PQQ, Carbonyl Catalysis and Quinoproteins: 220–224.

Moore-Morris T, Cattaneo P, Puceat M, et al. (2015) Origins of Cardiac Fibroblasts. *Journal of molecular and cellular cardiology* 91: 1.

Morfino P, Aimo A, Castiglione V, et al. (2023) Treatment of cardiac fibrosis: from neuro-hormonal inhibitors to CAR-T cell therapy. *Heart Failure Reviews* 28(2): 555–569.

Murphy-Ullrich JE and Sage EH (2014) Revisiting the matricellular concept. *Matrix Biology* 37. Matricellular Proteins: 1–14.

Nakamura Y, Yoshiyama M, Omura T, et al. (2003) Beneficial effects of combination of ACE inhibitor and angiotensin II type 1 receptor blocker on cardiac remodeling in rat myocardial infarction. *Cardiovascular Research* 57(1): 48–54.

Nakazawa Y, Taniyama Y, Sanada F, et al. (2018) Periostin blockade overcomes chemoresistance via restricting the expansion of mesenchymal tumor subpopulations in breast cancer. *Scientific Reports* 8(1). Nature Publishing Group: 4013.

Nam BY, Park JT, Kwon YE, et al. (2017) Periostin-Binding DNA Aptamer Treatment Ameliorates Peritoneal Dialysis-Induced Peritoneal Fibrosis. *Molecular Therapy Nucleic Acids* 7. Elsevier: 396–407.

Nielsen SH, Mouton AJ, DeLeon-Pennell KY, et al. (2019) Understanding cardiac extracellular matrix remodeling to develop biomarkers of myocardial infarction outcomes. *Matrix Biology* 75–76. Matrix Modeling and Remodeling: 43–57.

Noppe G, Dufeys C, Buchlin P, et al. (2014) Reduced scar maturation and contractility lead to exaggerated left ventricular dilation after myocardial infarction in mice lacking AMPKα1. *Journal of Molecular and Cellular Cardiology* 74: 32–43.

Norris RA, Damon B, Mironov V, et al. (2007) Periostin regulates collagen fibrillogenesis and the biomechanical properties of connective tissues. *Journal of Cellular Biochemistry* 101(3): 695–711.

Norris RA, Borg TK, Butcher JT, et al. (2008) Neonatal and Adult Cardiovascular Pathophysiological Remodeling and Repair. *Annals of the New York Academy of Sciences* 1123(1): 30–40.

Norris RA, Moreno-Rodriguez R, Hoffman S, et al. (2009) The many facets of the matricelluar protein periostin during cardiac development, remodeling, and pathophysiology. *Journal of Cell Communication and Signaling* 3(3–4): 275–286.

Ongstad E and Kohl P (2016) Fibroblast-Myocyte Coupling in the Heart: Potential Relevance for Therapeutic Interventions. *Journal of molecular and cellular cardiology* 91: 238–246.

periostin Null Mice Exhibit Dwarfism, Incisor Enamel Defects, and an Early-Onset Periodontal Disease-Like Phenotype: Molecular and Cellular Biology: Vol 25, No 24 (n.d.). Available at: https://www.tandfonline.com/doi/abs/10.1128/mcb.25.24.11131-11144.2005 (accessed 4 December 2024).

Petrov VV, Fagard RH and Lijnen PJ (2002) Stimulation of collagen production by transforming growth factor-beta1 during differentiation of cardiac fibroblasts to myofibroblasts. *Hypertension (Dallas, Tex.: 1979)* 39(2): 258–263.

Pillai ICL, Li S, Romay M, et al. (2017) Cardiac Fibroblasts Adopt Osteogenic Fates and Can Be Targeted to Attenuate Pathological Heart Calcification. *Cell Stem Cell* 20(2). Elsevier: 218-232.e5.

Porter KE and Turner NA (2009) Cardiac fibroblasts: At the heart of myocardial remodeling. *Pharmacology & Therapeutics* 123(2): 255–278.

Qiao B, Liu X, Wang B, et al. (2024) The role of periostin in cardiac fibrosis. *Heart Failure Reviews* 29(1): 191–206.

Querejeta R, López B, González A, et al. (2004) Increased collagen type I synthesis in patients with heart failure of hypertensive origin: relation to myocardial fibrosis. *Circulation* 110(10): 1263–1268.

Qureshi R, Kindo M, Arora H, et al. (2017) Prokineticin receptor-1-dependent paracrine and autocrine pathways control cardiac tcf21+ fibroblast progenitor

cell transformation into adipocytes and vascular cells. *Scientific Reports* 7(1). Nature Publishing Group: 12804.

Rickard AJ, Morgan J, Tesch G, et al. (2009) Deletion of mineralocorticoid receptors from macrophages protects against deoxycorticosterone/salt-induced cardiac fibrosis and increased blood pressure. *Hypertension (Dallas, Tex.: 1979)* 54(3): 537–543.

Rickard AJ, Morgan J, Bienvenu LA, et al. (2012) Cardiomyocyte Mineralocorticoid Receptors Are Essential for Deoxycorticosterone/Salt-Mediated Inflammation and Cardiac Fibrosis. *Hypertension* 60(6). American Heart Association: 1443–1450.

Rodríguez C and Martínez-González J (2019) The Role of Lysyl Oxidase Enzymes in Cardiac Function and Remodeling. *Cells* 8(12): E1483.

Rodríguez-Sinovas A, Sánchez JA, Valls-Lacalle L, et al. (2021) Connexins in the Heart: Regulation, Function and Involvement in Cardiac Disease. *International Journal of Molecular Sciences* 22(9): 4413.

Rog-Zielinska EA, Norris RA, Kohl P, et al. (2016) The Living Scar – Cardiac Fibroblasts and the Injured Heart. *Trends in Molecular Medicine* 22(2). Elsevier: 99–114.

Rosin NL, Sopel MJ, Falkenham A, et al. (2015) Disruption of Collagen Homeostasis Can Reverse Established Age-Related Myocardial Fibrosis. *The American Journal of Pathology* 185(3): 631–642.

Ruifrok AC and Johnston DA (2001) Quantification of histochemical staining by color deconvolution. *Analytical and Quantitative Cytology and Histology* 23(4): 291–299.

Russo I, Cavalera M, Huang S, et al. (2019) Protective Effects of Activated Myofibroblasts in the Pressure-Overloaded Myocardium Are Mediated Through Smad-Dependent Activation of a Matrix-Preserving Program. *Circulation Research* 124(8). American Heart Association: 1214–1227.

Rzucidlo EM, Martin KA and Powell RJ (2007) Regulation of vascular smooth muscle cell differentiation. *Journal of Vascular Surgery* 45(6, Supplement). Current Topics in Clinical and Basic Vascular Research: A25–A32.

Sahadevan P and Allen BG (2022) Isolation and culture of adult murine cardiac atrial and ventricular fibroblasts and myofibroblasts. *Methods* 203: 187–195.

Salvarani N, Maguy A, De Simone SA, et al. (2017) TGF-β1 (Transforming Growth Factor-β1) Plays a Pivotal Role in Cardiac Myofibroblast Arrhythmogenicity. *Circulation: Arrhythmia and Electrophysiology* 10(5). American Heart Association: e004567.

Sano M, Fukuda K, Sato T, et al. (2001) ERK and p38 MAPK, but not NF-κB, Are Critically Involved in Reactive Oxygen Species–Mediated Induction of IL-6 by Angiotensin II in Cardiac Fibroblasts. *Circulation Research* 89(8). American Heart Association: 661–669.

Santos GL, Hartmann S, Zimmermann W-H, et al. (2019) Inhibition of Rho-associated kinases suppresses cardiac myofibroblast function in engineered connective and heart muscle tissues. *Journal of Molecular and Cellular Cardiology* 134: 13–28.

Shimazaki M, Nakamura K, Kii I, et al. (2008) Periostin is essential for cardiac healingafter acute myocardial infarction. *Journal of Experimental Medicine* 205(2): 295–303.

Shivakumar K and Kumaran C (2001) L-type Calcium Channel Blockers and EGTA Enhance Superoxide Production in Cardiac Fibroblasts. *Journal of Molecular and Cellular Cardiology* 33(2): 373–377.

Silva AC, Pereira C, Fonseca ACRG, et al. (2021) Bearing My Heart: The Role of Extracellular Matrix on Cardiac Development, Homeostasis, and Injury Response. *Frontiers in Cell and Developmental Biology* 8. Frontiers.

Sivakumar P, Gupta S, Sarkar S, et al. (2008) Upregulation of lysyl oxidase and MMPs during cardiac remodeling in human dilated cardiomyopathy. *Molecular and Cellular Biochemistry* 307(1): 159–167.

Small EM (2012) The actin-MRTF-SRF gene regulatory axis and myofibroblast differentiation. *Journal of Cardiovascular Translational Research* 5(6): 794–804.

Smith-Mungo LI and Kagan HM (1998) Lysyl oxidase: Properties, regulation and multiple functions in biology. *Matrix Biology* 16(7): 387–398.

Snider P, Hinton RB, Moreno-Rodriguez RA, et al. (2008) Periostin Is Required for Maturation and Extracellular Matrix Stabilization of Noncardiomyocyte Lineages of the Heart. *Circulation Research* 102(7). American Heart Association: 752–760.

Souders CA, Bowers SLK and Baudino TA (2009) Cardiac Fibroblast: The Renaissance Cell. *Circulation Research* 105(12): 1164–1176.

Stockand JD and Meszaros JG (2003) Aldosterone stimulates proliferation of cardiac fibroblasts by activating Ki-RasA and MAPK1/2 signaling. *American Journal of Physiology. Heart and Circulatory Physiology* 284(1): H176-184.

Tallquist MD and Molkentin JD (2017) Redefining the identity of cardiac fibroblasts. *Nature Reviews Cardiology* 14(8): 484–491.

Titus AS, V H and Kailasam S (2020) Coordinated regulation of cell survival and cell cycle pathways by DDR2-dependent SRF transcription factor in cardiac fibroblasts. *American Journal of Physiology-Heart and Circulatory Physiology* 318(6). American Physiological Society: H1538–H1558.

Travers JG, Kamal FA, Robbins J, et al. (2016) Cardiac Fibrosis: The Fibroblast Awakens. *Circulation Research* 118(6): 1021–1040.

Ubil E, Duan J, Pillai ICL, et al. (2014) Mesenchymal–endothelial transition contributes to cardiac neovascularization. *Nature* 514(7524). Nature Publishing Group: 585–590.

V H, Titus AS, Cowling RT, et al. (2019) Collagen receptor cross-talk determines α-smooth muscle actin-dependent collagen gene expression in angiotensin II-stimulated cardiac fibroblasts. *The Journal of Biological Chemistry* 294(51): 19723–19739.

Valiente-Alandi I, Potter SJ, Salvador AM, et al. (2018) Inhibiting Fibronectin Attenuates Fibrosis and Improves Cardiac Function in a Model of Heart Failure. *Circulation* 138(12): 1236–1252.

Vasquez C, Mohandas P, Louie KL, et al. (2010) Enhanced Fibroblast–Myocyte Interactions in Response to Cardiac Injury. *Circulation Research* 107(8). American Heart Association: 1011–1020.

Verheule S and Schotten U (2021) Electrophysiological Consequences of Cardiac Fibrosis. *Cells* 10(11): 3220.

Voloshenyuk TG, Landesman ES, Khoutorova E, et al. (2011) Induction of cardiac fibroblast lysyl oxidase by TGF-β1 requires PI3K/Akt, Smad3, and MAPK signaling. *Cytokine* 55(1): 90–97.

Wang EY, Rafatian N, Zhao Y, et al. (2019) Biowire Model of Interstitial and Focal Cardiac Fibrosis. *ACS Central Science* 5(7). American Chemical Society: 1146–1158.

Wang H, Leinwand LA and Anseth KS (2014) Roles of transforming growth factor-β1 and OB-cadherin in porcine cardiac valve myofibroblast differentiation. *The FASEB Journal* 28(10): 4551.

Wang Y, Li Q, Tao B, et al. (2023) Fibroblasts in heart scar tissue directly regulate cardiac excitability and arrhythmogenesis. *Science*. American Association for the Advancement of Science. Epub ahead of print 29 September 2023. DOI: 10.1126/science.adh9925.

Weber KT (1989) Cardiac interstitium in health and disease: the fibrillar collagen network. *Journal of the American College of Cardiology* 13(7): 1637–1652.

Weber KT, Jalil JE, Janicki JS, et al. (1989) Myocardial collagen remodeling in pressure overload hypertrophy. A case for interstitial heart disease. *American Journal of Hypertension* 2(12 Pt 1): 931–940.

Weber KT, Sun Y, Bhattacharya SK, et al. (2013) Myofibroblast-mediated mechanisms of pathological remodelling of the heart. *Nature Reviews Cardiology* 10(1). Nature Publishing Group: 15–26.

Wu J, Li J, Xu H, et al. (2023) Periostin drives extracellular matrix degradation, stemness, and chemoresistance by activating the MAPK/ERK signaling pathway in triple–negative breast cancer cells. *Lipids in Health and Disease* 22(1): 153.

Yang F, Zhang X-L, Liu H-H, et al. (2024) Post translational modifications of connexin 43 in ventricular arrhythmias after myocardial infarction. *Molecular Biology Reports* 51(1): 329.

Yang J, Savvatis K, Kang JS, et al. (2016) Targeting LOXL2 for cardiac interstitial fibrosis and heart failure treatment. *Nature Communications* 7(1). Nature Publishing Group: 13710.

Yue L, Xie J and Nattel S (2011) Molecular determinants of cardiac fibroblast electrical function and therapeutic implications for atrial fibrillation. *Cardiovascular Research* 89(4): 744–753.

Zhang X, Zhou W, Niu Y, et al. (2022) Lysyl oxidase promotes renal fibrosis via accelerating collagen cross-link driving by β-arrestin/ERK/STAT3 pathway. *The FASEB Journal* 36(8): e22427.

Zhang Y, Kanter EM and Yamada KA (2010) Remodeling of Cardiac Fibroblasts Following Myocardial Infarction Results in Increased Gap Junction Intercellular Communication. *Cardiovascular pathology : the official journal of the Society for Cardiovascular Pathology* 19(6): e233.

Zhu F, Li P and Sheng Y (2022) Treatment of myocardial interstitial fibrosis in pathological myocardial hypertrophy. *Frontiers in Pharmacology* 13: 1004181.

ANNEXURES

List of publications from Thesis

Radhakrishnan S, Shenoy SJ, Devidasan I, Shaji BV, Gopal S, Sreekumaran S, Sp A, Sivaraman DM, Mohan N. Periostin regulates lysyl oxidase through ERK1/2 MAPK-dependent serum response factor in activated cardiac fibroblasts. Cell Biochem Funct. 2024 Jun;42(4): e4066. doi: 10.1002/cbf.4066. PMID: 38822669. doi: 10.1002/cbf.4066

Conference presentations

1. Radhakrishnan Sruthi, Devidasan Indraja, Mohan Neethu. Periostin-dependent Regulation of Lysyl Oxidase and Its Implications in Cardiac Wall Stiffening. International Conference on "Biotechnology – the way forward" (ICBWF-2024). November 2024

2. Radhakrishnan Sruthi, Devidasan Indraja, Shaji V. Binchu, Shenoy J. Sachin, Mohan Neethu. Molecular regulation of Lysyl Oxidase and its implications in cardiac wall stiffening post myocardial injury. International Society for Heart Research & International Academy of Cardiovascular Sciences. 2023 February

3. Radhakrishnan Sruthi, Devidasan Indraja, Mohan Neethu. Periostin mediated regulation of Lysyl Oxidase: Implications in cardiac wall stiffening. Heart failure Conflux. 2022 February

4. Radhakrishnan Sruthi, Devidasan Indraja, Mohan Neethu. Periostin mediated regulation of Lysyl Oxidase in cardiac fibroblasts: Implications in cardiac wall stiffening. National Conference on Science Day- Remembering the Legacy of Sir C.V Raman. February, 2022

5. Radhakrishnan Sruthi, Devidasan Indraja, Mohan Neethu. Discoidin Domain Receptor 2 (DDR2)-mediated regulation of Connexin43 in cardiac fibroblasts: Implications for conduction abnormalities in cardiac fibrosis. Heart failure Conflux. 2020 February

Curriculum Vitae

Sruthi Radhakrishnan
PhD student
Division of Cellular & Molecular Cardiology
Department of Pathology
SCTIMST, Kerala.
sruthiradhakrishnan23@outlook.com

EDUCATION

Ph.D.- Division of Cellular and Molecular Cardiology, Sree Chitra Tirunal Institute for Medical Sciences and Technology, Trivandrum, India- 2019 - (Ongoing)

- **Thesis title**: "Molecular regulation of Lysyl oxidase and Connexin 43 in cardiac fibroblasts: Implications for cardiac wall stiffening and conduction abnormalities"

M.Sc.- Industrial Biotechnology - Bharathiar University, Coimbatore, India- 2010-2012.

B.Sc.- Biotechnology – Calicut University, Kozhikode, India- 2007-2010.

EXPERIENCE

1. Senior Research Fellow, ICMR, Sree Chitra Tirunal Institute for Medical Sciences and Technology, Trivandrum, India, July, 2022- On-going (As part of Ph.D. programme)

2. Principal Investigator, WISE-KIRAN, Sree Chitra Tirunal Institute for Medical Sciences and Technology, Trivandrum, India, November 2018- May 2022(As part of Ph.D. programme).

3. Project Associate, Sree Chitra Tirunal Institute for Medical Sciences and Technology, Trivandrum, India, August 2018- November 2018

4. Research Associate, Novozymes South Asia Pvt Ltd, Bangalore, India, July 2014-May 2016

PUBLICATIONS

1. **Radhakrishnan S,** Shenoy SJ, Devidasan I, Shaji BV, Gopal S, Sreekumaran S, Sp A, Sivaraman DM, Mohan N*. Periostin regulates lysyl oxidase through ERK1/2 MAPK-dependent serum response factor in activated cardiac fibroblasts. Cell Biochem Funct. 2024 Jun;42(4): e4066. doi: 10.1002/cbf.4066.

CONFERENCE PRESENTATIONS

- Radhakrishnan Sruthi, Devidasan Indraja, Mohan Neethu. Periostin-dependent Regulation of Lysyl Oxidase and Its Implications in Cardiac Wall Stiffening. International Conference on "Biotechnology – the way forward" (ICBWF-2024), organized by Kerala University from 20-22nd November 2024

- Radhakrishnan Sruthi, Devidasan Indraja, Shaji V. Binchu, Shenoy J. Sachin, Mohan Neethu. Molecular regulation of Lysyl Oxidase and its implications in cardiac wall stiffening post myocardial injury. Advances In Cardiovascular Medicine and Research (ACMR) 2023, organized by IACS & ISHR held at PGIMER Chandigarh from 16-18th February 2023

- Radhakrishnan Sruthi, Devidasan Indraja, Mohan Neethu. Periostin mediated regulation of Lysyl Oxidase: Implications in cardiac wall stiffening. Heart failure Conflux, organized by SCTIMST from 5-7th February 2022

- Radhakrishnan Sruthi, Devidasan Indraja, Mohan Neethu. Periostin mediated regulation of Lysyl Oxidase in cardiac fibroblasts: Implications in cardiac wall stiffening. National Conference on Science Day- Remembering the Legacy of Sir C.V Raman, organized by SCTIMST on 28th February 2022

- Radhakrishnan Sruthi, Devidasan Indraja, Mohan Neethu. Discoidin Domain Receptor 2 (DDR2)-mediated regulation of Connexin43 in cardiac fibroblasts: Implications for conduction abnormalities in cardiac fibrosis. Heart failure Conflux 2020. organized by SCTIMST from 5-7th February 2020

- Devidasan Indraja, Radhakrishnan Sruthi, Mohan Neethu. Survival and fate of c-Kit+ cardiac cells in the injured myocardium: Role of Angiotensin II. Heart failure Conflux. February, 2023

- Devidasan Indraja, Radhakrishnan Sruthi, Mohan Neethu. Role of Angiotensin II in determining the fate of c-Kit+ cardiac cells in the injured myocardium. International Society for Heart Research & International Academy of Cardiovascular Sciences. February, 2023

TECHNICAL SKILLS

- Mammalian (primary and cell line) cell culture, mammalian cell transfection, siRNA mediated gene silencing and plasmid overexpression
- Cell-based assays
- Bacterial cell culture and transformation
- Rat handling, ECG (ADInstruments) and Echocardiographic (Mindray) data analysis
- Histology- Haematoxylin & Eosin staining, Picrosirius red staining, Immunohistochemistry and Immunofluorescence
- Western Blotting, SDS-PAGE, PCR and Molecular Cloning techniques
- Brightfield, Phase contrast and Fluorescence Microscopy
- Data analysis using GraphPad Prism, Image J and String for protein-protein interaction networks

AWARDS

- **University Gold medal** (University topper) for academic excellence in the year 2010-2012 for Undergraduate degree
- **University Gold medal** (University topper) for academic excellence in the year 2007-2010 for Postgraduate degree
- Winner, BioVERS'21, Bio-Rad India Life Sciences educational quiz.
- First Prize in poster presentation on Science Day- Remembering the Legacy of Sir C.V Raman, organized by SCTIMST on 28th February 2022

SHORT TERM COURSE

- Certificate course in **BIOCON**, India- **KECK GRADUATE INSTITUTE**, California programme in Biosciences
  Biocon KGI Certificate Program in Biosciences is a certificate programme in partnership with Keck Graduate Institute, California, and biopharmaceutical industry, BIOCON, India on Training on 'Biologics Process Development and Manufacturing'.

APPENDICES

ETHICS COMMITTEE APPROVAL

SREE CHITRA TIRUNAL INSTITUTE FOR MEDICAL SCIENCES AND TECHNOLOGY.
BIOMEDICAL TECHNOLOGY WING.

INSTITUTIONAL ANIMAL ETHICS COMMITTEE

SCT/ABS/IAEC-99/8 Date: 22.01.2019

To,
Dr. Neethu Mohan,
Division of Cellular and Molecular Cardiology.

The Institutional Animal Ethics Committee reviewed and discussed application to conduct the following proposal on 02.01.2019 in IAEC meeting held at Sree Chitra Tirunal Institute for Medical Sciences and Technology, Thiruvananthapuram.

B Form No - **SCT/IAEC-298/JANUARY/2019/99:** *Transcriptional and translational regulation of Periostin and its interaction with DDR2 in cardiac fibrosis.*

No. of Animals requested: Sprague dawley rat-180nos

SREE CHITRA TIRUNAL INSTITUTE FOR MEDICAL SCIENCES AND TECHNOLOGY.
BIOMEDICAL TECHNOLOGY WING.

INSTITUTIONAL ANIMAL ETHICS COMMITTEE

SCT/ABS/IAEC-106/01 Date: 27/07/2020

To,
Dr. Neethu mohan,
Division of cellular and molecular cardiology

The Institutional Animal Ethics Committee reviewed and discussed application to conduct the following proposal on 27.07.2020 in IAEC meeting held at Sree Chitra Tirunal Institute for Medical Sciences and Technology, Thiruvananthapuram.

B Form No - **SCT/IAEC-360/JULY/2020/106:** ***Role of connexin in cardiac fibroblast phenotypic transformation and extra cellular matrix synthesis in cardiac diseases***

No. of Animals requested: Rats, Wistar, Males, 72 nos

PLAGIARISM CHECK REPORT